eman ta zabal zazu

Universidad del País Vasco
Euskal Herriko Unibertsitatea

Shortcuts to adiabaticity in the double well

Sofía Martínez Garaot

Supervisor:

Prof. Juan Gonzalo Muga Francisco

Departamento de Química-Física
Facultad de Ciencia y Tecnología
Universidad del País Vasco/Euskal Herriko Unibertsitatea
(UPV/EHU)

Leioa, Febrero 2016

"El aprendizaje es experiencia, todo lo demás es información."

Albert Einstein

Acknowledgements

Al final de este largo camino me gustaría agradecer a todos aquellos que de alguna forma u otra han estado ayudándome y apoyándome. Mi primera idea era poner una larga lista de nombres en la que quedasen reflejadas todas y cada una de las personas que me han acompañado durante esta etapa pero finalmente he pensado que todo aquel que me conoce encontrará un hueco donde ubicar su nombre en estas líneas.

En primer lugar tengo que agradecer a mi director por haber confiado en mí y haberme guiado durante estos años. A mis colaboradores por haberme enseñado tanto. A mis compañeros de despacho porque todos ellos son parte de este trabajo. Al resto de compañeros de la universidad por todos los momentos vividos. A todas mis amigas y amigos por estar siempre a mi lado. A mi familia, a mis padres y a Pau. Y por último, a ti, por animarme cada día. Gracias a todos.

Esta Tesis ha sido financiada a través de una beca predoctoral concedida por la Universidad del País Vasco/Euskal Herriko Unibertsitatea (UPV/EHU).

Contents

List of Figures

Zuentzat

List of publications

I) **The results of this Thesis are based on the following articles**

Published Articles

1. E. Torrontegui, S. Martínez-Garaot, A. Ruschhaupt, and J. G. Muga
Shortcuts to adiabaticity: Fast-forward approach
Phys. Rev. A **86**, 013601 (2012).

2. E. Torrontegui, S. Martínez-Garaot, M. Modugno, X. Chen, and J. G. Muga
Engineering fast and stable splitting of matter waves
Phys. Rev. A **87**, 033630 (2013).

3. S. Martínez-Garaot, E. Torrontegui, X. Chen, M. Modugno, D. Guéry-Odelin, S.-Y. Tseng, and J. G. Muga
Vibrational Mode Multiplexing of Ultracold Atoms
Phys. Rev. Lett. **111**, 213001 (2013).

4. S. Martínez-Garaot, S.-Y. Tseng, and J. G. Muga
Compact and high conversion efficiency mode-sorting asymmetric Y junction using shortcuts to adiabaticity
Opt. Lett. **39**, 2306 (2014).

5. S. Martínez-Garaot, E. Torrontegui, and J. G. Muga
Shortcuts to adiabaticity in three-level systems using Lie transforms
Phys. Rev. A **89**, 053408 (2014).

6. S. Martínez-Garaot, A. Ruschhaupt, J. Gillet, Th. Busch, and J. G. Muga
Fast quasiadiabatic dynamics
Phys. Rev. A **92**, 043406 (2015).

7. S. Martínez-Garaot, M. Palmero, D. Guéry-Odelin, and J. G. Muga
Fast bias inversion of a double well without residual particle excitation
Phys. Rev. A **92**, 053406 (2015).

II) Other articles produced during the Thesis period

Published Articles not included in this Thesis

8. S. Ibáñez, S. Martínez-Garaot, X. Chen, E. Torrontegui, and J. G. Muga
Shortcuts to adiabaticity for non-Hermitian systems
Phys. Rev. A **84**, 023415 (2011).

9. S. Ibáñez, S. Martínez-Garaot, X. Chen, E. Torrontegui, and J. G. Muga
Erratum: Shortcuts to adiabaticity for non-Hermitian systems
Phys. Rev. A **86**, 019901 (2012).

10. E. Torrontegui, S. Martínez-Garaot, and J. G. Muga
Hamiltonian engineering via invariants and dynamical algebra
Phys. Rev. A **89**, 043408 (2014).

11. M. Palmero, S. Martínez-Garaot, J. Alonso, J. P. Home, and J. G. Muga
Fast expansions and compressions of trapped-ion chains
Phys. Rev. A **91**, 053411 (2015).

12. M. Palmero, S. Martínez-Garaot, U. G. Poschinger, A. Ruschhaupt, and J. G. Muga
Fast separation of two trapped ions
New J. Phys. **17**, 093031 (2015).

III) Review Articles

13. E. Torrontegui, S. Ibáñez, S. Martínez-Garaot, M. Modugno, A. del Campo, D. Guéry-Odelin, A. Ruschhaupt, X. Chen, and J. G. Muga
Shortcuts to adiabaticity
Adv. At. Mol. Opt. Phys. **62**, 117 (2013).

Introduction

During the last three decades, the research in quantum optics has experienced a phenomenal boost, largely driven by the rapid progress in microfabrication technologies, precision measurements, coherent radiation sources, and theoretical work. Many quantum optical systems are employed to test and illustrate the fundamental notions of quantum theory. They have also practical applications for communications, quantum information processing, metrology and the development of new quantum-based technologies, whose physical aspects have by now become an integral part of quantum optics. Frequently, the manipulated systems are quite simple, such as one or a few ions or neutral atoms in harmonic or double wells. Bose-Einstein condensates involve of course many more atoms, but may still be described by mean-field theories. Controlling these systems accurately has become a major goal in contemporary Physics. Serge Haroche and David J. Wineland won the Nobel Prize in 2012 after developing methods for manipulating individual ions in Paul traps or photons in cavities while preserving their quantum-mechanical nature.

This Thesis contributes to this goal by proposing fast operations for one to few ultra cold atoms, or Bose-Einstein condensates, in a double well potential, extending the results as well to optical waveguide systems. "Fast" is to be understood with respect to adiabatic processes. The "adiabatic" concept may have two different meanings: the thermodynamical one and the quantum one. In thermodynamics, an adiabatic process is the one in which there is no heat transfer between system and environment. In quantum mechanics, as stated by Born and Fock (1928) in the adiabatic theorem: "a physical system remains in its instantaneous eigenstate when a given perturbation is acting on it slowly enough and if there is a gap between the eigenvalue and the rest of the Hamiltonian's spectrum". In terms of the instantaneous eigenvalues E_n and their corresponding instantaneous eigenvectors $|\phi_n\rangle$, the adiabaticity condition, i.e., the condition that has to be

satisfied to follow the adiabatic dynamics, can be written as

$$\hbar \left| \frac{\langle \phi_n(t) | \partial_t \phi_m(t) \rangle}{E_n(t) - E_m(t)} \right| \ll 1, \ n \neq m.$$

In this Thesis, we shall always understand "adiabatic" in the quantum-mechanical sense. Quantum adiabatic processes are in principle useful to drive or prepare states in a robust and controllable manner, and have also been proposed to solve complicated computational problems. However, they are prone to suffer noise and decoherence or loss problems due to the long times involved. This is often problematic because some applications require many repetitions or too long times.

Shortcuts to adiabaticity (STA) are alternative fast processes that reproduce the same final populations, or even the same final state, as the adiabatic process in a finite, shorter time. The expression "shortcut to adiabaticity" was introduced in 2010 by Chen *et al.* [1] to describe protocols that speed up a quantum adiabatic process, usually, although not necessarily, through a non-adiabatic route. There are many different approaches to design the shortcuts. For example, the counterdiabatic or transitionless tracking approach formulated by Demirplak and Rice (2003, 2005, 2008) [2–4] or independently by Berry (2009) [5], based on adding counterdiabatic terms to a reference Hamiltonian H_0 to achieve adiabatic dynamics with respect to H_0. Moreover, Lewis-Riesenfeld invariants (1969) [6] were used to inverse engineer a time-dependent Hamiltonian $H(t)$ from the invariant $I(t)$. Masuda and Nakamura (2010) developed a "fast-forward technique" for several manipulations [7]. There are also alternative methods that use the dynamical symmetry of the Hamiltonian or based on distributing the adiabaticity parameter homogeneously in time, or Optimal Control Theory (OCT) [8]. In this Thesis I will not only apply these existing methods but also develop new ones.

Since adiabatic processes are ubiquitous, the shortcuts span a broad range of applications in atomic, molecular, and optical physics, such as fast transport, splitting and expansion of ions or neutral atoms; internal population control, and state preparation (for nuclear magnetic resonance or quantum information), vibrational mode multiplexing or demultiplexing, cooling cycles, many-body state engineering or correlations microscopy [8]. The Thesis focuses on the double well potential, which is an interesting model to study some of the most fundamental quantum effects, like interference or tunneling. Using utracold atoms it has become possible to study the double well at an unprecedented level of precision and

control. This has allowed the observation of Josephson oscillations, nonlinear self-trapping and recently, second-order tunneling effects. Few-body systems are lately of much interest as they enable us to study finite-size effects for a deeper understanding of the microscopic mechanics in utracold atoms, and for the possibility of realizing operations involving a few qubits. Also, double wells for single atoms and Bose-Einstein condensates have been used for precise measurement in interferometry experiments. For trapped ions, the double well is used to implement basic operations for quantum information processing, for example, separation or recombination of ions, Fock states creation, or tunable spin-spin interactions and entanglement.

The Thesis is divided into six chapters: The first chapter is devoted to fast splitting of matter waves. The fast-forward approach is applied to speed up the process and a two dynamical-mode model is introduced. This two-mode model will be an important test-bed model during the whole Thesis. Linear and non-linear matter waves (interacting Bose-Einstein condensates) are studied. Chapter 2 deals with an interacting few-body boson gas in a two-site potential. In particular, we investigate how to accelerate an insulator-superfluid transition and the implementation of a $1:2$ and $1:3$ beam splitter. To achieve these goals, a new STA method based on Lie transforms is worked out. In chapter 3 I present one more new STA method that uses the time dependence of a control parameter to delocalize in time the transition probability among adiabatic levels. Some general properties are described and the approach is used to speed up basic operations in three different systems: a two-mode model, interacting bosons in a double well and a few-particle system on a ring. In chapter 4 the invariant-based inverse engineering approach is used to accelerate multiplexing or demultiplexing processes. The shortcut is designed in the two-mode model and then it is mapped into a realizable coordinate potential. Chapter 5 extends the results of the previous chapter to optical wave guides systems. Finally, chapter 6 provides a strategy based on the compensating force-approach to implement a fast bias inversion both in neutral atoms and in trapped ions. Combining this fast bias inversion with fast multiplexing and demultiplexing processes, population inversions using only trap deformations can be achieved.

Due to the length of the manuscript and the different topics discussed, the notation is consistent within each chapter, but not necessarily throughout the Thesis.

Chapter 1

Engineering fast and stable splitting of matter waves

When attempting to split a coherent noninteracting atomic cloud by bifurcating the initial trap into two well separated wells, slow adiabatic following is unstable with respect to any slight trap asymmetry, and the matter wave "collapses" to the deepest well. A generic fast chopping splits the wave but it also excites it. Shortcuts to adiabaticity engineered to speed up the unperturbed adiabatic process through nonadiabatic transients provide, instead, quiet and robust balanced splitting. For a Bose-Einstein condensate in the mean-field limit, the interatomic interaction makes the splitting, adiabatic or via shortcuts, more stable with respect to trap asymmetry. Simple formulas are provided to distinguish different regimes.

1.1 Introduction

The splitting of a wave packet is an important operation in matter wave interferometry [9–12]. A strategy to improve the interferometer performance is to suppress the interaction [13, 14], so let us first consider a non-interacting Bose-Einstein condensate. For this system, a complete wave splitting into two separated branches is a peculiar operation because adiabatic following, rather than robust, is intrinsically unstable with respect to a small external potential asymmetry [15]. The potential is assumed here to evolve from a single well to a final double-well where tunnelling is negligible [16]. The ground-state wave function "collapses" into the final lower well (or more generally into the one that holds the lowest ground state as in [15]) and a very slow trap potential bifurcation fails to split the wave except for perfectly symmetrical potentials. A fast bifurcation remedies this but the price is typically a strong excitation which is also undesired, as it produces loss of contrast in the interference patterns when recombining the two waves [17]. We propose here a way around these problems by using shortcuts to adiabaticity that speed up the adiabatic process along a nonadiabatic route [1]. Wave splitting via shortcuts avoids the final excitation and is significantly more stable with respect to asymmetry than the adiabatic following. Specifically we shall use a streamlined version [18] of the fast-forward (FF) technique of Masuda and Nakamura [7] applied to the Gross-Pitaevskii (GP) or Schrödinger equations. There have previously been found some obstacles to apply the invariants-based method (quadratic-in-momentum invariants do not satisfy the required boundary conditions [18]) and the transitionless-driving algorithm [2] (because of difficulties in implementing counter-diabatic terms in practice).

In Sec. 1.2 we summarize the FF approach for condensates (interacting or not) in one dimension and its application to splitting. In Sec. 1.3 the effect of a small asymmetric perturbation is studied for noninteracting matter waves, and Sec. 1.4 analyzes and interprets the results with the aid of a moving two-mode model. Sec. 1.5 studies the remarkable stability with respect to the asymmetry achieved due to interatomic interactions in the mean-field limit, and different regimes are distinguished. Finally, Sec. 1.6 discusses the results and open questions.

1.2 Fast-forward approach

The FF method [7, 18, 19] may be used to generate external potentials V_{FF} and drive the matter wave from an initial single well to a final symmetric double-well. The starting point is the three-dimensional (3D) time-dependent GP equation,

$$i\hbar\partial_t|\psi(t)\rangle = H(t)|\psi(t)\rangle, \tag{1.1}$$

where $H(t) = T + G(t) + V(t)$ includes kinetic energy T, external potential V, and mean field potential G. We are assuming an external local potential, where "local" means here $\langle\mathbf{x}|V(t)|\mathbf{x}'\rangle = V(\mathbf{x},t)\delta(\mathbf{x}-\mathbf{x}')$. The kinetic and mean field terms in the coordinate representation have the usual forms,

$$\langle\mathbf{x}|T|\psi(t)\rangle = \frac{-\hbar^2}{2m}\nabla^2\psi(\mathbf{x},t), \tag{1.2}$$

$$\langle\mathbf{x}|G(t)|\psi(t)\rangle = g|\psi(\mathbf{x},t)|^2\psi(\mathbf{x},t). \tag{1.3}$$

The GP equation (1.1) is used to describe a Bose-Einstein condensate within the mean field approximation and it takes into account the atom-atom interaction through g, the atom-atom coupling constant. In the case of vanishing coupling constant $g = 0$ the GP equation simplifies to the Schrödinger equation.

By solving Eq. (1.1) in coordinate space, $V(\mathbf{x},t)$ may be written as

$$V(\mathbf{x},t) = \frac{i\hbar\langle\mathbf{x}|\partial_t\psi(t)\rangle - \langle\mathbf{x}|T+G(t)|\psi(t)\rangle}{\langle\mathbf{x}|\psi(t)\rangle}, \tag{1.4}$$

with $\langle\mathbf{x}|\psi(t)\rangle = \psi(\mathbf{x},t)$. By introducing into Eq. (1.4) the ansatz

$$\langle\mathbf{x}|\psi(t)\rangle = r(\mathbf{x},t)e^{i\phi(\mathbf{x},t)}, \quad r(\mathbf{x},t),\phi(\mathbf{x},t)\in\mathbb{R}, \tag{1.5}$$

we get

$$V(\mathbf{x},t) = i\hbar\frac{\dot{r}}{r} - \hbar\dot{\phi} + \frac{\hbar^2}{2m}\left(\frac{2i\nabla\phi\cdot\nabla r}{r} + i\nabla^2\phi - (\nabla\phi)^2 + \frac{\nabla^2 r}{r}\right) - gr^2, \tag{1.6}$$

where the dot means time derivative. The real and imaginary parts are

$$\mathrm{Re}[V(\mathbf{x},t)] = -\hbar\dot{\phi} + \frac{\hbar^2}{2m}\left(\frac{\nabla^2 r}{r} - (\nabla\phi)^2\right) - gr^2, \tag{1.7}$$

$$\mathrm{Im}[V(\mathbf{x},t)] = \hbar\frac{\dot{r}}{r} + \frac{\hbar^2}{2m}\left(\frac{2\nabla\phi\cdot\nabla r}{r} + \nabla^2\phi\right). \tag{1.8}$$

Our purpose is to design a local and real potential such that an initial eigenstate of the initial Hamiltonian, $H(0)$, typically the ground state, but it could be otherwise, evolves in a time t_f into the corresponding eigenstate of the final Hamiltonian, $H(t_f)$. We assume that the full Hamiltonian and the corresponding eigenstates are known at the boundary times.

By construction the potential of Eq. (1.6) is local. If we impose $Im[V(\mathbf{x},t)]=0$, i.e.,

$$\frac{\dot{r}}{r}+\frac{\hbar}{2m}\left(\frac{2\nabla\phi\cdot\nabla r}{r}+\nabla^2\phi\right)=0, \tag{1.9}$$

then we get from Eq. (1.7) a local and real potential.

In the inversion protocol $r(\mathbf{x},t)$ is designed first, and Eq. (1.9) is solved for ϕ to get $V_{FF}(\mathbf{x},t):=\mathrm{Re}[V(\mathbf{x},t)]$ from Eq. (1.7). To ensure that the initial and final states are eigenstates of the stationary GP equation we impose $\dot{r}=0$ at $t=0$ and t_f. Then Eq. (1.9) has solutions $\phi(\mathbf{x},t)$ independent of $\mathbf{x}$ at the boundary times [18]. Using this in Eq. (1.7) at $t=0$, and multiplying by $e^{i\phi(0)}$, we get

$$\left[-\frac{\hbar^2}{2m}\nabla^2+V(\mathbf{x},0)+g|\psi(\mathbf{x},0)|^2\right]\psi(\mathbf{x},0)=-\hbar\dot{\phi}(0)\psi(\mathbf{x},0).$$

The initial state $\psi(\mathbf{x},0)$ is an eigenstate of the stationary GP equation with chemical potential $-\hbar\dot{\phi}(0)=\mu(0)$. Note that the above solution of ϕ (with $\dot{r}=0$ at boundary times) admits the addition of an arbitrary function that depends only on time and modifies the zero of energy. A similar result is found at t_f.

In the remainder of this chapter we will restrict to the one dimensional case so the potential in Eq. (1.4) is reduced to

$$V(x,t)=\frac{i\hbar\langle x|\partial_t\psi(t)\rangle-\langle x|T+G|\psi(t)\rangle}{\langle x|\psi(t)\rangle}, \tag{1.10}$$

with $\langle x|T|\psi(t)\rangle=\frac{-\hbar^2}{2m}\psi''(x,t)$ and $\langle x|G(t)|\psi(t)\rangle=g_1N|\psi(x,t)|^2\psi(x,t)$. The primes denote derivatives with respect to x, g_1 is the effective 1D-coupling constant of the Bose-Einstein condensate, and N is the number of atoms. For the numerical examples we consider ^{87}Rb atoms. Using in Eq. (1.10) the ansatz

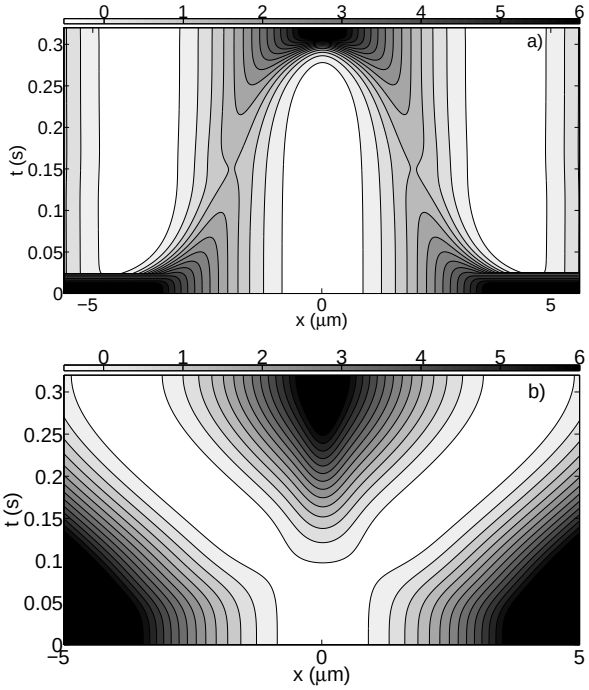

FIGURE 1.1: Contour plot of V_{FF} in units $\hbar\omega$ from Eq. (1.11) for (a) a three-well interpolation and (b) a Y-shaped form. Parameters: $\omega = 780$ rad/s, and $t_f = 320$ ms.

$\langle x|\psi(t)\rangle = r(x,t)e^{i\phi(x,t)}$, $\quad r(x,t), \phi(x,t) \in \mathbb{R}$, the real and imaginary parts will be

$$\mathrm{Re}[V(x,t)] = -\hbar\dot{\phi} + \frac{\hbar^2}{2m}\left(\frac{r''}{r} - (\phi')^2\right) - g_1 N r^2, \tag{1.11}$$

$$\mathrm{Im}[V(x,t)] = \hbar\frac{\dot{r}}{r} + \frac{\hbar^2}{2m}\left(\frac{2\phi' r'}{r} + \phi''\right), \tag{1.12}$$

where the dot means time derivative.

In the following two sections we consider first $g_1 = 0$ and split an initial single Gaussian state $f(x,0) = e^{-x^2/2a_0^2}$ ($a_0 = \sqrt{\hbar/m\omega}$) into a final double Gaussian $f(x,t_f) = e^{-(x-x_f)^2/2a_0^2} + e^{-(x+x_f)^2/2a_0^2}$. In previous works [7, 18] use has been made of the interpolation $r(x,t) = z(t)\big\{[1-\mathcal{R}(t)]f(x,0) + \mathcal{R}(t)f(x,t_f)\big\}$, where $\mathcal{R}(t)$ is a smooth, monotonously increasing function from 0 to 1, and $z(t)$ is a normalization function. This produces a triple-well potential at intermediate times. Here we use instead the two-bump form $r(x,t) = z(t)[e^{-[x-x_0(t)]^2/2a_0^2} + e^{-[x+x_0(t)]^2/2a_0^2}]$, which generates simpler Y-shaped potentials (see Fig. 1.1). We impose $\dot{x}_0(0) = \dot{x}_0(t_f) = 0$, so $\dot{r} = 0$ at the boundary times. In the numerical examples $x_0(s) = x_f(3s^2 - 2s^3)$, where $s = t/t_f$, and $x_f = 4\,\mu$m (see e.g. [20]); Equation (1.12) is solved with the initial conditions $\phi(x=0) = \frac{\partial\phi}{\partial x}|_{x=0} = 0$.

1.3 Effect of the perturbation

Assume now a perturbed Hamiltonian $H_\lambda = T + V_\lambda$ with $V_\lambda = V_{FF} + \lambda\theta(x)$, where $\theta(x)$ is the step function and λ the potential imbalance. Except in the final discussion, we assume that λ is some uncontrollable and hard-to-avoid small perturbation, typically unknown, due to imperfections of the experimental setting. The adiabatic splitting becomes unstable, as we shall see, but the instability does not depend strongly on this particular form, chosen for simplicity. It would also be found, for example, for a linear-in-x perturbation, a smoothed step, slightly different frequencies for the final right and left traps, or a shifted central barrier [15]. In the final potential configuration, with negligible tunneling, the two wells are independent, and the global ground state is localized in one of them.

To analyze the effects of the perturbation on the wavefunction structure and on the shortcut dynamics, we compute several wavefunction overlaps:

- $F_S = |\langle\psi_0^-(t_f)|\psi_\lambda^-(t_f)\rangle|$, the (black) short-dashed line in Fig. 1.2, is the "structural fidelity" between the (perfectly split) ground state $\psi_0^-(t_f)$ of the unperturbed potential $V_{FF}(t_f)$ and the final ground state $\psi_\lambda^-(t_f)$ of the perturbed potential V_λ. This would be the fidelity found with the desired split state if the process were adiabatic. $F_S(\lambda)$ decays extremely rapidly from 1 at $\lambda = 0$ to $1/\sqrt{2}$, which corresponds to the collapse of the ground state of the perturbed potential V_λ into the deeper well.

- $F_D^{(0)} = |\langle\psi_0^-(t_f)|\psi(t_f)\rangle|$, the (blue) long-dashed line in Fig. 1.2, is the fidelity between the state dynamically evolved with H_λ, $\psi(x,t_f) = \langle x|e^{iH_\lambda t_f/\hbar}|\psi(0)\rangle$, and $\psi_0^-(t_f)$. $\psi(0) = \psi_\lambda^-(0)$ is the initial ground state with $V_\lambda(0)$. If $\psi(0) = \psi_0^-(0)$ is used instead, the results are indistinguishable; see the overlap $F_I = |\langle\psi_\lambda^-(0)|\psi_0^-(0)\rangle| \approx 1$, [green dotted line] in Fig. 1.2. The flat $F_D^{(0)}(\lambda)$ at small λ, in sharp contrast to the rapid decay of $F_S(\lambda)$, demonstrates the robustness of the balanced splitting produced by the shortcut. Shorter process times t_f make the splitting more and more stable [compare Figs. 1.2(a)-1.2(c)]. (We assume condensate lifetimes of the order of seconds; see e.g., [21].) In principle, t_f may be reduced arbitrarily. In practice, this reduction implies an increase in transient energy excitation that requires accurate potential engineering for higher energies [22]. Considering that the time-averaged standard deviation of the energy $\overline{\Delta E}$ should be limited at some value a general bound is $t_f > h/(4\overline{\Delta E})$ [23]. For the trap frequency in the examples

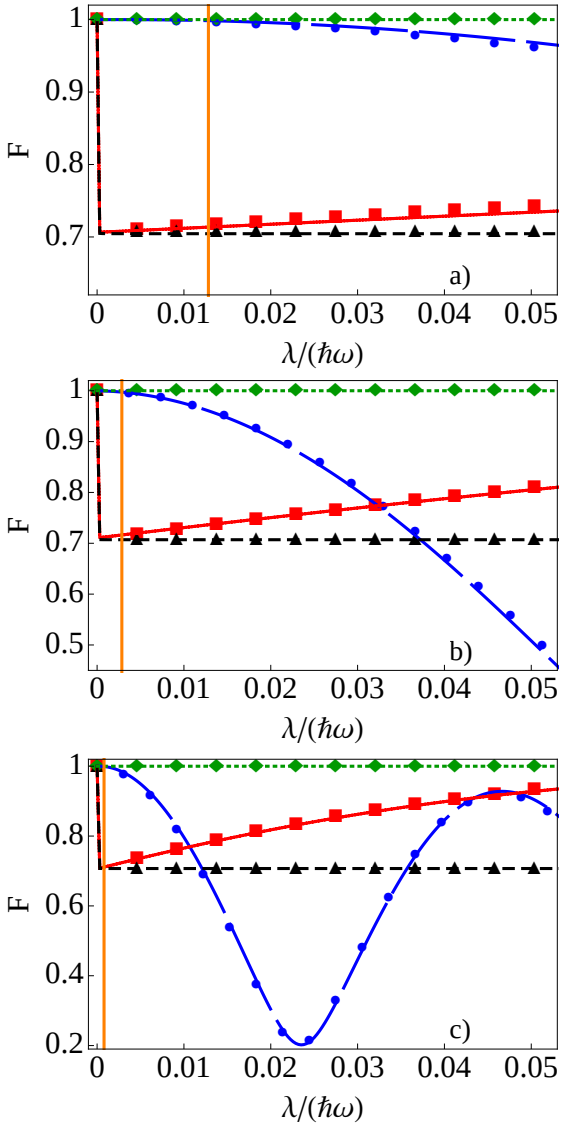

FIGURE 1.2: Different fidelities versus the perturbation parameter λ for the FF approach (lines) and the two-mode model (symbols). $F_D^{(0)}$: (blue) long-dashed line and circles; F_D: (red) solid line and squares; F_S: (black) short-dashed line and triangles; F_I: (green) dotted line and diamonds. The vertical (orange) line is at $0.2/(t_f\omega)$. (a) $t_f = 20$ ms. (b) $t_f = 90$ ms. (c) $t_f = 320$ ms. $\omega = 780$ rad/s.

(780 rad/s) and setting $\overline{\Delta E} = \hbar\omega$ the bound saturates for a time $t_f = 2$ ms, 10 times shorter than our shortest time in Fig. 2.

- $F_D = |\langle\psi(t_f)|\psi_\lambda^-(t_f)\rangle|$ [solid (red) line in Fig. 1.2] is the fidelity between the dynamically evolved state $\psi(t_f)$ and the final ground state $\psi_\lambda^-(t_f)$ for the perturbed potential. If the process is adiabatic, then $F_D \approx 1$. For very small perturbations $F_D \approx F_S$. In this regime the dynamical wave function $\psi(t_f)$ is not affected by the perturbation and becomes $\psi_0^-(t_f)$, up to a phase

factor; note that $F_D^{(0)} \approx 1$ there. We understand and quantify below this important regime as a sudden process in a moving-frame interaction picture. As λ increases, the energies of the ground and excited states of V_λ separate and the process becomes less sudden and more adiabatic. In Fig. 1.2(c) for $t_f = 320$ ms and for large values of λ, F_D approaches 1 again, the final evolved state collapses to one side and becomes the ground state of V_λ. For the shorter final times in Figs. 1.2(a) and 1.2(b), larger λ values are needed so that F_D approaches 1 adiabatically.

1.4 Moving two-mode model

Static two-mode models have been previously used to analyze splitting processes or double-well dynamics [11, 24, 25]. Here we add the separation motion of left and right basis functions to provide analytical estimates and insight. In terms of a (dynamical) orthogonal bare basis $|L(t)\rangle = \begin{pmatrix} 0 \\ 1 \end{pmatrix}$, $|R(t)\rangle = \begin{pmatrix} 1 \\ 0 \end{pmatrix}$ our two-mode Hamiltonian model is

$$H(t) = \frac{1}{2}\begin{pmatrix} \lambda & -\delta(t) \\ -\delta(t) & -\lambda \end{pmatrix}, \tag{1.13}$$

where $\delta(t)$ is the tunneling rate [11, 24, 25]. We may consider λ constant through a given splitting process, for the time being, and equal to the perturbative parameter that defines the asymmetry. A more detailed approach discussed later does not produce any significant difference. The instantaneous eigenvalues are

$$E_\lambda^{\pm}(t) = \pm\frac{1}{2}\sqrt{\lambda^2 + \delta^2(t)}, \tag{1.14}$$

and the normalized eigenstates take the form

$$\begin{aligned} |\psi_\lambda^+(t)\rangle &= \sin\left(\tfrac{\alpha}{2}\right)|L(t)\rangle - \cos\left(\tfrac{\alpha}{2}\right)|R(t)\rangle, \\ |\psi_\lambda^-(t)\rangle &= \cos\left(\tfrac{\alpha}{2}\right)|L(t)\rangle + \sin\left(\tfrac{\alpha}{2}\right)|R(t)\rangle, \end{aligned} \tag{1.15}$$

where $\alpha = \alpha(t)$ is the mixing angle given by $\tan\alpha = \delta(t)/\lambda$.

The bare basis states $\{|L(t)\rangle, |R(t)\rangle\}$ are symmetrical and orthogonal-moving left and right states. Initially they are close to each other and $\delta(0) \gg \lambda$. The instantaneous eigenstates of H are the symmetric ground state $|\psi_0^-(0)\rangle = \frac{1}{\sqrt{2}}(|L(0)\rangle + |R(0)\rangle)$ and the antisymmetric excited state $|\psi_0^+(0)\rangle = \frac{1}{\sqrt{2}}(|L(0)\rangle - |R(0)\rangle)$ of the single well. At t_f we distinguish two extremes:

i) For $\delta(t_f) \gg \lambda$ the final eigenstates of H tend to symmetric and antisymmetric splitting states $|\psi_\lambda^\mp(t_f)\rangle = \frac{1}{\sqrt{2}}(|L(t_f)\rangle \pm |R(t_f)\rangle)$;

ii) For $\delta(t_f) \ll \lambda$ the final eigenfunctions of H collapse and become right-and left-localized states: $|\psi_\lambda^-(t_f)\rangle = |L(t_f)\rangle$ and $|\psi_\lambda^+(t_f)\rangle = |R(t_f)\rangle$.

Since $\delta(t_f)$ is set as a small number to avoid tunneling in the final configuration, the transition from one to the other regime explains the sharp drop of F_S at small $\lambda \approx \delta(t_f)$.

1.4.1 Moving-frame interaction picture

We define now a moving-frame interaction-picture (IP) wave function $\psi^A = A^\dagger \psi^S$, where $A = \sum_{\beta=L,R} |\beta(t)\rangle\langle\beta(0)|$ and ψ^S is the Schrödinger-picture wave function. ψ^A obeys

$$i\hbar\dot{\psi}^A = (H_A - K_A)\psi^A, \tag{1.16}$$

with

$$H_A = A^\dagger H A, \tag{1.17}$$

$$K_A = i\hbar A^\dagger \dot{A}, \tag{1.18}$$

but for real $\langle x|R(t)\rangle$ and $\langle x|L(t)\rangle$, the symmetry $\langle x|R(t)\rangle = \langle -x|L(t)\rangle$ makes $K_A = 0$.

Inverting Eq. (1.15) the bare states may be written in terms of the ground and first excited states and energies. The two-level model approximates the actual dynamics by first identifying $|\psi_0^\pm(t)\rangle$ and $E_0^\pm(t)$ with the instantaneous ground and excited states and energies of the unperturbed FF Hamiltonian.[1] We combine them to compute the bare basis in coordinate representation and then the matrix elements $\langle\beta'|H_\lambda|\beta\rangle = H_\lambda^{\beta'\beta}$, for $\beta \neq \beta'$. From Eq. (1.13), $\delta(t) = -2H_\lambda^{RL} =$

[1] Contrast this with the variational approach in [26].

$-2H_\lambda^{LR}$.[2] Once all matrix elements are set we solve the dynamics in the moving frame for the two-mode Hamiltonian. The initial state may be the ground state of the perturbed or unperturbed initial potential. The agreement with the exact results is excellent (see the symbols of Fig. 1.2), which denotes the absence of higher excited states. This two-level model thus provides a powerful interpretative and control tool. To gain more insight we now perform further approximations.

1.4.2 Sudden and adiabatic approximations

The fidelities at low λ may be understood with the sudden approximation in the IP. Its validity requires [27]

$$t_f \ll \frac{\hbar}{\Delta\overline{H_A}}, \tag{1.19}$$

where $\Delta\overline{H_A} = [\langle\psi(0)|\overline{H_A}^2|\psi(0)\rangle - \langle\psi(0)|\overline{H_A}|\psi(0)\rangle^2]^{1/2}$. We take $|\psi(0)\rangle = |\psi_0^-(0)\rangle$ and $\overline{H_A} = \frac{1}{t_f}\int_0^{t_f} dt' H_A(t')$, where the matrix elements of $H_A(t')$ in the basis $\{|\beta(0)\rangle\}$ coincide with the matrix elements of H in Eq. (1.13), when the latter are expressed in the basis $\{|\beta(t')\rangle\}$. The condition for the sudden approximation to hold becomes

$$\lambda \ll \frac{2\hbar}{t_f}. \tag{1.20}$$

Vertical lines mark $\lambda = 0.2\hbar/t_f$ in Fig. 1.2 and demonstrate that indeed this condition sets the range in which $F_D^{(0)} \approx 1$ so that the fast protocol provides balanced splitting in spite of the asymmetry.

The increase in F_D with increasing λ can be explained using the adiabatic approximation. The adiabaticity condition is here [29]

$$|\langle\psi_\lambda^-(t)|\partial_t\psi_\lambda^+(t)\rangle| \ll \frac{1}{\hbar}|E_\lambda^-(t) - E_\lambda^+(t)|, \tag{1.21}$$

which, using Eqs. (1.14) and (1.15), takes the form

$$\left|\frac{\hbar\lambda\dot{\delta}(t)}{2[\lambda^2+\delta(t)^2]^{3/2}}\right| \ll 1. \tag{1.22}$$

[2] For $\beta = \beta'$, we may consistently calculate $\lambda'(t) := 2(H_\lambda^{RR} - V_0) = -2(H_\lambda^{LL} - V_0)$, where $V_0 = [E_\lambda^-(t) + E_\lambda^+(t)]/2$ is a shift to match the zero-energy point between the FF and the two-mode models. λ' differs slightly from the constant λ at short times, but the results of substituting λ by λ' are hardly distinguishable in the calculations, so the treatment with λ is preferred for simplicity.

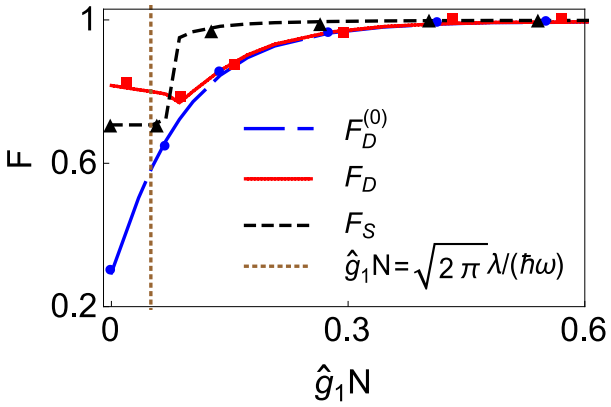

FIGURE 1.3: Fidelities vs dimensionless coupling constant for $\lambda/(\hbar\omega) = 0.02$, $t_f = 320$ ms, and $x_f = 4$ μm. Lines are the same as in Fig. 1.2. Symbols are for a two-level model like Eq. (1.13) with the nonlinear diagonal terms $g_2|c_{R,L}|^2$ added, where $g_2 = g_1 \int dx|R(x)|^4 = g_1 \int dx|L(x)|^4$ and $|c_{R,L}|^2$ are populations for left and right states [28]. The vertical line is at $\widehat{g_1}N = \sqrt{2\pi}\lambda/\hbar\omega$; see the Appendix A.

1.5 Interacting Bose-Einstein condensates

We now generalize the results of the two previous sections for a condensate with interatomic interaction in the mean-field framework. We calculate the ground states $\chi_N(x)$ and $\chi_{\frac{N}{2}}(x)$ of a harmonic trap that holds a Bose-Einstein condensate with N and $N/2$ atoms and define $f(x,t) = [1-\mathcal{R}(t)]\chi_N(x) + \mathcal{R}(t)\chi_{\frac{N}{2}}(x)$, where $\mathcal{R}(t) = 3(t/t_f)^2 - 2(t/t_f)^3$. $r(x,t)$ is constructed as

$$r(x,t) = \big\{f[x - x_0(t), t] + f[x + x_0(t), t]\big\}/z(t), \tag{1.23}$$

where $z(t)$ is a normalization factor and $x_0(t) = x_f\mathcal{R}(t)$. We then get V_{FF} from Eq. (1.11) and evolve the initial ground state with the GP equation using the perturbed potential $V_\lambda(t)$.

The fidelities are shown in Fig. 1.3 versus the dimensionless coupling constant $\widehat{g_1}N = g_1N/(\hbar\omega a_0)$. Note the stabilization of $F_D^{(0)}$ towards 1 upon increasing the interaction (this implies more stable shortcuts). F_D increases too, as the dynamics tends to be more adiabatic. The structural fidelity jumps to 1 around $\widehat{g_1}N = \sqrt{2\pi}\lambda/\hbar\omega$ from the linear case value $1/\sqrt{2}$, i.e., balanced splitting by

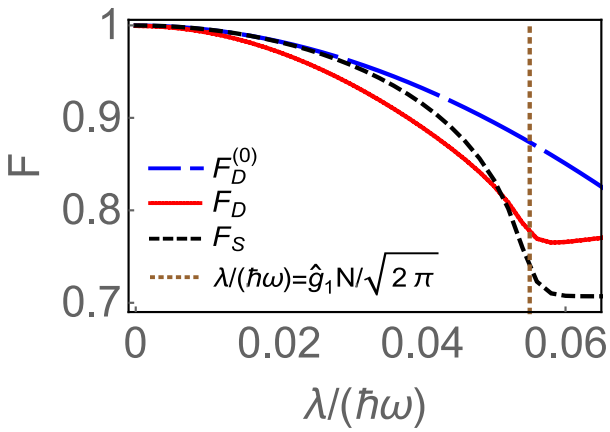

FIGURE 1.4: Fidelities for a Bose-Einstein condensate; lines are the same as in Fig. 1.2. Equation (1.23) is used to design the potential V_{FF}. Parameters: $x_f = 4$ μm, $\omega = 780$ rad/s, $\widehat{g}_1 N$=0.138, and $t_f = 45$ ms.

adiabatic following is robust versus trap asymmetry for $\widehat{g}_1 N \gg \lambda/\hbar\omega$ (see the Appendix A). The extra filling of the lower well increases the nonlinear interaction there opposing the external potential imbalance.

The two-level model may also be extended to interacting condensates with minor modifications, also providing an accurate description (see Fig. 1.3). Adiabaticity fails eventually when decreasing t_f and/or g_1, but the shortcut provides then balanced splitting (see the example of Fig. 1.4): for small λ, adiabatic following would be stable (see F_S and compare to the sharp drop in Fig. 1.2 for linear dynamics), but the process is not quite adiabatic ($F_D < F_S$) for the chosen time, $t_f = 45$ ms -more time would be needed. The shortcut is nevertheless more stable than the hypothetical adiabatic process ($F_D^{(0)} > F_S$).

1.6 Discussion

We have designed simple Y-shaped (position and time dependent) potential traps to fully split noninteracting matter waves rapidly without final excitation, avoiding the instability of the adiabatic approach with respect to slight trap asymmetries. We also avoid or mitigate in this manner the decoherence and noise that affect slow adiabatic following [16, 17]. The bifurcation may be experimentally implemented with optical traps created with the aid of spatial light modulators [30]. A simpler approximate approach would involve two Gaussian beams. Further manipulations, such as the application of differential ac Stark phase shifts could be combined with the proposed technique [16]. Also, a differential phase

among the two final wave parts will develop due to the imbalance, allowing for precision metrology [20, 21], without the time limitations of methods based on adiabatic splitting [21]. In addition, optimal control methods [9–11] complement the present approach to further improve stability and/or optimize other variables such as the transient excitation.

A unique feature of the above application of shortcuts to adiabaticity, compared to previous ones [1, 31–33], is that the shortcut does not attempt to reproduce the result of an adiabatic following of the perturbed asymmetrical system in a shorter time. (The assumption has been made so far that the perturbation is uncontrolled and, possibly, unknown.) Instead, the shortcut reproduces the balanced splitting of the adiabatic following corresponding to the unperturbed, perfectly symmetrical system. In other words, shortening the time here is not really the goal, but it means to achieve stability.

Other operations may actually make positive use of the instability due to potential asymmetries. In particular, the ground- and first-excited-state components of the initial trap could be spatially separated by a controlled, slightly asymmetrical adiabatic bifurcation. Moreover, both states would become ground states of the right and left final traps, so the process may as well be used as a population inversion protocol from the excited to the ground state.

We have also analyzed and exemplified the effect of interatomic interactions for a condensate in the mean-field regime. The interaction changes the behavior of the system with respect to asymmetry, stabilizing dramatically balanced splitting. The total adiabatic collapse of the wave onto one of the two final separated wells requires, in this case, a significant perturbation, proportional to the coupling constant. Compared to the noninteracting case, this offers different manipulation opportunities, in particular, the possibility of considering the asymmetric perturbation as a known, controllable parameter, so that the imbalance between the two wells may be prepared at will. Examples of this type of manipulation may be found in [34–36]. Shortcuts to adiabaticity and, in particular, the FF approach may be readapted to that scenario by designing the fast protocol taking into account the known, controlled asymmetry. The emphasis would be again, as in most applications of the shortcuts, on accelerating and reproducing the result of a slow process.

Shortcuts to adiabaticity could play other roles in systems described by a double-well with varying parameters. They have been applied, in particular, to speed up the generation of spin-squeezed many-body states in bosonic Josephson junctions [37]. Here we suggest other applications: for example, Stickney and Zozulya [38] have described a wave-function recombination instability due to the weak nonlinearity of the condensate. Specifically, they consider an initially weak ground symmetric mode of the double-well which is exponentially amplified at the expense of an initially strong excited asymmetric mode when the wells are recombined. Similarly to the instability due to asymmetry described in this chapter for noninteracting waves, the nonlinear instability is in fact enhanced by adiabatic following. A shortcut-to-adiabaticity strategy as the one followed in this chapter would stabilize the recombination. Our present results may as well be applied to design Y-junctions in planar optical waveguides [39–41], since the equation that describes the field in the paraxial approximation is formally identical to the linear Schrödinger equation, with the longitudinal coordinate playing the role of time. Finally, partial splitting, in which the final two wells are not completely separated and tunnelling is still allowed, may as well be considered.

Chapter 2

Shortcuts to adiabaticity in three-level systems using Lie transforms

Sped-up protocols that drive a system quickly to the same populations that can be reached by a slow adiabatic process may involve Hamiltonian terms which are difficult to realize. We use the dynamical symmetry of the Hamiltonian to find, by means of Lie transforms, alternative Hamiltonians that achieve the same goals without the problematic terms. We apply this technique to three-level systems (two interacting bosons in a double well, and beam splitters with two and three output channels) driven by Hamiltonians that belong to the four-dimensional algebra U3S3.

2.1 Introduction

"Shortcuts to adiabaticity" are manipulation protocols that take the system quickly to the same populations, or even the same state, that can be reached by a slow adiabatic process [8]. Adiabaticity is ubiquitous in preparing a system state in atomic, molecular, and optical physics, so many applications of this concept have been worked out, in both theory and experiment [8]. Some of the engineered Hamiltonians that speed up the adiabatic process in principle may involve terms which are difficult or impossible to realize in practice. In simple systems the dynamical symmetry of the Hamiltonian can be used to eliminate the problematic terms and provide instead feasible Hamiltonians. Examples are single particles transported or expanded by harmonic potentials [42, 43], or two-level systems [31, 33, 44]. In this chapter we extend this program to three-level systems whose Hamiltonians belong to a four-dimensional dynamical algebra. This research was motivated by a recent observation by Opatrný and Mølmer [45]. Among other systems they considered two (ultracold) interacting bosons in a double well within a three-state approximation. Specifically, the aim was to speed up a transition from a "Mott-insulator" state with one particle in each well, to a delocalized "superfluid" state. The reference adiabatic process consisted in slowly turning off the interparticle interaction while increasing the tunneling rate. To speed up this process they applied a method of generating shortcuts based on adding a "counterdiabatic" (cd) term to the original time-dependent Hamiltonian [2–5, 31], but the evolution with the cd term turns out to be difficult to realize in practice [45]. In this chapter we shall use the symmetry of the Hamiltonian (its dynamical algebra) to find an alternative shortcut by means of a Lie transform, namely, a unitary operator in the Lie group associated with the Lie algebra. Since other physical systems have the same Hamiltonian structure the results are applicable to them too. Specifically, the analogy between the time-dependent Schrödinger equation and the stationary-wave equation for a waveguide in the paraxial approximation [46–51] is used to design short-length optical beam splitters with two and three output channels.

In Sec. 2.2 we describe the theoretical model for two bosons in two wells. In Sec. 2.3 we summarize the counterdiabatic or transitionless tracking approach and apply it to the bosonic system. Section 2.4 sets the approach based on unitary Lie transforms to produce alternative shortcuts. In Sec. 2.5 we introduce the insulator-superfluid transition and apply the shortcut designed in the previous

section. In Sec. 2.6 we apply the technique to generate beam splitters with two and three output channels. Section 2.7 discusses the results and open questions. Finally, in the Appendix B some features of the Lie algebra of the system are discussed.

2.2 The model

An interacting boson gas in a two-site potential is described within the Bose-Hubbard approximation [52, 53] by

$$H_0 = \frac{U}{2}\sum_{j=1}^{2} n_j(n_j-1) - J(a_1 a_2^\dagger + a_1^\dagger a_2), \tag{2.1}$$

where a_j ($a_j^\dagger$) are the bosonic particle annihilation (creation) operators at the jth site and n_j is the occupation number operator. The on-site interaction energy is quantified by the parameter U and the hopping energy by J. They are assumed to be controllable functions of time. For two particles the Hamiltonian in the occupation number basis $|2,0\rangle = \begin{pmatrix} 1 \\ 0 \\ 0 \end{pmatrix}$, $|1,1\rangle = \begin{pmatrix} 0 \\ 1 \\ 0 \end{pmatrix}$, and $|0,2\rangle = \begin{pmatrix} 0 \\ 0 \\ 1 \end{pmatrix}$ is given by [45]

$$H_0 = \begin{pmatrix} U & -\sqrt{2}J & 0 \\ -\sqrt{2}J & 0 & -\sqrt{2}J \\ 0 & -\sqrt{2}J & U \end{pmatrix} = UG_4 - 4JG_1, \tag{2.2}$$

where

$$G_1 = \frac{1}{2\sqrt{2}}\begin{pmatrix} 0 & 1 & 0 \\ 1 & 0 & 1 \\ 0 & 1 & 0 \end{pmatrix}, \quad G_4 = \begin{pmatrix} 1 & 0 & 0 \\ 0 & 0 & 0 \\ 0 & 0 & 1 \end{pmatrix}. \tag{2.3}$$

This Hamiltonian belongs to the vector space (Lie algebra) spanned by G_1, G_4, and two more generators,

$$G_2 = \frac{1}{2\sqrt{2}}\begin{pmatrix} 0 & -i & 0 \\ i & 0 & i \\ 0 & -i & 0 \end{pmatrix}, G_3 = \frac{1}{4}\begin{pmatrix} 1 & 0 & 1 \\ 0 & -2 & 0 \\ 1 & 0 & 1 \end{pmatrix}, \tag{2.4}$$

with nonzero commutation relations

$$\begin{aligned}
[G_1, G_2] &= iG_3, \\
[G_2, G_3] &= iG_1, \\
[G_3, G_1] &= iG_2, \\
[G_4, G_1] &= iG_2, \\
[G_2, G_4] &= iG_1.
\end{aligned} \tag{2.5}$$

This four-dimensional Lie algebra, U3S3 [54], is described in more detail in the Appendix B. To find the Hermitian basis we calculate $[G_1, G_4]$, and then all commutators of the result with previous elements. This operation is repeated for all operator pairs until no new linearly independent operator appears.

To diagonalize the Hamiltonian (2.2) it is useful to parameterize U and J as [45]

$$\begin{aligned}
U &= E_0 \cos\varphi, \\
J &= \frac{E_0}{4} \sin\varphi,
\end{aligned} \tag{2.6}$$

where $E_0 = E_0(t)$ and $\varphi = \varphi(t)$, so that

$$H_0 = E_0 \begin{pmatrix} \cos\varphi & -\frac{1}{2\sqrt{2}}\sin\varphi & 0 \\ -\frac{1}{2\sqrt{2}}\sin\varphi & 0 & -\frac{1}{2\sqrt{2}}\sin\varphi \\ 0 & -\frac{1}{2\sqrt{2}}\sin\varphi & \cos\varphi \end{pmatrix}. \tag{2.7}$$

The instantaneous eigenvalues are

$$E_1 = \frac{E_0}{2}(\cos\varphi - 1), \tag{2.8}$$

$$E_2 = E_0 \cos\varphi, \tag{2.9}$$

$$E_3 = \frac{E_0}{2}(\cos\varphi + 1), \tag{2.10}$$

corresponding to the normalized eigenstates

$$|\phi_1\rangle = \begin{pmatrix} \frac{1}{2}\sqrt{1-\cos\varphi} \\ \frac{1}{\sqrt{2}}\sqrt{1+\cos\varphi} \\ \frac{1}{2}\sqrt{1-\cos\varphi} \end{pmatrix}, \tag{2.11}$$

$$|\phi_2\rangle = \frac{1}{\sqrt{2}}\begin{pmatrix} 1 \\ 0 \\ -1 \end{pmatrix}, \tag{2.12}$$

$$|\phi_3\rangle = \begin{pmatrix} \frac{1}{2}\sqrt{1+\cos\varphi} \\ -\frac{1}{\sqrt{2}}\sqrt{1-\cos\varphi} \\ \frac{1}{2}\sqrt{1+\cos\varphi} \end{pmatrix}. \tag{2.13}$$

2.3 Counterdiabatic or transitionless tracking approach

For the transitionless driving or counterdiabatic approach formulated by Demirplak and Rice [2–4] or equivalently by Berry [5], the starting point is a time-dependent reference Hamiltonian

$$H_0(t) = \sum_n |n_0(t)\rangle E_n^{(0)}(t)\langle n_0(t)|. \tag{2.14}$$

The approximate time-dependent adiabatic solution of the dynamics with H_0 takes the form

$$|\psi_n(t)\rangle = e^{i\xi_n(t)}|n_0(t)\rangle, \tag{2.15}$$

where the adiabatic phase reads

$$\xi_n(t) = -\frac{1}{\hbar}\int_0^t dt' E_n^{(0)}(t') + i\int_0^t dt'\langle n_0(t')|\partial_{t'} n_0(t')\rangle. \tag{2.16}$$

Defining now the unitary operator

$$A(t) = \sum_n e^{i\xi_n(t)}|n_0(t)\rangle\langle n_0(0)|, \tag{2.17}$$

a Hamiltonian $H(t) = i\hbar\dot{A}A^{\dagger}$ can be constructed to drive the system exactly along the adiabatic paths of $H_0(t)$ as

$$\begin{aligned} H(t) &= H_0(t) + H_{cd}(t), \\ H_{cd}(t) &= i\hbar \sum_n \left[|\dot{n}_0(t)\rangle\langle n_0(t)| - \langle n_0(t)|\dot{n}_0(t)\rangle |n_0(t)\rangle\langle n_0(t)| \right], \end{aligned} \tag{2.18}$$

where $H_{cd}(t)$ is purely nondiagonal in the $\{|n_0(t)\rangle\}$ basis and the overdot represents time derivative.

We may change the $E_n^{(0)}(t)$, and therefore $H_0(t)$ itself, keeping the same $|n_0(t)\rangle$. We could for example make all the $E_n^{(0)}(t)$ zero, or set $\xi_n(t) = 0$ [5]. Taking into account this freedom the Hamiltonian for transitionless driving can be generally written as

$$H(t) = -\hbar \sum_n |n_0(t)\rangle \dot{\xi}_n \langle n_0(t)| + i\hbar \sum_n |\partial_t n_0(t)\rangle\langle n_0(t)|. \tag{2.19}$$

Subtracting $H_{cd}(t)$, the generic H_0 is

$$H_0(t) = \sum_n |n_0(t)\rangle \left[i\hbar \langle n_0(t)|\partial_t n_0(t)\rangle - \hbar\dot{\xi}_n \right] \langle n_0(t)|. \tag{2.20}$$

For our system $[|n_0(t)\rangle \to |\phi_n\rangle]$, the counterdiabatic term takes the form

$$H_{cd} = i\hbar(|\dot{\phi}_1\rangle\langle\phi_1| + |\dot{\phi}_3\rangle\langle\phi_3|). \tag{2.21}$$

Taking into account Eqs. (2.11), (2.12), (2.13), and their respective time derivatives we get

$$H_{cd} = -\hbar\dot{\varphi}G_2. \tag{2.22}$$

Implementing this interaction is quite challenging as discussed in detail in [45]. In particular, a rapid switching between G_1 and G_4, to implement G_2 through their commutator, is not a practical option [45]. Our goal in the following is to design an alternative Hamiltonian to perform the shortcut without G_2.

2.4 Alternative driving protocols via Lie transforms

The main goal here is to define a new shortcut different from the one described by $i\hbar\partial_t\psi(t) = H(t)\psi(t)$, where $H(t) = H_0(t) + H_{cd}(t)$. A wave function $\psi_I(t)$, which represents the alternative dynamics, is related to $\psi(t)$ by a unitary operator $B(t)$,

$$\psi_I(t) = B^\dagger(t)\psi(t), \tag{2.23}$$

and obeys $i\hbar\partial_t\psi_I(t) = H_I(t)\psi_I(t)$, where

$$H_I(t) = B^\dagger(t)[H(t) - K(t)]B(t), \tag{2.24}$$

$$K(t) = i\hbar\dot{B}(t)B^\dagger(t). \tag{2.25}$$

These are formally the same expressions that define an interaction picture. However, in this application the "interaction picture" portrays a different physical setting from the original one [33]. In other words, H_I is not a mathematical aid to facilitate a calculation in some transformed space, but rather a physically realizable Hamiltonian different from H. Similarly, ψ_I represents in general different dynamics from ψ. The transformation provides indeed an alternative shortcut if $B(0) = B(t_f) = 1$, so that $\psi_I(t_f) = \psi(t_f)$ for a given initial state $\psi_I(0) = \psi(0)$. Moreover, if $\dot{B}(0) = \dot{B}(t_f) = 0$ also the Hamiltonians coincide at initial and final times, $H(0) = H_I(0)$ and $H(t_f) = H_I(t_f)$. These boundary conditions may be relaxed in some cases as we shall see.

We carry out the transformation by exponentiating a member G of the dynamical Lie algebra of the Hamiltonian,

$$B(t) = e^{-i\alpha G}, \tag{2.26}$$

where $\alpha = \alpha(t)$ is a time-dependent real function to be determined. This type of unitary operator $B(t)$ constitutes a "Lie transform". Lie transforms have been used, for example, to develop efficient perturbative approaches that try to set the perturbation term of a Hamiltonian in a convenient form in both classical and quantum systems [55, 56].

Note that K in Eq. (2.25) becomes $-\hbar\dot{\alpha}G$ and commutes with G. Then, H_I, given now by

$$\begin{aligned} B^{\dagger}(H-K)B &= e^{i\alpha G}(H-K)e^{-i\alpha G} \\ &= H-\hbar\dot{\alpha}G+i\alpha[G,H]-\frac{\alpha^2}{2!}[G,[G,H]]-i\frac{\alpha^3}{3!}[G,[G,[G,H]]]+\cdots, \end{aligned} \tag{2.27}$$

depends only on G, H, and its repeated commutators with G, so it stays in the algebra. If we can choose G and α so that the undesired generator components in H cancel out and the boundary conditions for B are satisfied, the method provides a feasible, alternative shortcut. In the existing applications of the method [8, 33], and in this chapter we proceed by trial an error, testing different generators. In the present application we want the Hamiltonian H_I to keep the structure of the original one, with nonvanishing components proportional to G_1 and G_4. We may quickly discard by inspection G_1, G_2, and G_3 as candidates for G. Choosing $G \to G_4$ in Eq. (2.26), and substituting into Eqs. (2.24) and (2.27), the series of repeated commutators may be summed up. H_I becomes

$$\begin{aligned} H_I &= (E_0\cos\varphi-\hbar\dot{\alpha})\,G_4 \\ &- (E_0\sin\varphi\cos\alpha+\hbar\dot{\varphi}\sin\alpha)\,G_1 \\ &- (E_0\sin\varphi\sin\alpha-\hbar\dot{\varphi}\cos\alpha)\,G_2. \end{aligned} \tag{2.28}$$

To cancel the G_2 term, we choose

$$\alpha(t)=\operatorname{arccot}\left[\frac{E_0(t)}{\hbar\dot{\varphi}(t)}\sin[\varphi(t)]\right]. \tag{2.29}$$

Substituting Eq. (2.29) into Eq. (2.28) we have finally

$$\begin{aligned} H_I &= \left[\frac{\cos\varphi E_0^3\sin^2\varphi+\hbar^2\sin\varphi\dot{E}_0\dot{\varphi}+\hbar^2E_0\left(2\cos\varphi\dot{\varphi}^2-\sin\varphi\ddot{\varphi}\right)}{E_0^2\sin^2\varphi+\hbar^2\dot{\varphi}^2}\right]G_4 \\ &- \left[E_0\sin\varphi\sqrt{1+\frac{\hbar^2\csc^2\varphi\dot{\varphi}^2}{E_0^2}}\right]G_1, \end{aligned} \tag{2.30}$$

which has the same structure (generators) as the reference Hamiltonian but different time-dependent coefficients.

2.5 Insulator-Superfluid transition

On changing the U/J ratio, the system may go from a Mott-insulator (the two particles isolated in separate wells) to a superfluid state (in which each particle is distributed with equal probability in both wells). From Eq. (2.11), the Mott-insulator ground state is $|\phi_1\rangle = |1,1\rangle$ and in the superfluid regime the ground state becomes $|\phi_1\rangle = \frac{1}{2}|2,0\rangle + \frac{1}{\sqrt{2}}|1,1\rangle + \frac{1}{2}|0,2\rangle$. To design a reference process (one that performs the transition when driven slowly enough) we consider polynomial functions for $E_0(t)$ and $\varphi(t)$. Since we want to drive the system from $|1,1\rangle$ to $\frac{1}{2}|2,0\rangle + \frac{1}{\sqrt{2}}|1,1\rangle + \frac{1}{2}|0,2\rangle$, we impose in Eq. (2.11)

$$\begin{aligned} \varphi(0) &= 0, \\ \varphi(t_f) &= \pi/2. \end{aligned} \tag{2.31}$$

To have the wells isolated at $t = 0$ but connected (allowing the particles to pass from one to the other) at $t = t_f$ we also set

$$\begin{aligned} E_0(0) &= 0, \\ E_0(t_f) &\neq 0, \end{aligned} \tag{2.32}$$

so that $J(0) = U(0) = 0$ and $J(t_f) \neq 0$. Moreover, for a smooth connection with the asymptotic regimes ($t < 0$, $t > t_f$) we set

$$\begin{aligned} \dot{\varphi}(0) &= 0, \\ \dot{\varphi}(t_f) &= 0. \end{aligned} \tag{2.33}$$

This implies that $H_{cd}(0) = H_{cd}(t_f) = 0$; see Eq. (2.22). The condition

$$\ddot{\varphi}(t_f) = 0 \tag{2.34}$$

is also needed to implement alternative shortcuts, in particular, to satisfy $\dot{B}(t_f) = 0$. At intermediate times, we interpolate the functions as $E_0(t) = \sum_{j=0}^{1} a_j t^j$ and $\varphi(t) = \sum_{j=0}^{4} b_j t^j$, where the coefficients are found by solving Eqs. (2.31), (2.32), (2.33) and (2.34). These functions are shown in Fig. 2.1. In this and other figures $\tau = E_0^{max} t/\hbar$, where E_0^{max} is the maximum value of $E_0(t)$.

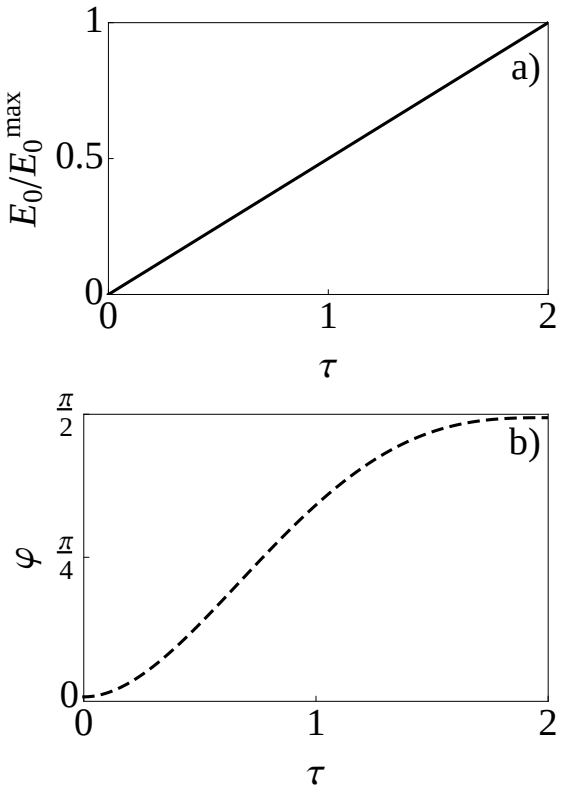

FIGURE 2.1: Functions in $H_I(t)$: (a) $E_0(t)$ and (b) $\varphi(t)$. Parameters: $\tau = E_0^{max}t/\hbar$ where E_0^{max} is the maximum value of $E_0(t)$ and $\tau_f = 2$.

The actual time evolution of the state

$$|\Psi(t)\rangle = c_1(t)|2,0\rangle + c_2(t)|1,1\rangle + c_3(t)|0,2\rangle \tag{2.35}$$

is given by solving Schrödinger's equation with the different Hamiltonians. For this particular transition, $|\Psi(0)\rangle = |\phi_1(0)\rangle$ and the ideal target state is (up to a global phase factor) $|\Psi(t_f)\rangle = |\phi_1(t_f)\rangle$.

The dynamics versus time τ is shown in Fig. 2.2 for $\tau_f = 2$. For this short time $H_0(t)$ fails to drive the populations to 1/2 and 1/4, whereas when $H_{cd}(t)$ is added the intended transition occurs successfully. As for the alternative Hamiltonian in Eq. (2.30), with $B = e^{-i\alpha G_4}$, and α in Eq. (2.29), we find

$$\begin{aligned} &B(t_f) = 1, \\ &\dot{B}(0) = \dot{B}(t_f) = 0 \end{aligned} \tag{2.36}$$

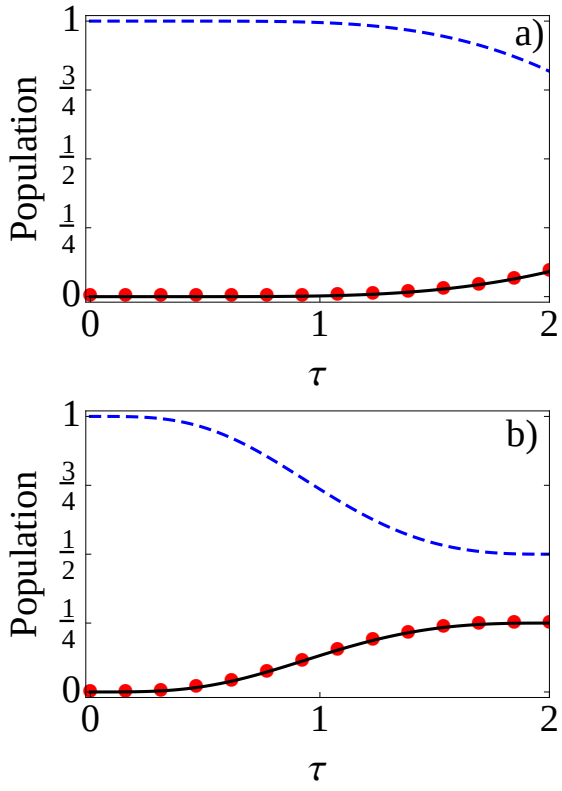

FIGURE 2.2: Bare-state populations for (a) $H_0(t)$; (b) $H(t)$ and $H_I(t)$. $|c_1(t)|^2$ (red circles), $|c_2(t)|^2$ (short-dashed blue line) and $|c_3(t)|^2$ (solid black line). Parameters: $\tau = E_0^{max}t/\hbar$ with E_0^{max} the maximum value of $E_0(t)$, $\tau_f = 2$.

[Eq. (2.34) is necessary to have $\dot{\alpha}(t_f) = 0$ and consequently $\dot{B}(t_f) = 0$], whereas

$$B(0) = \begin{pmatrix} e^{-i\pi/2} & 0 & 0 \\ 0 & 1 & 0 \\ 0 & 0 & e^{-i\pi/2} \end{pmatrix} \neq 1. \tag{2.37}$$

However $B^\dagger(0)|1,1\rangle = |1,1\rangle$ so $\psi^I(0) = \psi(0)$ and H_I provides the desired shortcut.

Solving numerically the dynamics for $H_I(t)$ we obtain a perfect insulator-superfluid transition [see Fig. 2.2(b)]. Notice that, as G_4 is diagonal in the bare basis, the bare populations are the same for the dynamics driven by H and H_I; see Fig. 2.2(b).

In order to compare our approach with other protocols we reformulate H_I as

$$H_I = \begin{pmatrix} U^I & -\sqrt{2}J^I & 0 \\ -\sqrt{2}J^I & 0 & -\sqrt{2}J^I \\ 0 & -\sqrt{2}J^I & U^I \end{pmatrix} = U^I G_4 - 4J^I G_1. \tag{2.38}$$

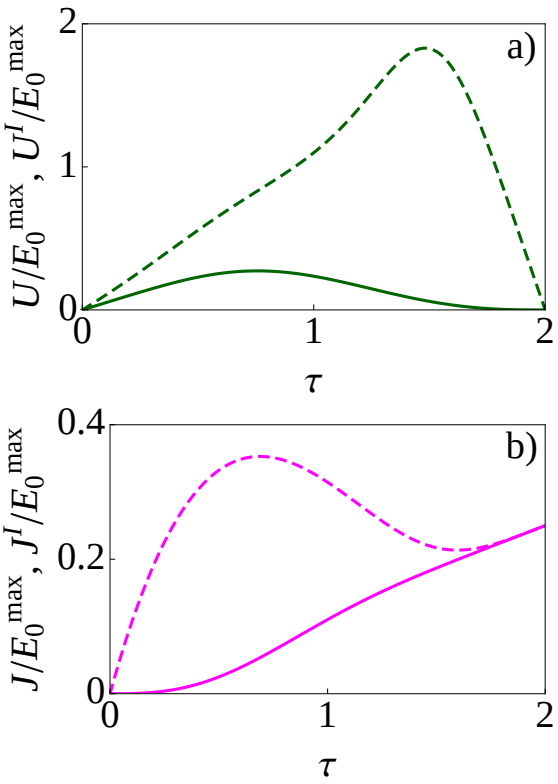

FIGURE 2.3: (a) Interaction energy for the reference Hamiltonian H_0 (solid green line) and for H_I (short-dashed green line). (b) Hopping energy for H_0 (solid magenta line) and H_I (short-dashed magenta line). The same parameters as in Fig. 2.1.

Comparing Eqs. (2.38) and (2.30) we find that

$$\begin{aligned} U^I &= \frac{1}{(E_0)^2 \sin^2\varphi + \hbar^2(\dot{\varphi})^2} \left\{ \cos\varphi (E_0)^3 \sin^2\varphi \right. \\ &+ \left. \hbar^2 \sin\varphi \dot{E}_0 \dot{\varphi} + \hbar^2 E_0 \left[2\cos\varphi(\dot{\varphi})^2 - \sin\varphi\ddot{\varphi} \right] \right\}, \\ J^I &= \frac{1}{4} E_0 \sin\varphi \sqrt{1 + \frac{\hbar^2 \csc^2\varphi (\dot{\varphi})^2}{(E_0)^2}}. \end{aligned} \tag{2.39}$$

Figure 2.3 shows the functions U_I and J_I. We have set $H_I(t_b) = H_0(t_b)$, for $t_b = 0, t_f$, since $H_{cd}(t_b) = 0$ and $\dot{B}(t_b) = 0$. In the same way as Eq. (2.6) we can rewrite the above energies as

$$\begin{aligned} U^I &= E_0^I \cos\varphi^I, \\ J^I &= \frac{E_0^I}{4} \sin\varphi^I, \end{aligned} \tag{2.40}$$

where $E_0^I = E_0^I(t)$ and $\varphi^I = \varphi^I(t)$. The inverse transformation is

$$\begin{aligned} \varphi^I &= \arctan\left(4\frac{J^I}{U^I}\right), \\ E_0^I &= \frac{U^I}{\cos\varphi'}. \end{aligned} \tag{2.41}$$

Consider a simple protocol with $E_0(t) = E_0^M(t) = const$ and a linear $\varphi^M(t)$ from 0 and $\pi/2$ [45]. Setting the value of E_0^M so that $\int E_0^M dt = \int E_0^I dt$, it is found that the simple protocol needs $\tau_f = 18.8$ to perform the transition with a 0.9999 fidelity. In other words, the protocol based on H_I is 9.4 times faster according to this criterion.

2.6 Beam splitters

The three-level Hamiltonian (2.2) describes other physical systems apart from two bosons in two wells. For example, it represents in the paraxial approximation, and substituting time by a longitudinal coordinate three coupled waveguides [46–51], where J is controlled by waveguide separation and U by the refractive index. In particular J and U may be manipulated to split an incoming wave in the central waveguide into two output channels (corresponding to the external waveguides) or three output chanels [50, 51]. The Hamiltonian also represents a single particle in a triple well [57], where U plays the role of the bias of the outer wells with respect to the central one and, J the coupling coefficient between adjacent wells. The beam splitting may thus depict the evolution of the particle wave function from the central well either to the two outer wells or to three of them with equal probabilities.

For three-well or three-waveguide systems[1] the minimal channel basis for left, center and right wave functions is $|L\rangle = \begin{pmatrix} 1 \\ 0 \\ 0 \end{pmatrix}$, $|C\rangle = \begin{pmatrix} 0 \\ 1 \\ 0 \end{pmatrix}$, and $|R\rangle = \begin{pmatrix} 0 \\ 0 \\ 1 \end{pmatrix}$.

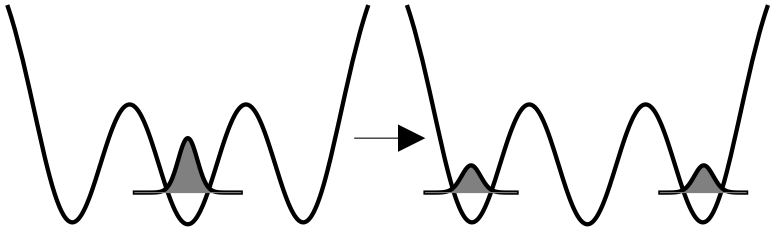

FIGURE 2.4: Schematic representation of a $1:2$ beam splitter.

2.6.1 1:2 beam splitter

To implement a $1:2$ beam splitter (see Fig. 4.3), the goal is to drive the eigenstate from $|\phi_1(0)\rangle = |C\rangle$ to $|\phi_1(t_f) = \frac{1}{\sqrt{2}}(|L\rangle + |R\rangle)$. As in the previous section we use polynomial functions for $E_0(t)$ and $\varphi(t)$ to set a reference process. We impose

$$\begin{aligned} \varphi(0) &= 0, \\ \varphi(t_f) &= \pi \end{aligned} \tag{2.42}$$

in Eq. (2.11). The wells (waveguides) should be isolated at initial and final times. If morever all wells are at equal heights at those times we set

$$\begin{aligned} E_0(0) = E_0(t_f) &= 0, \\ E(t_f/2) &\neq 0 \end{aligned} \tag{2.43}$$

to satisfy $H_0(0) = H_0(t_f) = 0$. We also impose

$$\begin{aligned} \dot{\varphi}(0) &= 0, \\ \dot{\varphi}(t_f) &= \pi \end{aligned} \tag{2.44}$$

to smooth the functions at the time boundaries and make $H_{cd}(t_b) = 0$. In addition

$$\ddot{\varphi}(t_f) = 0 \tag{2.45}$$

is imposed to satisfy $\dot{B}(t_f) = 0$. At intermediate times $E_0(t) = \sum_{j=0}^{2} a_j t^j$ and $\varphi(t) = \sum_{j=0}^{4} b_j t^j$, with the coefficients deduced from Eqs. (2.42), (2.43), (2.44) and (2.45). These functions are shown in Fig. 2.5.

[1] The Hamiltonian (2.2) also describes a three-level atom under appropriate laser interactions; see [49].

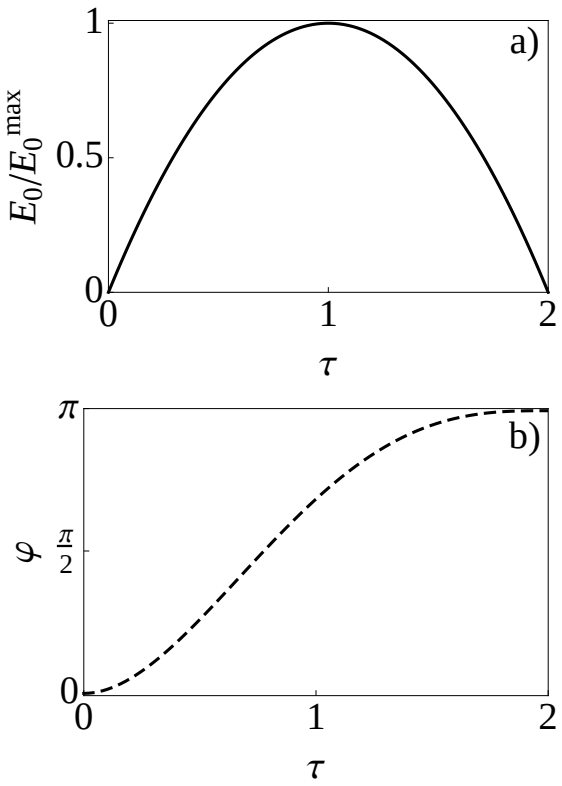

FIGURE 2.5: (a) $E_0(t)$ and (b) $\varphi(t)$. $\tau = E_0^{max}t/\hbar$ where E_0^{max} is the maximum value of $E_0(t)$. $\tau_f = 2$.

Figure 2.6 shows the dynamics for $\tau_f = 2$. This time (corresponding to the splitter length in the optical system) is too short for the reference Hamiltonian $H_0(t)$ to drive the bare-basis populations to 0 and 1/2. On adding $H_{cd}(t)$ the transition occurs as desired. As in Sec. 2.4, we construct an alternative shortcut $H_I(t)$ without G_2 using the transformation $B = e^{-i\alpha G_4}$. With α in Eq. (2.29), $\dot{B}(0) = \dot{B}(t_f) = 0$, whereas

$$B(0) = B(t_f) = \begin{pmatrix} e^{-i\pi/2} & 0 & 0 \\ 0 & 1 & 0 \\ 0 & 0 & e^{-i\pi/2} \end{pmatrix}. \tag{2.46}$$

This is enough for our objective as $B^\dagger(0)|C\rangle = |C\rangle$, and $B^\dagger(t_f)|\psi(t_f)\rangle = -i|\psi(t_f)\rangle$.

Solving numerically the dynamics for $H_I(t)$ we obtain a perfect $1:2$ beam splitting [see Figs. 2.7 and 2.6(c)].

To compare the new shortcut and the simple approach with $E_0^M = const$ and $\varphi^M(t) = \frac{t}{t_f}\pi$, we set $\int E_0^M dt = \int E_0^I dt$. The constant-$E_0$ protocol needs $\tau_f \geqslant 18.6$

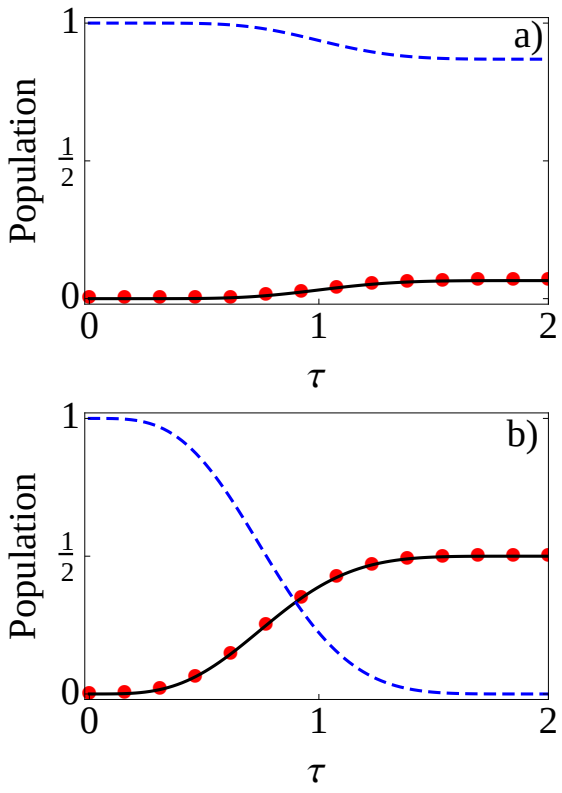

FIGURE 2.6: Bare-state populations for (a) $H_0(t)$, and (b) $H(t)$ and $H_I(t)$. $|c_1(t)|^2$ (red circles), $|c_2(t)|^2$ (short-dashed blue line) and $|c_3(t)|^2$ (solid black line). Parameters: $\tau = E_0^{max}t/\hbar$ with E_0^{max} the maximum value of $E_0(t)$, and $\tau_f = 2$.

to achieve 0.9999 fidelity, so the protocol driven by H_I is 9.3 times faster.

2.6.2 1:3 beam splitter

We also describe briefly a $1:3$ beam splitter; see Figs. 2.8-2.11. The aim is to drive the system from $|\phi_1(0)\rangle = |C\rangle$ to equal populations in $|L\rangle$, $|C\rangle$, and $|R\rangle$. To design a reference protocol we use polynomial interpolation for $E_0(t)$ and $\varphi(t)$ (see Fig. 2.9), with the same boundary conditions as for the $1:2$ splitter but with $\varphi(t_f) = 0.60817\pi = \arccos(-1/3)$ and the additional condition $\dot{E}_0(t_f) = 0$ [to satisfy $U^I(t_f) = U(t_f)$ so that $H_I(t_f) = H_0(t_f)$]. The Lie transform may be applied as before on the protocol with the counterdiabatic correction; see Fig. 2.10(b).

A simple protocol with E_0^M and $\varphi(t) = \frac{t}{t_f}0.60817\pi$ needs $\tau_f = 22$, if $\int E_0^M dt = \int E_0^I dt$, for a 0.9999 fidelity, so the protocol based on H_I is 11 times faster.

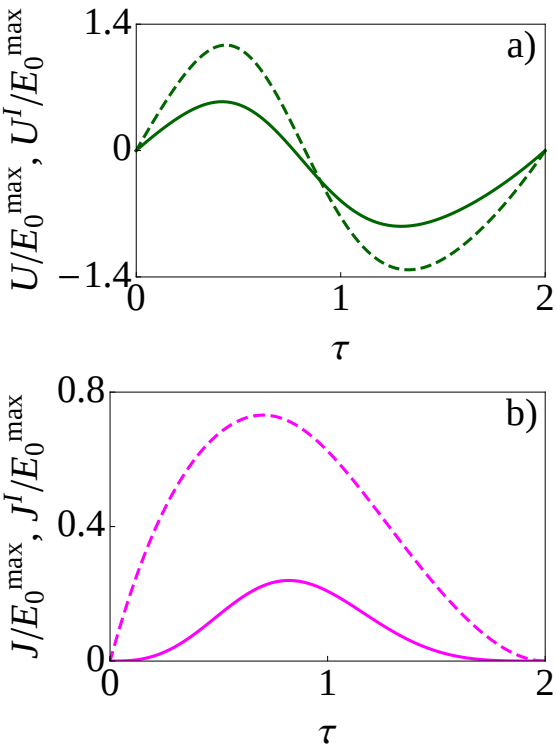

FIGURE 2.7: (a) Interaction energy for H_0 (solid green line) and H_I (short-dashed green line). (b) Hopping energy for H_0 (solid magenta line) and H_I (short-dashed magenta line). The same parameters as in Fig. 2.5.

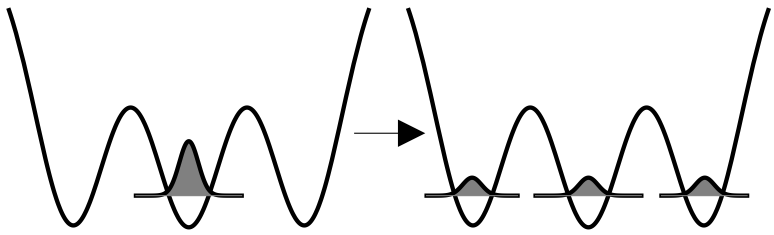

FIGURE 2.8: Schematic representation of the $1:3$ beam splitter.

2.7 Discussion

We started with shortcuts to adiabaticity for three-level systems with U3S3 symmetry (a four-dimensional Lie algebra) that include Hamiltonian terms which are difficult to implement in the laboratory. Alternative shortcuts without them have then been found by means of Lie transforms. These transformations are formally equivalent to IP transformations. However the resulting IP Hamiltonian and state represent a different physical process from the original (Schrödinger) Hamiltonian and dynamics. We have set shortcuts for different physical systems. For

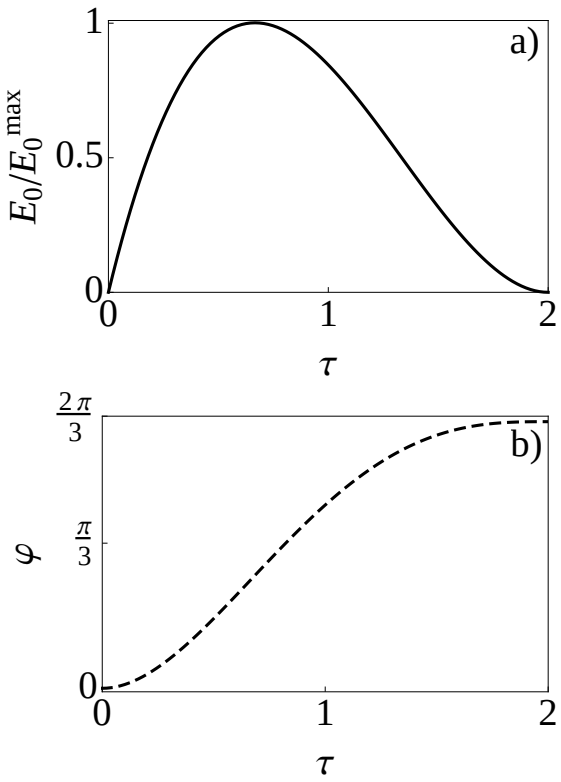

FIGURE 2.9: (a) $E_0(t)$ and (b) $\varphi(t)$. $\tau = E_0^{max}t/\hbar$, where E_0^{max} is the maximum value of $E_0(t)$. $\tau_f = 2$.

two particles in two wells we have implemented a fast insulator-superfluid transition. For coupled waveguides, or a particle in a triple well we have implemented fast beam splitting with one input channel and two or three output channels. In all cases the IP Hamiltonian involves only two realizable terms (generators).

A related method has been worked out in [58]. Both approaches rely on Lie algebraic methods and aim at constructing shortcuts to adiabaticity. However, we do not use dynamical invariants explicitly in the current approach, whereas the bottom-up approach in [58] engineers the Hamiltonian by making explicit use of its relation to dynamical invariants. In contrast, we start here from an existing, known shortcut –for example the one generated by a counterdiabatic method; then, a Lie transform is applied to generate alternative, feasible, or more convenient shortcuts, as in [33]. A connection between the transformation method and dynamical invariants is sketched briefly in the Appendix B but it deserves a separate study. We note that the dynamics of all our examples takes place in a degenerate eigenspace of an algebraic invariant which is not proportional to the unit matrix and commutes with all members of the algebra. The degeneracy is required to produce nontrivial dynamics, so identifying degenerate subspaces of

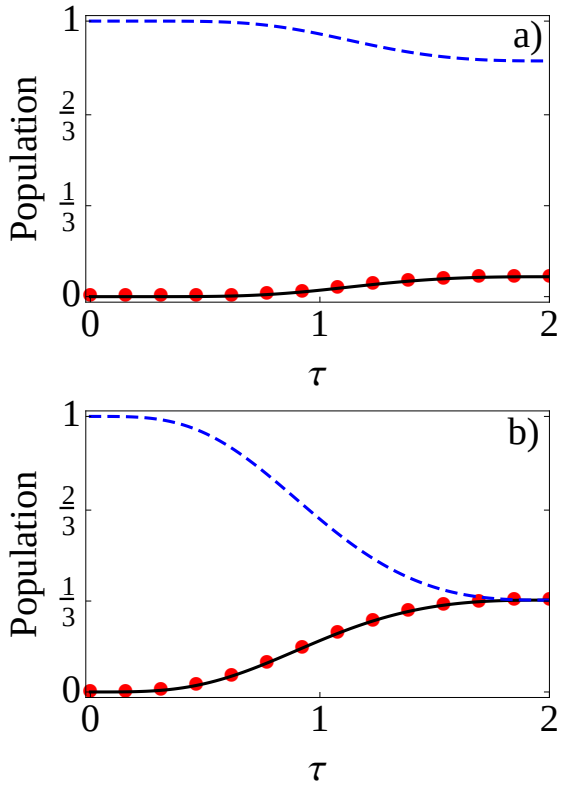

FIGURE 2.10: Bare-state populations for (a) $H_0(t)$, and (b) $H(t)$ and $H_I(t)$. $|c_1(t)|^2$ (red circles), $|c_2(t)|^2$ (short-dashed blue line) and $|c_3(t)|^2$ (solid black line). Parameters: $\tau = E_0^{max}t/\hbar$ with E_0^{max} the maximum value of $E_0(t)$, and $\tau_f = 2$.

nontrivial invariants, as well as the conditions allowing the cancellation of certain generators will be instrumental in finding further applications in systems described by other Lie algebras.

Optimal control theory (OCT) offers an alternative way to generate fast dynamics [59, 60]. In this chapter no optimization has been attempted, but the combination of shortcut-to-adiabaticity techniques offering multiple exact protocols with perfect fidelity, such as the one based on Lie transforms, and OCT, has been shown to be fruitful [61–63]. OCT may select among the protocols generated the ones that optimize a physically significant variable [61–63].

Within the scope of the algebra U3S3, other physical systems that could be treated are in quantum optics (three-level atoms) [64, 65], nanostructures (triple wells or dots) [66], optics (mode converters) [40, 41], or Bose-Einstein condensates in an accelerated optical lattice [67].

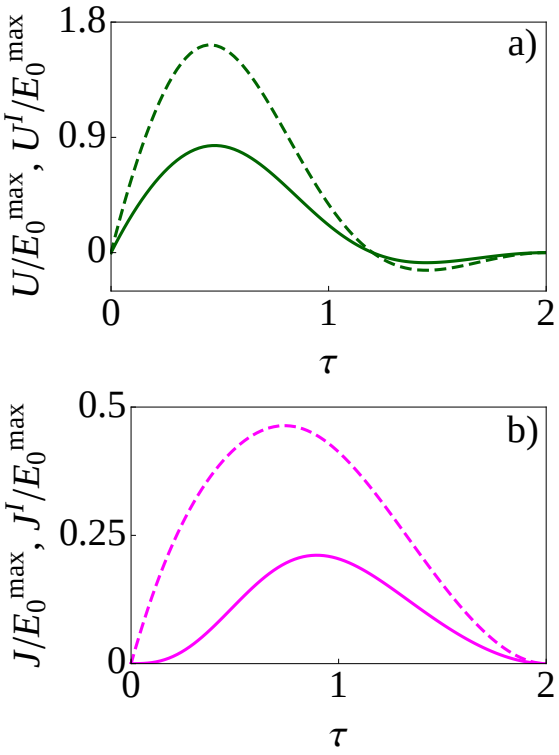

FIGURE 2.11: (a) Interaction energy for H_0 (solid green line) and H_I (short-dashed green line). (b) Hopping energy for H_0 (solid magenta line) and H_I (short-dashed magenta line). The same parameters as in Fig. 2.9

Chapter 3

Fast quasi-adiabatic dynamics

We work out the theory and applications of a fast quasi-adiabatic approach to speed up slow adiabatic manipulations of quantum systems by driving a control parameter as near to the adiabatic limit as possible over the entire protocol duration. We find characteristic time scales, such as the minimal time to achieve fidelity 1, and the optimality of the approach within the iterative superadiabatic sequence. Specifically, we show that the population inversion in a two-level system, the splitting and cotunneling of two-interacting bosons, and the stirring of a Tonks-Girardeau gas on a ring to achieve mesoscopic superpositions of many-body rotating and nonrotating states can be significantly speeded up.

3.1 Introduction

Developing technologies based on delicate quantum coherences of atomic systems is a major scientific and technical challenge due to pervasive noise-induced and manipulation errors. Shortening the process below characteristic decoherence times provides a way out to avoid the effects of noise, but the protocol (time dependence of control parameters) should still be robust with respect to offsets of the external driving parameters. Shortcuts to adiabaticity (STA) are a set of techniques to reduce the duration of slow adiabatic processes, minimizing noise effects while keeping or enhancing robustness [1, 8, 68]. There are different approaches but, as we have already discussed in the previous chapter, they are not always easy to implement in practice, because of the need to control many variables, or the difficulty to realize certain terms added to the original Hamiltonian to speed up the adiabatic dynamics. Here we work out the theory and present several applications of a simple, but effective, fast quasi-adiabatic (FAQUAD) approach that engineers the time dependence of a single control parameter $\lambda(t)$, without changing the structure of the original Hamiltonian, $H[\lambda(t)]$, to perform a process as quickly as possible while making it as adiabatic as possible at all times. The two goals are contradictory so a compromise is needed.

3.2 The method

We impose that the standard adiabaticity parameter [69] is constant throughout the process, and consistent with the boundary conditions (BC) of $\lambda(t)$ at $t = 0$ and $t = t_f$.

In the simplest scenario we assume that the adiabatic process driven by changing $\lambda(t)$ involves a passage through at least one avoided crossing. While real systems are in general multilevel, only the two quasicrossing levels (say E_1, E_2) in the instantaneous basis $\{|\phi_j\rangle\}$ need to be considered under the adiabaticity condition [69],

$$\hbar \left| \frac{\langle \phi_1(t)|\partial_t \phi_2(t)\rangle}{E_1(t) - E_2(t)} \right| \ll 1. \tag{3.1}$$

(More levels can be taken into account if necessary.) We then impose

$$\hbar \left| \frac{\langle \phi_1(t)|\partial_t \phi_2(t)\rangle}{E_1(t)-E_2(t)} \right| = \hbar \left| \frac{\langle \phi_1(t)|\frac{\partial H}{\partial t}|\phi_2(t)\rangle}{[E_1(t)-E_2(t)]^2} \right| = c, \tag{3.2}$$

and as $\lambda = \lambda(t)$ and $t = t(\lambda)$ we apply the chain rule to write

$$\dot{\lambda} = \mp \frac{c}{\hbar} \left| \frac{E_1(\lambda)-E_2(\lambda)}{\langle \phi_1(\lambda)|\partial_\lambda \phi_2(\lambda)\rangle} \right| = \mp \frac{c}{\hbar} \left| \frac{[E_1(\lambda)-E_2(\lambda)]^2}{\langle \phi_1(\lambda)|\frac{\partial H}{\partial \lambda}|\phi_2(\lambda)\rangle} \right|, \tag{3.3}$$

where the overdot is a time derivative and $\mp$ applies to a monotonous decrease or increase of $\lambda(t)$. Equation (3.3) must be solved with the BC $\lambda(0)$ and $\lambda(t_f)$, which fixes c and the integration constant. The corresponding FAQUAD solution, $\lambda_F(t)$, changes quickly when the transitions among instantaneous eigenstates are unlikely and slowly otherwise. An equation equivalent to Eq. (3.3) has been applied to specific models [29, 70–74], for example, the two-level system [72] and three-level lambda systems [71].

In this chapter, we derive important properties of FAQUAD including characteristic time scales, such as the minimal time to achieve fidelity 1, and its optimality within the iterative superadiabatic sequence. We also apply FAQUAD to several physical systems for which other shortcut techniques are difficult or impossible to implement, including a process for creating a collective superposition state between rotating and nonrotating atoms on a ring.

The FAQUAD strategy belongs to a family of processes that use the time dependence of a control parameter to delocalize in time the transition probability among adiabatic levels. In the parallel adiabatic transfer technique [75, 76] the level gap is required to be constant, which prevents it from being applicable when the initial and final gaps are different [see the Tonks-Girardeau (TG) gas example below]. The uniform adiabatic (UA) method developed in [77] relies on a comparison of *transition* and *relaxation* time scales and predicts (in a notation consistent with the one used in the work)

$$\dot{\lambda} = \mp \frac{c_{UA}}{\hbar} \left| \frac{[E_1(\lambda)-E_2(\lambda)]^2}{\partial [E_1(\lambda)-E_2(\lambda)]/\partial \lambda} \right|. \tag{3.4}$$

Furthermore, the local adiabaticity (LA) approach [78, 79] predicts an equation similar to Eq. (3.3), however without the factor $\langle \phi_1(\lambda)|\frac{\partial H}{\partial \lambda}|\phi_2(\lambda)\rangle$. This leads to a different constant, c_{LA}, and time dependence of the parameter, $\lambda_{LA}(t)$, and

therefore different minimal times as illustrated below. Note that in [78] Eq. (3.3) is also written down but not applied as such.

3.2.1 General Properties

We rewrite Eq. (3.3) in terms of $s = t/t_f$ and define $\tilde{\lambda}(s) := \lambda(st_f)$ so that

$$\dot{\lambda}(t) = \tilde{\lambda}' \frac{1}{t_f}, \tag{3.5}$$

where the prime is the derivative with respect to s. We get

$$\tilde{\lambda}' = \mp \frac{\tilde{c}}{\hbar} \left| \frac{E_1 - E_2}{\langle \phi_1 | \partial_{\tilde{\lambda}} \phi_2 \rangle} \right|_{\tilde{\lambda}}, \tag{3.6}$$

with

$$\tilde{c} = ct_f = \mp\hbar \int_{\tilde{\lambda}(0)}^{\tilde{\lambda}(1)} \frac{d\tilde{\lambda}}{\left| \frac{E_1 - E_2}{\langle \phi_1 | \partial_{\tilde{\lambda}} \phi_2 \rangle} \right|_{\tilde{\lambda}}}. \tag{3.7}$$

It is thus enough to solve the FAQUAD protocol once, i.e., using Eq. (3.6) we get $\tilde{\lambda}_F(s)$ and $\tilde{c}$ to satisfy $\tilde{\lambda}(s=0)$ and $\tilde{\lambda}(s=1)$, and then adapt (scale) the result for each t_f, as $\lambda_F(t = st_f) = \tilde{\lambda}_F(s)$, and $c = \tilde{c}/t_f$. Similarly, the gap

$$\omega_{12}(t) = \frac{E_1(t) - E_2(t)}{\hbar} \tag{3.8}$$

is given in terms of a universal gap function $\tilde{\omega}_{12}[\tilde{\lambda}_F(s)]$ as $\omega_{12}(t) = \tilde{\omega}_{12}[\tilde{\lambda}_F(t/t_f)]$. Depending on $\tilde{c}$, a large time t_f might be necessary to make the process fully adiabatic (i.e., with a small enough c) but, surprisingly, much shorter times for which the process is not fully adiabatic also lead to the desired results.

Since the system is nearly adiabatic, this is explained by adiabatic perturbation theory. In the adiabatic basis the wave function is expanded as [69, 80]

$$|\Psi(t)\rangle = \sum_n g_n(t) e^{i\beta_n(t)} |\phi_n(t)\rangle, \tag{3.9}$$

where

$$\beta_n(t) = -\frac{1}{\hbar} \int_0^t E_n(t')dt' + i \int_0^t \langle \phi_n(t') | \dot{\phi}_n(t') \rangle dt'. \tag{3.10}$$

From

$$i\hbar |\dot{\Psi}(t)\rangle = H(t) |\Psi(t)\rangle \tag{3.11}$$

we get, choosing $\langle\phi_n(t)|\dot{\phi}_k(t)\rangle$ to be real (in particular $\langle\phi_n(t)|\dot{\phi}_n(t)\rangle = 0$),

$$\dot{g}_n(t) = -\sum_{k\neq n} e^{iW_{nk}(t)}\langle\phi_n(t)|\dot{\phi}_k(t)\rangle g_k(t), \tag{3.12}$$

where

$$W_{nk}(t) = \int_0^t \omega_{nk}(t')dt' \tag{3.13}$$

is a dynamical-gap phase and

$$\omega_{nk}(t) \coloneqq \frac{E_n(t) - E_k(t)}{\hbar}. \tag{3.14}$$

Integrating,

$$g_n(t) - g_n(0) = -\sum_{k\neq n}\int_0^t e^{iW_{nk}(t')}\langle\phi_n(t')|\dot{\phi}_k(t')\rangle g_k(t')dt', \tag{3.15}$$

which is still exact. Assuming that the initial state is $|\phi_m(0)\rangle$ and approximating $g_k(t') = \delta_{km}$ one finds to first order, for $n \neq m$,

$$g_n^{(1)}(t) = -\int_0^t \langle\phi_n(t')|\dot{\phi}_m(t')\rangle e^{iW_{nm}(t')}dt', \tag{3.16}$$

which should satisfy $|g_n(t)| \ll 1$ for an adiabatic evolution. In FAQUAD, setting $n = 2$, $m = 1$ and neglecting transitions to further states, $\langle\phi_2(t)|\dot{\phi}_1(t)\rangle = cr\omega_{21}(t)$, with $r = \mathrm{sgn}[\langle\phi_2(t)|\dot{\phi}_1(t)\rangle\omega_{21}]$, so we find (higher-order corrections are also explicit)

$$g_2^{(1)}(t) = -r\int_0^t c\omega_{21}(t')e^{iW_{21}(t')}dt' = icr(e^{iW_{21}(t)} - 1). \tag{3.17}$$

Note the scaling $W_{21}(t_f) = t_f\Phi_{21}$ where $\Phi_{21} = \int_0^1 \tilde{\omega}_{21}(s)ds$, and $\tilde{\omega}_{21}(s) = \omega_{21}(st_f)$. The oscillation period for the final population with FAQUAD is $T = \frac{2\pi}{\Phi_{12}}$, which is also a good estimate of the minimal (final) time to pass through the avoided crossing with fidelity 1 [since $g_2^{(1)}(T) = 0$]. The upper envelope for the probability of level 2 is $4\tilde{c}^2/t_f^2$. The period, envelope, and Eq. (3.17) are important general results of this work. The oscillation is due to a quantum interference: $g_2^{(1)}(t_f)$ results from the sum of paths where the jump at time t' from 1 to 2 has an amplitude $c\omega_{21}(t')$. $e^{iW_{21}(t')}$ represents the dynamical phases before and after the jump, as

$$e^{iW_{21}(t')} = e^{\frac{-i}{\hbar}\int_0^{t'} dt'' E_2(t'')}e^{\frac{-i}{\hbar}\int_{t'}^{t_f} dt'' E_2(t'')}e^{\frac{i}{\hbar}\int_0^{t_f} dt'' E_2(t'')}, \tag{3.18}$$

where the last exponential is a phase factor independent of t'.

To illustrate these general properties, we will first examine the two-level model, a paradigmatic test bed. Then, to show the power of FAQUAD, we will apply it to more complicated atomic systems.

3.3 Population inversion

Consider first a two-mode model with a single avoided crossing. In the bare basis, $|1\rangle = \begin{pmatrix} 1 \\ 0 \end{pmatrix}$ and $|2\rangle = \begin{pmatrix} 0 \\ 1 \end{pmatrix}$, the time-dependent state is $|\Psi(t)\rangle = b_1(t)|1\rangle + b_2(t)|2\rangle$ and

$$H = \begin{pmatrix} 0 & -\sqrt{2}J \\ -\sqrt{2}J & U-\Delta \end{pmatrix}, \tag{3.19}$$

where the bias $\Delta = \Delta(t)$ is the control parameter, and $U > 0$ and $J > 0$ are constant. The instantaneous eigenvalues are

$$E_1 = \frac{1}{2}(U - \Delta - P), \tag{3.20}$$

$$E_2 = \frac{1}{2}(U - \Delta + P), \tag{3.21}$$

where $P = P(t) = \sqrt{8J^2 + U^2 - 2U\Delta(t) + \Delta^2(t)}$, and the normalized eigenstates are

$$|\phi_1\rangle = \frac{1}{\sqrt{1 + \frac{(U-\Delta+P)^2}{8J^2}}} \begin{pmatrix} \frac{1}{2\sqrt{2}J}(U - \Delta + P) \\ 1 \end{pmatrix}, \tag{3.22}$$

$$|\phi_2\rangle = \frac{1}{\sqrt{1 + \frac{(U-\Delta-P)^2}{8J^2}}} \begin{pmatrix} \frac{1}{2\sqrt{2}J}(U - \Delta - P) \\ 1 \end{pmatrix}. \tag{3.23}$$

The goal is to drive the eigenstate from $|\phi_1(0)\rangle = |2\rangle$ to $|\phi_1(t_f)\rangle = |1\rangle$. To design the reference adiabatic protocol we impose on $\Delta(t)$ the BC $\Delta(0) \gg U, J$ and $\Delta(t_f) = 0$. The FAQUAD protocol is shown in Fig. 3.1(a) compared to a linear-in-time $\Delta(t)$ and a constant $\Delta = U$. The final ground-state populations $|b_1(t_f)|^2$ versus dimensionless final time $\tau_f = Jt_f/\hbar$ are shown in Fig. 3.1(b). Since the dressed states are essentially pure bare states at initial and final times, their populations in bare and dressed state bases coincide at these times. For

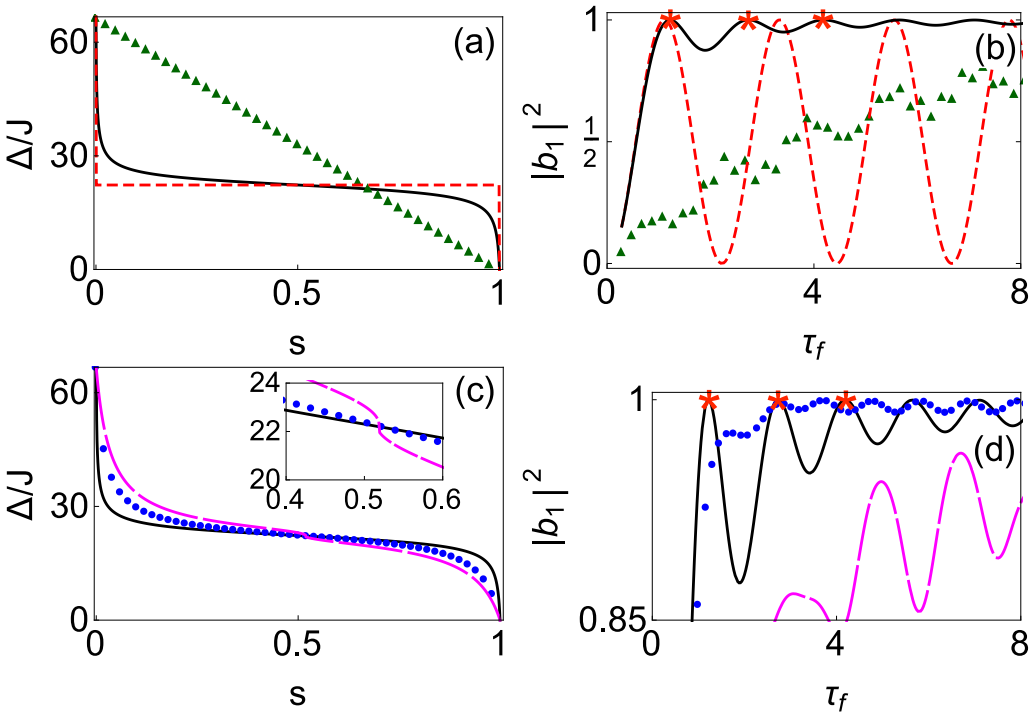

FIGURE 3.1: (a) Bias vs s for linear-in-time bias (green triangles), π pulse (short-dashed red line), and FAQUAD (solid black line). (b) Final ground-state population $|b_1(t_f)|^2$ vs $\tau_f = Jt_f/\hbar$ for linear-in-time bias (green triangles), π pulse (short-dashed red line), and FAQUAD (solid black line). (c) Bias vs s for FAQUAD (solid black line), LA approach (blue dots), and UA approach (long-dashed magenta line). The inset amplifies the kink of the UA approach. (d) $|b_1(t_f)|^2$ vs $\tau_f = Jt_f/\hbar$ for FAQUAD (solid black line), LA approach (blue dots), and UA approach (long-dashed magenta line). The stars in (b) and (d) correspond to integer multiples of the characteristic FAQUAD time scale $2\pi/\Phi_{12}$. $\Delta(0)/J = 66.7$, $U/J = 22.3$.

$\Delta = U$ between 0 and t_f, "Rabi oscillations" (we use a terminology appropriate for quantum optics but of course the two-level model is more broadly applicable) occur [see Fig. 3.1(b)]. The conditions for a π pulse or multiple π pulses are met periodically over t_f, alternated with times where the probability drops to zero because of destructive interference among two dressed states superposed with equal weights. By contrast the FAQUAD process is dominated by one dressed state and the influence of the transitions to the other one is minimized, because they are small in amplitude, and because at certain times they completely cancel each other out by destructive interference. The time interval between population maxima for FAQUAD is $2\pi/\Phi_{1,2}$ [also shown in Figs. 3.1(b) and 3.1(d) by stars], i.e., it is not governed by the Rabi frequency. The first maximum is at a small t_f similar to the one for the π pulse, but broader. The FAQUAD maxima are more stable with respect to errors in Δ as t_f increases, whereas the flat-pulse maxima

decrease their stability. Figure 3.1(b) also shows the poorer results of the linear ramp for $\Delta(t)$.

FAQUAD is compared to the LA and UA approaches in Figs. 3.1(c) and 3.1(d). It provides shortcuts at smaller process times (it achieves 0.9998 probability three times faster than LA) and an analytically predictable behavior via the perturbation theory analysis. Let us now consider more complicated atomic systems where FAQUAD can be applied whereas other STA techniques cannot.

3.4 Interacting bosons in a double well

Pairs of interacting bosons in a double-well potential may be manipulated to implement universal quantum logic gates for quantum computation or to observe fundamental phenomena such as cotunneling of two atoms [81, 82]. We shall speed up two processes: the splitting of the two particles from one to the two separate wells, and cotunneling (see Fig. 3.2). The boson dynamics in a double well with tight lateral confinement is described by a two-site Bose-Hubbard Hamiltonian[1] [82]. The Hamiltonian in the occupation number basis $|2,0\rangle = \begin{pmatrix} 1 \\ 0 \\ 0 \end{pmatrix}$, $|1,1\rangle = \begin{pmatrix} 0 \\ 1 \\ 0 \end{pmatrix}$, and $|0,2\rangle = \begin{pmatrix} 0 \\ 0 \\ 1 \end{pmatrix}$ is

$$H = \begin{pmatrix} U+\Delta & -\sqrt{2}J & 0 \\ -\sqrt{2}J & 0 & -\sqrt{2}J \\ 0 & -\sqrt{2}J & U-\Delta \end{pmatrix}, \tag{3.24}$$

where the bias $\Delta = \Delta(t)$ is the control function, J is the hopping energy, and U the interaction energy. We write the time-dependent states as $|\Psi(t)\rangle = c_1(t)|2,0\rangle + c_2(t)|1,1\rangle + c_3(t)|0,2\rangle$. Adiabatic processes that change $\Delta(t)$ slowly, keeping the U/J ratio constant, are possible to implement splitting or cotunelling. Speeding them up by a "counterdiabatic" approach is not possible in practice because of the need to apply new terms in the Hamiltonian which are difficult to implement. Alternative techniques, like the one introduced in Chapter 2, could not be applied [45] or are cumbersome [58, 83] because of the relatively large algebra involved. The FAQUAD approach provides a viable way out.

[1] This Hamiltonian is similar to the one in the previous chapter [Eq.(2.2)] but we add two diagonal terms that make the potential asymmetric.

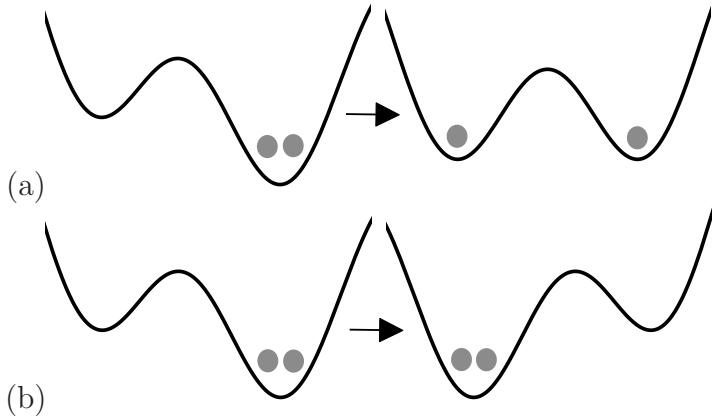

FIGURE 3.2: (a) Schematic representation of splitting from $|0,2\rangle$ to $|1,1\rangle$. (b) Cotunneling from $|0,2\rangle$ to $|2,0\rangle$.

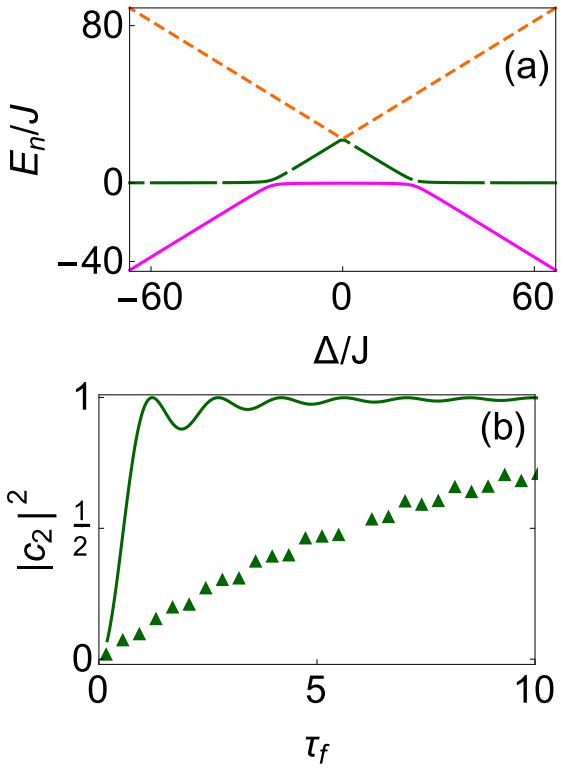

FIGURE 3.3: (a) Energy levels vs Δ. For $n = 1, 2, 3$: E_1 (solid magenta line), E_2 (long-dashed green line), and E_3 (short-dashed orange line). $U/J = 22.3$. (b) $|c_2|^2$ vs τ_f for linear-in-time bias (green triangles) and FAQUAD (solid green line). $\Delta(0)/J = 100$, $U/J = 33.45$, and $\tau_f = Jt_f/\hbar$.

- In a splitting process $\Delta(0) \gg U, J$ and $\Delta(t_f) = 0$ [see Fig. 3.2(a)]. The initial ground state is $|\phi_1\rangle = |0,2\rangle$ and the final ground state $|\phi_1\rangle = |1,1\rangle$. Figure 3.3(a) shows the dependence of the three eigenenergies with Δ. $\Delta_F(t)$ is very similar to the result for the two-level system in Fig. 3.1(a). The results of FAQUAD and the linear protocol are compared in Fig. 3.3(b). The probability of the first peak

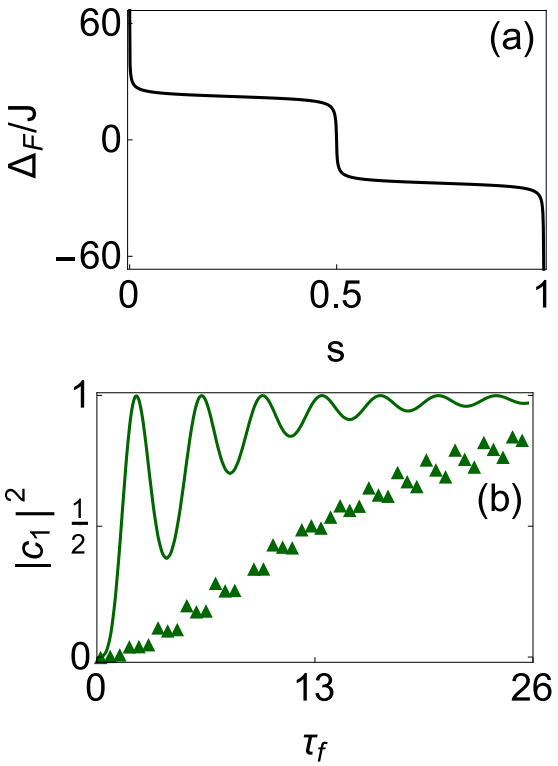

FIGURE 3.4: (a) Time dependence of the bias with FAQUAD. (b) $|c_1|^2$ vs τ_f for linear-in-time bias (green triangles) and FAQUAD (solid green line). $\Delta(0)/J = 66.7$, $U/J = 22.3$, and $\tau_f = Jt_f/\hbar$.

for FAQUAD, 0.998 at $\tau_f = 1.2$, is achieved with the linear ramp for $\tau_f = 43$.

- In a speeded-up cotunneling, shown in Fig. 3.2(b), the goal is to drive the system fast from $|\phi_1(0)\rangle = |0,2\rangle$ to $|\phi_1(t_f)\rangle = |2,0\rangle$ intermediated by $|1,1\rangle$ [the Hamiltonian (3.24) does not connect $|2,0\rangle$ and $|0,2\rangle$ directly]. We impose $\Delta(0) \gg U, J$ and $\Delta(t_f) = -\Delta(0)$ to have $|0,2\rangle$ and $|2,0\rangle$ as the ground states at initial and final times, respectively. The energy levels versus Δ are depicted in Fig. 3.3(a) for repulsive interaction ($U > 0$). Figure 3.4(a) shows the FAQUAD trajectory for $\Delta(t)$ for the repulsive strong-interaction regime, $U/J = 22.3$. Figure 3.4(b) depicts the final probabilities of the bare state $|2,0\rangle$ for FAQUAD and a linear protocol that needs about $\tau_f = 65$ to achieve the value of the first peak of the FAQUAD method ($|c_1|^2 = 0.998$ at $\tau_f = 2.3$). The minima in the FAQUAD probability go in this case below the lower envelope $1 - 4\tilde{c}^2/t_f^2$ predicted by perturbation theory. The reason is a leak through the narrow avoided crossing at $\Delta = 0$ from the second to the third energy level [see Fig. 3.3(a)]. The leak occurs at total process times in which the first avoided crossing produces a minimum of the ground-state probability.

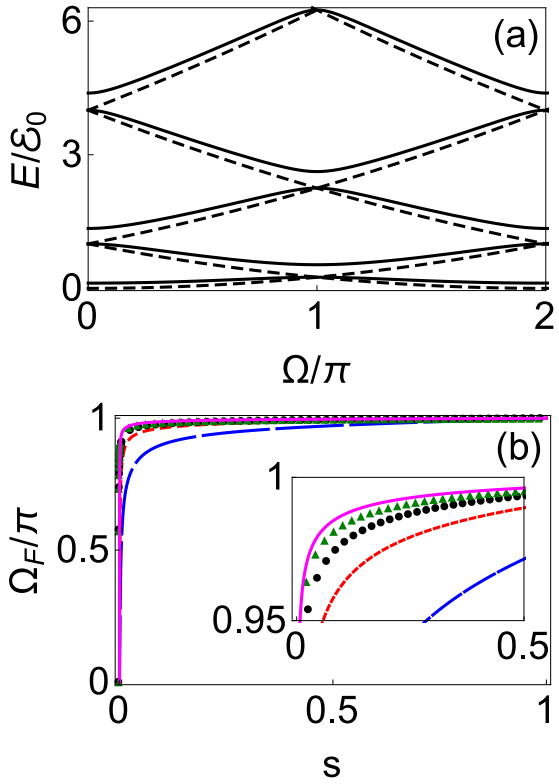

FIGURE 3.5: (a) Single-particle energy levels for $U_0 = 0$ (dashed lines) and $U_0ML/\hbar^2 = 4$ (solid lines) in units of $\mathcal{E}_0 = 2\pi^2\hbar^2/(ML^2)$. The ordering is $E_1(n = 0) < E_2(n = 1) < E_3(n = -1) < E_4(n = 2) < E_5(n = -2) < ....$ (b) $\Omega_F(s)$ for $N = 1, 3, 5, 7, 9$, from the bottom up to the top.

3.5 Collective superpositions of rotating and non-rotating atoms on a ring

Creating a macroscopic or mesoscopic superposition of a many-particle system is a difficult task and of interest for research in quantum information, quantum metrology and fundamental aspects of quantum mechanics. However, it was recently proposed that a low-dimensional gas of interacting bosons in the TG limit [84] placed on a ring can be perturbed in such a way, that a robust superposition of two angular momentum states can be achieved. This perturbation corresponds to the introduction of a narrow potential, which is then accelerated to a certain value to spin up the gas [85].

For a single particle this is described by

$$i\hbar\partial_t\psi(x,t) = \left\{ -\frac{\hbar^2}{2M}\frac{\partial^2}{\partial x^2} + U_0\delta[x - x_0(t)] \right\}\psi(x,t), \tag{3.25}$$

where the stirrer is represented by a δ function of strength U_0 and periodic BC are assumed. In a comoving frame one can then define $y = x - x_0(t)$ and the Hamiltonian is

$$H = \frac{1}{2M}\left[\hat{P}_y - \hbar\Omega(t)/L\right]^2 + U_0\delta(y), \tag{3.26}$$

where L is the ring perimeter, $\hbar\Omega(t) = M\dot{x}_0$ and $\hat{P}_y = -i\hbar\partial/\partial y$. The instantaneous energy eigenvalues are

$$E(n) = \frac{2\hbar^2\pi^2}{L^2M}\alpha_n^2, \tag{3.27}$$

and the α_n are solutions of

$$\frac{4\pi\hbar^2\alpha_n}{MLU_0} = \cot(\pi\alpha_n - \Omega/2) + \cot(\pi\alpha_n + \Omega/2). \tag{3.28}$$

For $U_0 \to 0$, the α_n tend to $n - \Omega/(2\pi)$, with $n = 0, \pm1, \pm2, \ldots$, where the different signs are for clockwise or counterclockwise rotation in the laboratory frame, and the nth eigenstates are plane waves with momentum $n\hbar 2\pi/L$. For $0 < \Omega < \pi$ the energies in the moving frame increase for $n \leqslant 0$ and decrease for $n > 0$. For $U_0 = 0$ the spectrum shows degeneracies at $\Omega = 0, \pi$, which turn into avoided crossings once the stirrer couples different angular momentum eigenstates, as shown in Fig. 3.5(a). Adiabatically increasing the stirring frequency from $\Omega = 0$ to π then, allows us to drive the system into a superposition of two angular momentum states, and for a TG gas with an odd number of particles N it can be shown that the ground state at $\Omega = \pi$ corresponds to macroscopic superposition between states with angular momentum zero and $N\hbar$.

To design an optimal $\Omega(t)$ for the TG gas, we note that the fidelity depends mostly on leakage from the highest occupied levels. This can be seen by considering the time evolved TG gas state $\Psi_{TG}(x_1, x_2, \ldots, x_N)$ defined by

$$\Psi_{TG} = \frac{1}{\sqrt{N!}}\prod_{i<j}\mathrm{sgn}(x_i - x_j)\sum_{\mu\in P}\epsilon_\mu\psi_{\mu_1}(x_1)\cdots\psi_{\mu_N}(x_N), \tag{3.29}$$

where P represents the set of all permutations of $\{0, 1, \ldots, N-1\}$, ϵ_μ is the antisymmetric tensor of the permutation μ, and ψ_i are the one-particle orbitals. Assuming that the system is isolated and contains only N eigenvectors ϕ_j, the orbitals can be expressed as $\psi_i = \sum_j U_{ij}\phi_j$ with U some unitary operator. If we now compare Ψ_{TG} to the ground state Φ_{TG} of the TG gas at the final Ω, we can

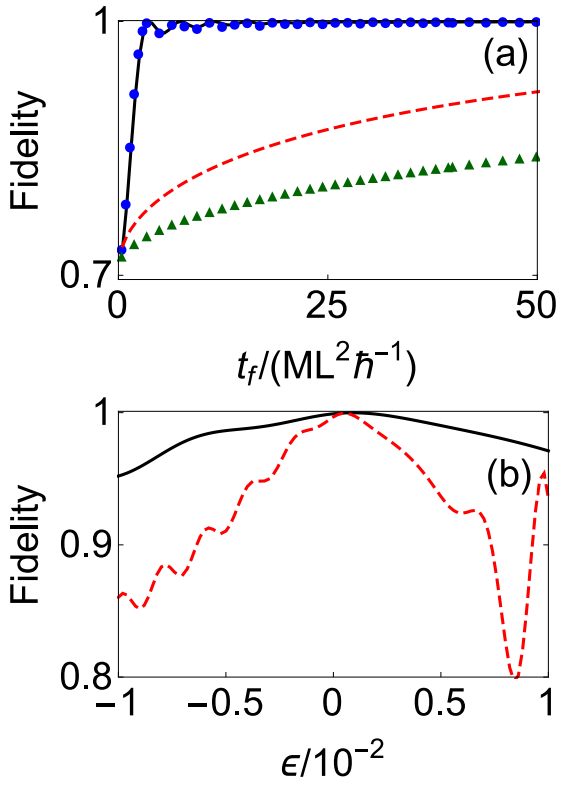

FIGURE 3.6: (a) Fidelity $|\langle\Psi_{TG}(t_f)|\Phi_{TG}\rangle|$ for $N = 3$ [FAQUAD (solid black line) and linear $\Omega(t)$ (short-dashed red line)] and $N = 9$ [FAQUAD (blue circles) and linear $\Omega(t)$ (green triangles)]. $\Psi_{TG}(t_f)$ is the time-evolved TG state starting from the ground state for $\Omega = 0$, and Φ_{TG} is the ground state of the TG gas at $\Omega = \pi$. (b) Fidelity $|\langle\Psi_{TG}(t_f)|\Phi_{TG}\rangle|$ vs ϵ if FAQUAD is applied following a *wrong* $\Omega_e(t) = \Omega_F(t)(1+\epsilon)$ for $N = 3$ (solid black line) and $N = 9$ (short-dashed red line). Here $U_0ML/\hbar^2 = 0.5$.

calculate the fidelity $F = |\langle\Phi_{TG}|\Psi_{TG}\rangle|$ as

$$\begin{aligned} F &= \frac{1}{N!}\left|\sum_{\nu,\mu}\epsilon_\nu\epsilon_\mu\langle\phi_{\nu_1}|\psi_{\mu_1}\rangle\cdots\langle\phi_{\nu_1}|\psi_{\mu_1}\rangle\right| \\ &= \frac{1}{N!}\left|\sum_{\nu,\mu}\epsilon_\nu\epsilon_\mu U_{\mu_1,\nu_1}\cdots U_{\mu_N,\nu_N}\right| \\ &= |\det(U)| = 1, \end{aligned} \tag{3.30}$$

since U is unitary. Of course, in reality the system we consider contains more than N eigenvectors and the fidelity does not remain 1, but this argument shows that leaking between two occupied states does not influence the fidelity of a TG gas at all; only leaks into modes above the Fermi level do, such as with nonzero mixing terms $U_{N,N+1}$. We should therefore optimize $\Omega_F(s)$ for the avoided crossing of the highest occupied level as shown in Fig. 3.5(b). The corresponding final-state

fidelities for $N = 3$ and 9 with respect to the exact ground states clearly outperform the ones for the linear ramp [see Fig. 3.6(a)]. The linear ramp fidelity deteriorates as N increases whereas, remarkably, the fidelity of the FAQUAD protocol stays constant. The effect of an error of the form $\Omega_e(t) = \Omega_F(t)(1+\epsilon)$ is shown in Fig. 3.6(b).

3.6 Discussion

The FAQUAD approach to speed up adiabatic manipulations of quantum systems achieves significant time shortenings by distributing homogeneously the adiabaticity parameter along the process while satisfying the boundary conditions of the control parameter. We have derived general time scales and we have demonstrated its applicability in different systems, in particular where other approaches are not available, and expect a broad range of applications in quantum, optical, and mechanical systems, due to the ubiquity of adiabatic methods.

A natural extension is to attempt a scheme similar to Eq. (3.2) in a superadiabatic rather than an adiabatic frame [86]. The set of nested frames is described in detail in [86]. A brief summary is provided here. Let us start with a Schrödinger picture Hamiltonian $H_0(t)$ and corresponding wave function $\psi_0(t)$. Defining the unitary operator

$$A_0(t) = \sum_n |\phi_n(t)\rangle\langle n| \tag{3.31}$$

with $|\phi_n(t)\rangle$ the adiabatic basis in Eqs. (3.22) and (3.23), and $|n\rangle$ the bare basis, the Hamiltonian that governs the dynamics of the interaction picture state $A_0^\dagger\psi_0$ is

$$H_1(t) = A_0^\dagger(H_0 - K_0)A_0, \tag{3.32}$$

where $K_0 = i\hbar\dot{A}_0A_0^\dagger$. For the two level model, taking into account Eq. (3.19) in Eq. (3.32) we get

$$H_1 = \begin{pmatrix} \frac{1}{2}(U-P-\Delta) & i\frac{\sqrt{2}J\hbar\dot{\Delta}}{P^2} \\ -i\frac{\sqrt{2}J\hbar\dot{\Delta}}{P^2} & \frac{1}{2}(U+P-\Delta) \end{pmatrix}, \tag{3.33}$$

with instantaneous eigenvalues

$$E_1^{(1)} = \frac{1}{2}\left(U - \Delta - \frac{\sqrt{P^6 + 8J^2\hbar^2\dot{\Delta}^2}}{P^2}\right), \tag{3.34}$$

$$E_2^{(1)} = \frac{1}{2}\left(U - \Delta + \frac{\sqrt{P^6 + 8J^2\hbar^2\dot{\Delta}^2}}{P^2}\right), \tag{3.35}$$

and normalized eigenstates

$$|\phi_1^{(1)}\rangle = \begin{pmatrix} \frac{-2iJ\hbar\dot{\Delta}}{(P^6+8J^2\hbar^2\dot{\Delta}^2)^{1/4}\sqrt{-P^3+\sqrt{P^6+8J^2\hbar^2\dot{\Delta}^2}}} \\ \frac{\sqrt{-P^3+\sqrt{P^6+8J^2\hbar^2\dot{\Delta}^2}}}{\sqrt{2}(P^6+8J^2\hbar^2\dot{\Delta}^2)^{1/4}} \end{pmatrix}, \tag{3.36}$$

$$|\phi_2^{(1)}\rangle = \begin{pmatrix} \frac{2iJ\hbar\dot{\Delta}}{(P^6+8J^2\hbar^2\dot{\Delta}^2)^{1/4}\sqrt{P^3+\sqrt{P^6+8J^2\hbar^2\dot{\Delta}^2}}} \\ \frac{\sqrt{P^3+\sqrt{P^6+8J^2\hbar^2\dot{\Delta}^2}}}{\sqrt{2}(P^6+8J^2\hbar^2\dot{\Delta}^2)^{1/4}} \end{pmatrix}. \tag{3.37}$$

The first superadiabatic frame is defined by the unitary operator

$$A_1(t) = \sum_n |\phi_n^{(1)}(t)\rangle\langle n|. \tag{3.38}$$

The state $A_1^\dagger\psi_1$ is governed by the Hamiltonian

$$H_2(t) = A_1^\dagger(H_1 - K_1)A_1, \tag{3.39}$$

where $K_1 = i\hbar\dot{A}_1A_1^\dagger$.

Note that superadiabaticity, i.e., the possibility to neglect K_1, does not necessarily imply adiabaticity, which amounts to neglecting K_0. Also, a shortcut to superadiabaticity is only a STA if the superadiabatic states $|\phi_n^{(1)}\rangle$ coincide, up to phase factors, with the eigenstates of H_0, $|\phi_n\rangle$, at boundary times. This will imply additional boundary conditions on the control parameter. The equation that substitutes Eq. (3.2) for the lowest superadiabatic scheme beyond the adiabatic level is

$$\hbar\left|\frac{\langle\phi_1^{(1)}(t)|\partial_t\phi_2^{(1)}(t)\rangle}{E_1^{(1)} - E_2^{(2)}}\right| = c. \tag{3.40}$$

Using Eqs. (3.34), (3.35), (3.36) and (3.37) in (3.40), we get a second-order differential equation for Δ:

$$\frac{\sqrt{2}J\hbar^2P^4(-3\dot{P}\dot{\Delta}+P\ddot{\Delta})}{(P^6+8J^2\hbar^2\dot{\Delta}^2)^{3/2}}=c. \tag{3.41}$$

To satisfy $|\phi_1^{(1)}(0)\rangle = |\phi_1(0)\rangle = |2\rangle$ and $|\phi_1^{(1)}(t_f)\rangle = |\phi_1(t_f)\rangle = |1\rangle$ (up to phase factors) we have to impose four boundary conditions,

$$\begin{aligned}&\Delta(0)\gg U,J,\ \ \Delta(t_f)=0,\\ &\dot{\Delta}(0)=0,\ \ \dot{\Delta}(t_f)\gg\Delta(0),U,J,\end{aligned} \tag{3.42}$$

that cannot be satisfied with two integration constants plus the c. The mismatch between number of conditions and free parameters actually gets worse when increasing the order of superadiabaticity in further iterations. In the second superadiabatic frame defined by the unitary operator

$$A_2(t)=\sum_n|\phi_n^{(2)}(t)\rangle\langle n|, \tag{3.43}$$

due to the $K_2 = i\hbar\dot{A}_2A_2^\dagger$ term, second-order derivatives of the control parameter appear in the superadiabatic eigenstates, so the number of boundary conditions necessary to satisfy $|\phi_1^{(2)}(0)\rangle = |2\rangle$ and $|\phi_1^{(2)}(t_f)\rangle = |1\rangle$ (up to phase factors) increases to 6. Moreover, the differential equation resulting from applying the FAQUAD concept in the second superadiabatic basis is of third order in Δ. Once again, the differential equation cannot satisfy the six boundary conditions with three integration constants plus the c. In general, as the order of the iteration increases, the number of boundary conditions to satisfy grows as $2n+2$, where n is the order of the iteration, while the order of the differential equation increases as $n+1$. Hence, the adiabatic frame is in fact optimal to apply the FAQUAD concept within the series of iterative superadiabatic frames, as it is the only one for which the number of conditions equals the number of free parameters available.

Chapter 4

Vibrational mode multiplexing of ultracold atoms

Sending multiple messages on qubits encoded in different vibrational modes of cold atoms or ions along a transmission waveguide requires us to merge first and then separate the modes at input and output ends. Similarly, different qubits can be stored in the modes of a trap and be separated later. We design the fast splitting of a harmonic trap into an asymmetric double well so that the initial ground vibrational state becomes the ground state of one of two final wells, and the initial first excited state becomes the ground state of the other well. This might be done adiabatically by slowly deforming the trap. We speed up the process by inverse engineering a double-function trap using dynamical invariants. The separation (demultiplexing) followed by an inversion of the asymmetric bias and then by the reverse process (multiplexing) provides a population inversion protocol based solely on trap reshaping.

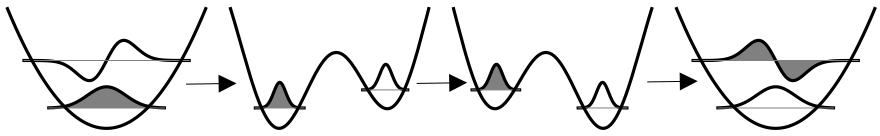

FIGURE 4.1: Population inversion using trap deformations in three steps: demultiplexing, bias inversion, and multiplexing.

4.1 Introduction

One of the main goals of atomic physics is to achieve an exhaustive control of atomic states and dynamics [87]. The ultracold domain is particularly suitable for this aim as it provides a rich scenario of quantum states and phenomena. Atom optics and atomtronics [88] intend to manipulate cold atoms in circuits and devices for applications in metrology, quantum information, or fundamental science. These devices are frequently inspired by electronics (e.g., the atom diode [89, 90], the transistor [88], atom chips [91]), or optics (e.g., beam splitters [92], or multiplexing [93, 94]).

In this chapter we shall focus on a cold-atom realization of multiplexing, a basic process in modern telecommunications. Multiplexing is the transmission of different messages via a single physical medium. A multiplexer combines signals from several emitters into a single medium, whereas a demultiplexer performs the reverse operation. The concept of multiplexing is relevant for quantum information processing (for its use in quantum repeaters, see [95, 96], or for trapped ions [97]). We envision here optical or magnetic waveguides for atoms holding several transverse orthogonal modes [98–101]. If the qubit is encoded in the internal state of the atom, several qubits may be carried out simultaneously by different modes. To develop such a quantum-information architecture, fast multiplexers or demultiplexers that could join the modes from different waveguides into one guide, or separate them, are needed. We shall discuss trap designs for demultiplexing since the multiplexer would simply operate in reverse. For a proof of principle, we propose the simplified setting of a single initial harmonic trap for noninteracting cold atoms whose first two eigenstates will be separated, as in the first step of Fig. 4.1, into two different wells. In a complete demultiplexing process, the final wells should be independent, with negligible tunneling. The challenge is to design the splitting (a) without final excitation of higher vibrational levels, (b) in a short time, and (c) with a realizable trap potential. Condition (a) may be achieved by an adiabatic asymmetric splitting [15, 102] in which, for moderate bias compared

to the vibrational quanta, the initial ground state becomes the ground state of the well with the lowest energy, and the excited state becomes the ground state of the other well (see Chapter 1). This adiabatic approach generally fails to satisfy the condition (b), which we shall implement applying STA [1, 8, 44, 73]. As for (c), we shall make use of a simple two-level model for the shortcut design, and then map it to a realistic potential recently implemented to realize an atomic Josephson junction [35]. Finally, several applications, such as separation of multiple modes, population inversion, or controlled excitation, will be discussed.

4.2 Slow adiabatic and fast quasi-adiabatic processes

Suppose that a harmonic potential evolves adiabatically into two well-separated and asymmetric wells as in the first step of Fig. 4.1. To accelerate the dynamics we shall use the moving two-level approximation presented in Chapter 1 (Section 1.4). This moving two-level approximation is based on a process where a symmetrical potential evolves from an initial harmonic trap to a final double well. Then, we construct a time-dependent orthogonal bare basis $|L(t)\rangle = \begin{pmatrix} 0 \\ 1 \end{pmatrix}$, $|R(t)\rangle = \begin{pmatrix} 1 \\ 0 \end{pmatrix}$ of left and right states, obtained by a linear combination of the instantaneous ground and first excited states. An approximate two-mode Hamiltonian model for a generally *asymmetrical* process is written in this basis as

$$H_{2\times 2}(t) = \frac{\hbar}{2}\begin{pmatrix} \lambda(t) & -\delta(t) \\ -\delta(t) & -\lambda(t) \end{pmatrix}, \tag{4.1}$$

where, for the double well configuration, $\delta(t)$ is the tunneling rate, and $\hbar\lambda(t)$ the relative gap, or bias, between the two wells. Note that, this Hamiltonian is just the Hamiltonian in Eq. (1.13) multiplied by a factor $\hbar$. For the initial harmonic potential at $t = 0$, $\lambda(0) = 0$ and $\delta(0) = \omega_0$. The instantaneous eigenvalues are

$$E_\lambda^{\pm}(t) = \pm\frac{\hbar}{2}\sqrt{\lambda^2(t) + \delta^2(t)}, \tag{4.2}$$

and the normalized eigenstates

$$\begin{aligned} |\psi_\lambda^+(t)\rangle &= \sin\left(\frac{\alpha}{2}\right)|L(t)\rangle - \cos\left(\frac{\alpha}{2}\right)|R(t)\rangle, \\ |\psi_\lambda^-(t)\rangle &= \cos\left(\frac{\alpha}{2}\right)|L(t)\rangle + \sin\left(\frac{\alpha}{2}\right)|R(t)\rangle, \end{aligned} \tag{4.3}$$

where the mixing angle $\alpha = \alpha(t)$ is given by $\tan\alpha = \delta(t)/\lambda(t)$. The boundary conditions on $\lambda(t)$ and $\delta(t)$ are

$$\begin{aligned} &\delta(0) = \omega_0, \\ &\lambda(0) = 0, \\ &\delta(t_f) = 0, \\ &\lambda(t_f) = \lambda_f, \end{aligned} \tag{4.4}$$

which correspond, at time $t = 0$, to a harmonic well, and at time t_f to two independent wells with asymmetry bias $\hbar\lambda_f$.

To design a FAQUAD process, we shall first assume the simplifying conditions: $\lambda(t) = \lambda$ constant and $\lambda/\delta(0) \ll 1$. Thus, $\alpha(0) \approx \pi/2$ and the initial eigenstates essentially coincide with the ground and first excited states of the harmonic oscillator. As we have seen in Chapter 1, for a constant λ, the adiabaticity condition reads [102]

$$\left|\frac{\lambda\dot{\delta}(t)}{2[\lambda^2 + \delta(t)^2]^{3/2}}\right| \ll 1. \tag{4.5}$$

To get the FAQUAD solution we proceed as in Chapter 3. Therefore, imposing a constant value c for the adiabaticity parameter and using the boundary conditions for δ in Eq. (4.4), we fix the integration constant and the value of c,

$$c = \frac{\omega_0}{2\lambda\sqrt{\omega_0^2 + \lambda^2}\, t_f}. \tag{4.6}$$

The solution of the differential equation for $\delta(t)$ takes finally the form

$$\delta_{fa}(t) = \frac{\omega_0\lambda(t_f - t)}{\sqrt{\lambda^2 t_f^2 + \omega_0^2 t(2t_f - t)}}. \tag{4.7}$$

Although this protocol can be work for shorter times for which the process is not fully adiabatic, the FAQUAD approach is limited by

$$t_f = \frac{2\pi}{\phi_{12}}, \tag{4.8}$$

where $\phi_{12} = \int_0^1 \tilde{\omega}_{12}(s)ds$, and $\tilde{\omega}_{12}(s) = \omega_{12}(st_f)$ [see Chapter 3, Subsection 3.2.1].

We shall now work out an alternative, faster protocol based on invariants, in which the boundary conditions on $\lambda(t)$ and $\delta(t)$ will be exactly satisfied.

4.3 Invariant-based inverse engineering

4.3.1 Lewis-Riesenfeld invariants

The Lewis-Riesenfeld [6] theory is applicable to a quantum system that evolves with a time-dependent Hermitian Hamiltonian $H(t)$, which supports a Hermitian dynamical invariant $I(t)$ satisfying

$$i\hbar\frac{\partial I(t)}{\partial t} - [H(t), I(t)] = 0. \tag{4.9}$$

Therefore, its expectation values for an arbitrary solution of the time-dependent Schrödinger equation

$$i\hbar\frac{\partial}{\partial t}|\Psi(t)\rangle = H(t)|\Psi(t)\rangle \tag{4.10}$$

do not depend on time. $I(t)$ can be used to expand $|\Psi(t)\rangle$ as a superposition of "dynamical modes" $|\psi_n(t)\rangle$,

$$\begin{aligned} |\Psi(t)\rangle &= \sum_n c_n|\psi_n(t)\rangle, \\ |\psi_n(t)\rangle &= e^{i\alpha_n(t)}|\phi_n(t)\rangle, \end{aligned} \tag{4.11}$$

where $n = 0, 1, \ldots$; c_n are time-independent amplitudes, and $|\phi_n(t)\rangle$ are orthonormal eigenvectors of the invariant $I(t)$,

$$I(t) = \sum_n |\phi_n(t)\rangle\lambda_n\langle\phi_n(t)|. \tag{4.12}$$

The λ_n are real constants, and the Lewis-Riesenfeld phases are defined as [6]

$$\alpha_n(t) = \frac{1}{\hbar}\int_0^t \left\langle \phi_n(t') \middle| i\hbar\frac{\partial}{\partial t'} - H(t') \middle| \phi_n(t') \right\rangle dt'. \tag{4.13}$$

We use, for simplicity, a notation for a discrete spectrum of $I(t)$ but the generalization to a continuum or mixed spectrum is straightforward. We also assume a non-degenerate spectrum.

4.3.2 Inverse engineering

Supose that we want to drive the system from an initial Hamiltonian $H(0)$ to a final one $H(t_f)$, in such a way that the populations in the initial and final instantaneous bases are the same, but admitting transitions at intermediate times. To inverse engineer a time-dependent Hamiltonian $H(t)$ and achieve this goal, we may first define the invariant through its eigenvalues and eigenvectors. The Lewis-Riesenfeld phases $\alpha_n(t)$ may also be chosen as arbitrary functions to write down the time-dependent unitary evolution operator U

$$U = \sum_n e^{i\alpha_n(t)} |\phi_n(t)\rangle\langle\phi_n(0)|. \tag{4.14}$$

U obeys $i\hbar\dot{U} = H(t)U$, where the dot means time derivative. Solving formally this equation for $H(t) = i\hbar\dot{U}U^\dagger$, we get

$$H(t) = -\hbar\sum_n |\phi_n(t)\rangle\dot{\alpha}_n\langle\phi_n(t)| + i\hbar\sum_n |\partial_t\phi_n(t)\rangle\langle\phi_n(t)|. \tag{4.15}$$

According to Eq. (4.15), for a given invariant there are many possible Hamiltonians corresponding to different choices of phase functions $\alpha_n(t)$. In general $I(0)$ does not commute with $H(0)$, so the eigenstates of $I(0)$, $|\phi_n(0)\rangle$, do not coincide with the eigenstates of $H(0)$. $H(t_f)$ does not necessarily commute with $I(t_f)$ either. If we impose $[I(0), H(0)] = 0$ and $[I(t_f), H(t_f)] = 0$, the eigenstates will coincide, which guarantees a state transfer without final excitations. In typical applications, the Hamiltonians $H(0)$ and $H(t_f)$ are given, and set the initial and final configurations of the external parameters. Then we define $I(t)$ and its eigenvectors accordingly, so that the commutation relations are obeyed at the boundary times and, finally, $H(t)$ is designed via Eq. (4.15). While the $\alpha_n(t)$ may be taken

as fully free time-dependent phases in principle, they may also be constrained by a pre-imposed or assumed structure of $H(t)$.

We will focus now on the two-level system, so for the Hamiltonian in Eq. (4.1), there is a dynamical invariant $I(t)$ of the form [44]

$$I(t) = \frac{\hbar}{2}\Omega_0 \begin{pmatrix} \cos\theta(t) & \sin\theta(t)e^{i\varphi(t)} \\ \sin\theta(t)e^{-i\varphi(t)} & -\cos\theta(t) \end{pmatrix}, \tag{4.16}$$

where $\varphi(t)$ and $\theta(t)$ are auxiliary (azymuthal and polar) angles, and Ω_0 is an arbitrary constant with units of frequency. The role of the invariant is therefore to drive the initial eigenstates of $H_{2\times2}(0)$ to the eigenstates of $H_{2\times2}(t_f)$. In our application this implies a unitary mapping from the first two eigenstates of the harmonic oscillator to the ground states of the left and right final wells.

From the invariance property (4.9), choosing $H(t)$ as the Hamiltonian in (4.1), it follows that

$$\begin{aligned} \delta(t) &= -\dot{\theta}(t)/\sin\varphi(t), \\ \lambda(t) &= -\delta(t)\cot\theta(t)\cos\varphi(t) - \dot{\varphi}(t). \end{aligned} \tag{4.17}$$

The commutativity of $I(t)$ and $H_{2\times2}(t)$ at boundary times $t_b = 0, t_f$ imposes the conditions

$$\begin{aligned} &\lambda(t_b)\sin[\theta(t_b)]e^{i\varphi(t_b)} + \delta(t_b)\cos[\theta(t_b)] = 0, \\ &\lambda(t_b)\sin[\theta(t_b)]e^{-i\varphi(t_b)} + \delta(t_b)\cos[\theta(t_b)] = 0, \\ &\delta(t_b)\sin[\theta(t_b)]\sin[\varphi(t_b)] = 0. \end{aligned} \tag{4.18}$$

Taking into account Eq. (4.4), we get from Eq. (4.18),

$$\begin{aligned} &\theta(0) = \pi/2, \\ &\varphi(0) = \pi, \\ &\theta(t_f) = 0, \\ &\dot{\theta}(t_f) = 0. \end{aligned} \tag{4.19}$$

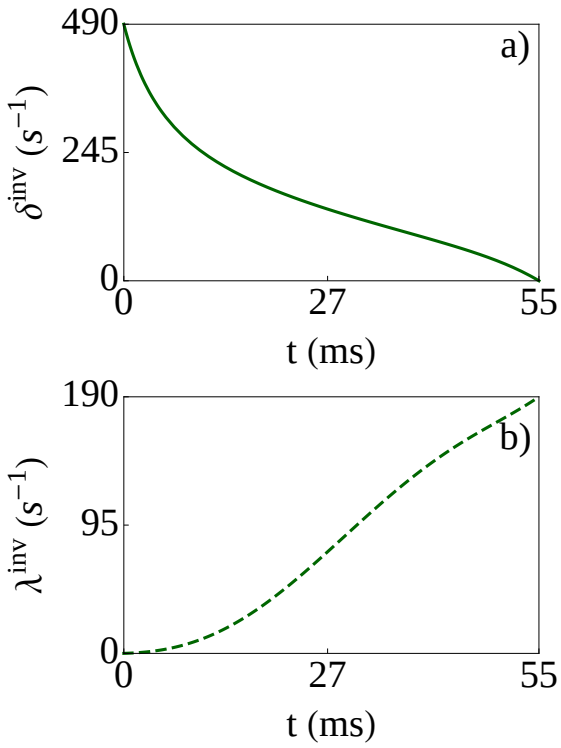

FIGURE 4.2: (a) $\delta^{\mathrm{inv}}(t)$ and (b) $\lambda^{\mathrm{inv}}(t)$. $\delta(0) = 2\pi \times 78$ Hz, $\lambda_f = 190$ s^{-1}, $\dot{\lambda}(0) = 190$ s^{-2}, and $t_f = 55$ ms.

These conditions lead to indeterminacies in Eq. (4.17). To resolve them we apply l'Hôpital's rule repeatedly and find additional boundary conditions,

$$\begin{aligned}
&\dot{\theta}(0) = \ddot{\theta}(0) = \dot{\varphi}(0) = 0,\\
&\dddot{\theta}(0) = -\omega_0 \dot{\lambda}(0),\\
&\ddot{\varphi}(0) = -\dot{\lambda}(0),\\
&\varphi(t_f) = \pi/2,\\
&\dot{\varphi}(t_f) = -\frac{\lambda_f}{3},
\end{aligned} \tag{4.20}$$

with $\dot{\lambda}(0) \neq 0$. At intermediate times, we interpolate the angles assuming a polynomial ansatz, $\theta(t) = \sum_{j=0}^{5} a_j t^j$ and $\varphi(t) = \sum_{j=0}^{4} b_j t^j$, where the coefficients are found by solving the equations for the boundary conditions. Thus, we obtain the Hamiltonian functions $\delta^{\mathrm{inv}}(t)$ and $\lambda^{\mathrm{inv}}(t)$ from Eq. (4.17). Figure 4.2 provides an example of parameter trajectories.

4.4 Mapping to coordinate space

Our purpose now is to map the 2×2 Hamiltonian into a realizable potential,

$$V(x,t) = \frac{1}{2}m\omega^2 x^2 + V_0 \cos^2\left[\frac{\pi(x-\Delta x)}{d_l}\right]. \tag{4.21}$$

This form has already been implemented [35] with optical dipole potentials, combining a harmonic confinement due to a crossed beam dipole trap with a periodic light shift potential provided by the interference pattern of two mutually coherent laser beams. The control parameters are in principle the frequency ω, the displacement Δx of the optical lattice relative to the center of the harmonic well, the amplitude V_0 and the lattice constant d_l, but in the following examples we fix d_l and Δx; the other two parameters offer enough flexibility and are easier to control as time-dependent functions. To perform the mapping, we minimize numerically

$$F[V_0(t), \omega(t)] = [\delta^{\mathrm{id}}(t) - \delta(t)]^2 + [\lambda^{\mathrm{id}}(t) - \lambda(t)]^2, \tag{4.22}$$

using the simplex method. The functions $\delta^{\mathrm{id}}(t)$ and $\lambda^{\mathrm{id}}(t)$ are designed according to the shortcuts discussed before, and (following the same procedure as in Chapter 1) $\delta(t)$ and $\lambda(t)$ are computed as

$$\delta(t) = -\frac{2}{\hbar}\langle L(t)|H|R(t)\rangle = -\frac{2}{\hbar}\langle R(t)|H|L(t)\rangle, \tag{4.23}$$

$$\lambda(t) = \frac{2}{\hbar}\langle R(t)|H-\Lambda|R(t)\rangle = -\frac{2}{\hbar}\langle L(t)|H-\Lambda|L(t)\rangle, \tag{4.24}$$

where $H = H(V_0(t), \omega(t); \Delta x, d_l) = -\frac{\hbar^2}{2m}\frac{\partial^2}{\partial x^2} + V$ is the full Hamiltonian in coordinate space with a kinetic energy term and the potential (4.21) and $\Lambda(t) = [E_\lambda^-(t) + E_\lambda^+(t)]/2$ is a shift defined from the first two levels $E_\mp$ of H to match the zero-energy point between the coordinate and the two-level system. Finally,

$$\begin{aligned} |R(t)\rangle &= (|g(t)\rangle + |e(t)\rangle)/2^{1/2}, \\ |L(t)\rangle &= (|g(t)\rangle - |e(t)\rangle)/2^{1/2} \end{aligned} \tag{4.25}$$

form the base, where $|g(t)\rangle$ is the ground state and $|e(t)\rangle$ the first excited state of the symmetrical Hamiltonian $H_0(V_0(t), \omega(t); \Delta x = 0, d_l)$, defined as H but with $\Delta x = 0$, which we diagonalize numerically. In our calculations, $\delta(t)$ and $\lambda(t)$ become indistinguishable from their ideal counterparts. Figure 4.3 depicts $V_0(t)$

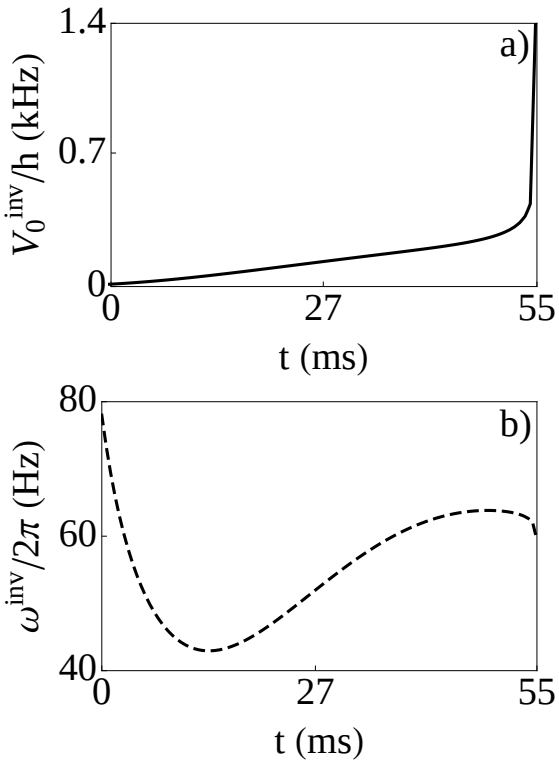

FIGURE 4.3: Lattice height V_0, and trap frequency $\omega/(2\pi)$ using invariant-based engineering and mapping. $\Delta x = 200$ nm.

and $\omega(t)$ for the parameters of Fig. 4.2. We use ^{87}Rb atoms and a lattice spacing $d_l = 5.18$ μm. The sharp final increase of $V_0(t)$ makes the two wells totally independent, but for most applications this strict condition may be relaxed to avoid intrawell excitations.

Figure 4.4 demonstrates perfect transfer for the ground (a) and the excited state (b) using the very same protocol in both cases, the one depicted in Figs. 4.2 and 4.3. (Thanks to the superposition principle, the same protocol would produce a perfect demultiplexing for any linear combination of the ground and excited states.) Initial and final states are represented, solving the Schrödinger equation with the potential (4.21). We stop the process 2 ms before the nominal time t_f, as the fidelity reaches a stable maximum there, and a further increase of V_0 is not required. We also include the results for the protocol in which ω is kept constant and $V_0(t)$ is a linear ramp (with the same durations as the shortcut protocols). For this linear protocol the final state includes a significant density in the "wrong" well. This simple linear-V_0 approach needs $t_f \gtrsim 0.7$ s to become adiabatic and produce the same fidelity, 0.9997, found for a shortcut protocol ten times faster, $t_f = 0.07$ s, the rightmost point in Fig. 4.5 (a). Figure 4.6 compares the populations in the instantaneous basis of the (full, coordinate-space) Hamiltonian for the shortcut and

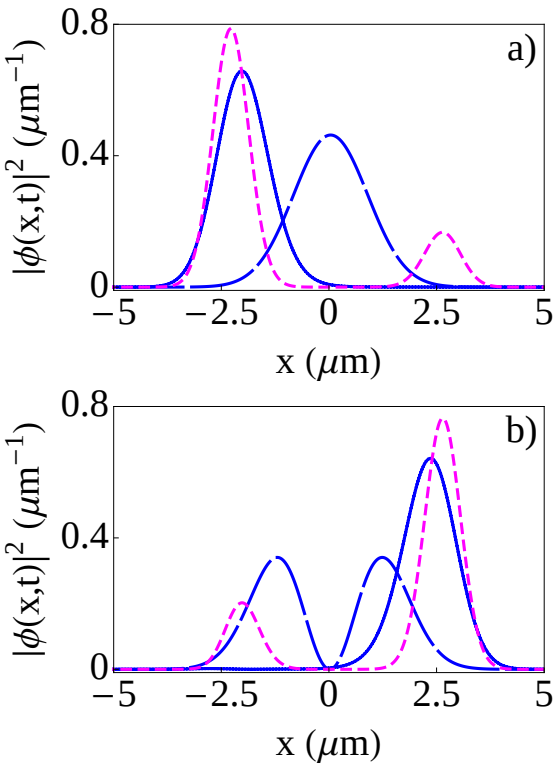

FIGURE 4.4: (a): Ground state at $t = 0$ (long-dashed, blue line); final state with the shortcut (solid, blue line, indistinguishable from the ground state of the final trap); final state with linear ramp for $V_0(t)$ and $\omega = 2\pi \times 78$ Hz (short-dashed, magenta line). (b): Same as (a) for the first excited state. Parameters like in Fig. 4.3 at $t = 53$ ms. The linear ramp for $V_0(t)$ ends in the same value used for the shortcut.

the linear protocols when the system starts in the ground state, corresponding to Fig. 4.4 (a). The shortcut protocol implies a transient exchange between ground and (first) excited levels but finally takes the system to the desired ground state. In contrast to the linear protocol, the excitation is permanent, leading to a poor final fidelity.

In the two-level model, t_f may be reduced arbitrarily, but in the coordinate space Hamiltonian, levels 0-1 will only be "independent" as long as higher levels are not excited. These excitations are the limiting factor to shorten the times further with the current mapping scheme. Some guidance is provided by the Anandan-Aharonov relation $t_f > h/(4\overline{\Delta E})$, where $\overline{\Delta E}$ is the time average of the standard deviation [23].

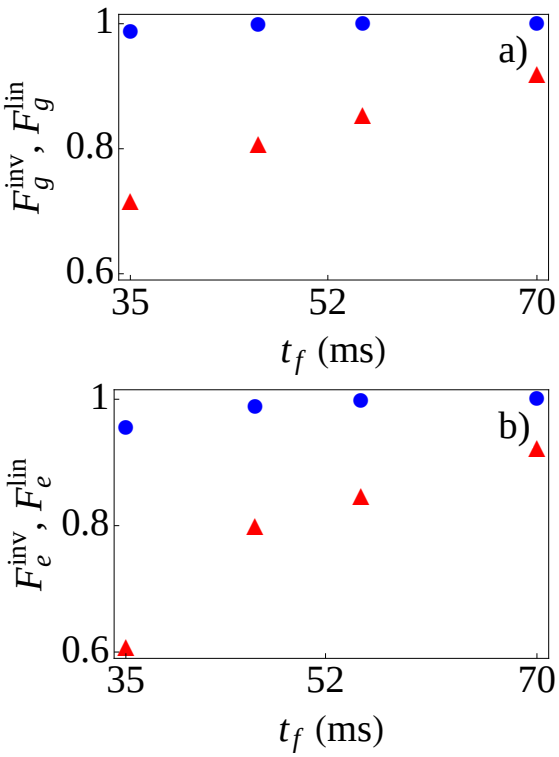

FIGURE 4.5: Fidelities with respect to the final ground state starting at the ground state (a) and with respect to the final first excited state starting at the excited state (b) versus final time t_f, via shortcuts (F_g^{inv} and F_e^{inv}, blue circles), or linear ramping of $V_0(t)$ (F_g^{lin} and F_e^{lin}, red triangles). The fidelity is computed at 2 ms less than the nominal t_f. Other parameters as in Figs. 4.2, 4.3, and 4.4.

4.5 Discussion

Vibrational multiplexing may be combined with internal-state multiplexing [97] to provide a plethora of possible operations. Motivated by the prospective use of multiplexing or demultiplexing for quantum information processing, we have applied shortcuts to adiabaticity techniques to speed up the spatial separation of vibrational modes of a harmonic trap. A similar approach would separate n modes into n wells so as to deliver more information into different processing sites. The number of modes that could be separated will depend on the asymmetric bias in relation to other potential parameters: the bias among the extreme wells should not exceed the vibrational quanta in the final wells. The bias determines possible speeds, too, as smaller biases generally imply longer times.

Chapter 1 dealt also with splitting operations and shortcuts to adiabaticity, but the objective was the opposite to our aim here. Since adiabatic following from a harmonic trap to an asymmetric double well collapses the ground state wave to

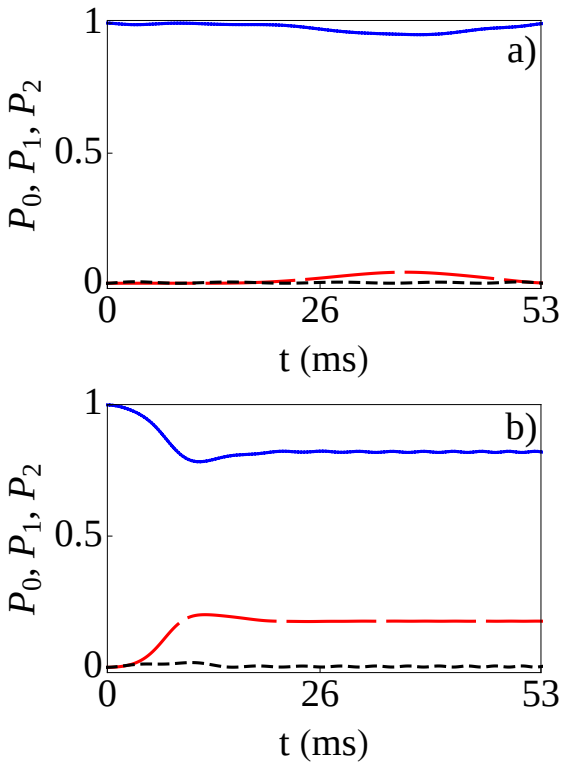

FIGURE 4.6: Populations of the states for the shortcuts (a) and the linear ramp for $V_0(t)$ (b). Ground state (P_0, solid blue line); first excited state (P_1, long-dashed red line); second excited state (P_2, short-dashed black line). Parameters as in Fig. 4.4 (a).

one of the two wells, a FF technique [7, 18] was applied to *avoid* the collapse and achieve perfect, balanced splitting, as required, e.g., for matter-wave interferometry. The idea was that for a fast nonadiabatic shortcut, the perturbative effect of the asymmetry becomes negligible. The stabilizing effect of interactions was also characterized within a mean-field treatment. In the present chapter, the objective is to send each mode of the initial harmonic trap as fast as possible to a different final well, so we needed a different methodology. Instead of FF, which demands an arbitrary control of the potential function in position and time, we have restricted the potential to a form with a few controllable parameters (in practice we have let only two of them evolve in time). Inverse engineering of the Hamiltonian is carried out for a two-level model using invariants of motion, and the resulting (analytical) Hamiltonian is then mapped to real space. The discrete Hamiltonian is useful as it provides a simple picture to understand and design the dynamics at will. The method provides also a good basis to apply OCT, which complements invariant-based engineering (see. e.g. [62]) by selecting among the fidelity-1 protocols according to other physical requisites. As for interactions and nonlinearities,

they will generally spoil a clean multiplexing or demultiplexing processes, so we have only examined linear dynamics here.

An application of the demultiplexing schemes discussed in this work is the population inversion of the first two levels of the harmonic trap without making use of internal state excitations [103]. This is useful to avoid decoherence effects induced by decay, or for species without an appropriate (isolated two-level) structure. The scheme is based on the three steps shown in Fig. 4.1. A mechanical excitation of the ground state level into the first excited state of a fixed anharmonic potential was implemented by shaking the trap along a trajectory calculated with an OCT algorithm [104]. Our proposed approach relies instead on a smooth potential deformation. This type of inversion could be applied to interacting Bose-Einstein condensates as long as the initial states are pure ground or excited levels. The production of twin-atom beams from the excited state is an outstanding application [105].

Asymmetric double wells may also be used for other state-control operations such as preparing nonequilibrium Fock states through a ladder excitation process. The vibrational number may be increased by one at every step. Each excitation would start and finish with demultiplexing and multiplexing operations from the harmonic oscillator to the double well and vice versa, as described in the main text. Between them the two wells are independent and their height or width can be adjusted to produce the desired level ordering. For an even-to-odd vibrational number transition, this requires an inversion of the bias, as in Fig. 4.1; transitions from odd to even levels are performed by deepening the left well until the initially occupied level on the right well surpasses one of the levels in the left well. The steps may be repeated until a given Fock state is reached. Operating in reverse mode, a given excited state could be taken down to the ground state, as in sideband cooling, just with trap deformations, as we will see in Chapter 6.

Open questions left for future work include optimizing the robustness of parameter trajectories versus noise and perturbations [68], or finding time bounds in terms of average energies, similar to the ones for harmonic trap expansions [22] or transport [42]. The present results may also be applied for optical waveguide design, as we will see in the next chapter, or to two-dimensional systems as a way to generate vortices.

Chapter 5

Compact and high conversion efficiency mode-sorting asymmetric Y junction using shortcuts to adiabaticity

We propose a compact and high conversion efficiency asymmetric Y junction mode multiplexer/demultiplexer for applications in on-chip mode-division multiplexing. Traditionally, mode-sorting is achieved by adiabatically separating the arms of a Y junction. We shorten the device length using invariant-based inverse engineering and achieve better conversion efficiency than the adiabatic device.

5.1 Introduction

As optical communications over single-mode optical waveguides are quickly approaching their capacity limits, using multiple spatial modes in optical transmission systems to increase information capacity has attracted lots of attention[106, 107]. In mode-division multiplexing (MDM) systems [108], the multiple propagating modes in the system provide the extra degrees of freedom for potential capacity increase. However, to avoid intermodal dispersion, one needs to be able to excite and detect the spatial modes independently in MDM systems. So far, most of the efforts for the multiplexing or demultiplexing in MDM systems are focused on fiber-based systems, but there is also interest in realizing integrated multimode systems [109–111]. In integrated optical waveguides, the asymmetric Y junction can be designed to function as a mode sorter [93, 94, 112]. The asymmetric Y junction has a two-modes stem and two diverging single-mode arms with different widths. When the fundamental (second) mode of the stem propagates through the junction, it evolves into the fundamental mode of the wider (narrower) output arm, and vice versa. The mode sorting behavior can be attributed to the fact that a mode would evolve into the mode of the output arm with the closest effective index [93]. However, this smooth evolution can only occur when the variation at the junction is slow enough, such that the evolution is adiabatic, reducing the coupling between the local eigenmodes (supermodes) of the structure. However, the adiabatic criterion often leads to a small branching angle between the arms, and thus, a long device length to achieve the desired arm separation. The challenge in the integrated mode-sorting Y junction multiplexer or demultiplexer design is thus to reduce the device lengths while minimizing the cross talk between the arms.

So far the efforts have been focused on optimizing the device length without violating the adiabatic criterion [113]. There have also been attempts to find the optimal shape function that minimizes the coupling between the supermodes [114]. These approaches are based on the adiabatic approximation, and a well-known criterion for mode-sorting operation of the asymmetric Y junction is given by the mode conversion factor (MCF) as [93]

$$\mathrm{MCF} = \frac{|\beta_A - \beta_B|}{\theta \gamma_{AB}}, \tag{5.1}$$

where θ is the branching angle of the Y junction arms, β_A and β_B are the propagation constants of the modes supported by single mode arms A and B, and

$$\gamma_{AB} = 0.5\sqrt{(\beta_A + \beta_B)^2 - (2k_0 n)^2} \tag{5.2}$$

with n the cladding refractive index and k_0 the free-space wavenumber. When the MCF is larger (smaller) than 0.43, an asymmetric Y junction acts as a mode sorter (power divider). For a given material system n, branching waveguides dimensions β_A and β_B, and branch separation D, the required device length $L = D/\theta$ is limited by θ, obtained from Eq. (5.1). Moreover, as long as there is finite coupling between the supermodes in the adiabatic evolution, the conversion efficiency will only be unity at specific operating points [115, 116].

Recently, many coherent quantum phenomena have been exploited to implement light manipulation in waveguide structures based on the analogies between quantum mechanics and wave optics [46]. At the same time, the development in new ways to manipulate quantum systems with high-fidelity and in a short interaction time using STA [8] has inspired the design of a family of novel coupled-wave devices [40, 41, 51, 117–119]. In particular, the invariant-based inverse engineering approach [44, 74], introduced in Chapter 4, provides a versatile tool for the design of fast and robust waveguide couplers [118], in which the system dynamics are described using the eigenstates of the invariant I corresponding to the system Hamiltonian H. While previous works [40, 41, 51, 119] have focused on grating-assisted mode conversion in multimode waveguides, in this chapter, we apply the STA to design short asymmetric Y junction mode multiplexer or demultiplexer beyond the adiabatic limit.

5.2 The model

We consider the asymmetric Y junction shown schematically in Fig. 5.1, in which a two-modes stem waveguide evolves to two single-mode waveguides A (wider) and B (narrower) in a length L. The evolution of the fundamental modal

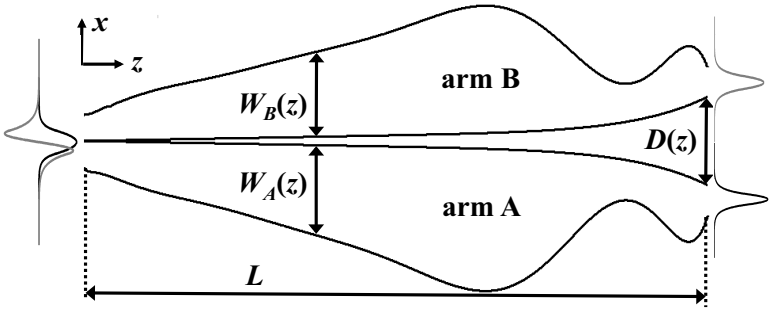

FIGURE 5.1: Schematic of the asymmetric Y junction.

amplitudes in waveguides A and B can be described by the coupled mode equations as

$$\frac{d}{dz}\begin{bmatrix} A \\ B \end{bmatrix} = -i\begin{bmatrix} \lambda(z) & -\delta(z) \\ -\delta(z) & -\lambda(z) \end{bmatrix}\begin{bmatrix} A \\ B \end{bmatrix} = -iH\begin{bmatrix} A \\ B \end{bmatrix}, \tag{5.3}$$

where δ (real) is the coupling coefficient, and $\lambda = (\beta_B - \beta_A)/2$ describes the mismatch. For the two-modes stem waveguide at $z = 0$, $\lambda(0) = 0$ and $\delta(0) = \omega_0$. Solving for the eigenvectors of H, we find two adiabatic supermodes,

$$\begin{aligned} |a_A\rangle &= \sin\alpha|\Psi_1\rangle + \cos\alpha|\Psi_2\rangle, \\ |a_B\rangle &= \cos\alpha|\Psi_1\rangle - \sin\alpha|\Psi_2\rangle, \end{aligned} \tag{5.4}$$

where $|\Psi_1\rangle \equiv \binom{0}{1}$, $|\Psi_2\rangle \equiv \binom{1}{0}$, and $\alpha = (1/2)\tan^{-1}(\delta/\lambda)$. λ and δ are related to the branch geometry, which is yet to be specified. We impose the boundary conditions

$$\begin{aligned} &\delta(0) = \omega_0, \\ &\lambda(0) = 0, \\ &\delta(L) = 0, \\ &\lambda(L) = \lambda_L, \end{aligned} \tag{5.5}$$

such that the structure corresponds to a two-modes stem waveguide at $z = 0$ and two single-mode waveguides at $z = L$. For the conventional adiabatic Y junction design, the goal is to design the evolution of λ and δ through the device geometry such that the coupling between $|a_A\rangle$ and $|a_B\rangle$ are minimized. When the adiabatic criterion is not satisfied, and there is a finite coupling between $|a_A\rangle$ and $|a_B\rangle$, the mode-sorting performance will deteriorate. In the following, we use the invariant-based inverse engineering approach to design a protocol in which the mode-sorting

is achieved at a shorter length than required by the adiabatic criterion.

5.2.1 Invariant-based inverse engineering

Replacing the spatial variation z with the temporal variation t, Eq. (5.3) is equivalent to the time-dependent Schrödinger equation ($\hbar = 1$) describing the interaction dynamics of a two-state system, and H is the Hamiltonian.

As we have seen in the previous chapter, associated with H there are Hermitian dynamical invariants $I(t)$, fulfilling

$$\partial_t I + \frac{1}{i}[I, H] = 0, \tag{5.6}$$

so that their expectation values remain constant. I can be written as (where t is replaced by z and hereafter)[44]

$$I(z) = \frac{1}{2}\begin{pmatrix} \cos\theta & \sin\theta e^{i\varphi} \\ \sin\theta e^{-i\varphi} & -\cos\theta \end{pmatrix}, \tag{5.7}$$

where $\theta \equiv \theta(z)$ and $\varphi \equiv \varphi(z)$ are z-dependent angles. The eigenstates of the invariant $I(z)$ satisfy $I(z)|\phi_n(z)\rangle = \lambda_n|\phi_n(z)\rangle$, and they can be written as

$$\begin{aligned} |\phi_+(z)\rangle &= \begin{pmatrix} \cos\frac{\theta}{2}e^{-i\varphi} \\ \sin\frac{\theta}{2} \end{pmatrix}, \\ |\phi_-(z)\rangle &= \begin{pmatrix} \sin\frac{\theta}{2} \\ -\cos\frac{\theta}{2}e^{i\varphi} \end{pmatrix}. \end{aligned} \tag{5.8}$$

An invariant $I(z)$ of $H(z)$ satisfies $i\hbar\partial_z(I(z)|\Psi(z)\rangle) = H(z)(I(z)|\Psi(z)\rangle)$[6]. According to the Lewis-Riesenfeld theory, the state of the system can be written as

$$|\Psi(z)\rangle = \Sigma_n c_n e^{i\gamma_n(z)}|\phi_n(z)\rangle, \tag{5.9}$$

where the c_n are z-independent amplitudes, and the $\gamma_n(z)$ are Lewis-Riesenfeld phases. The z-independent c_n implies that the system state will follow the eigenstate of the invariant exactly without mutual coupling.

To engineer the Hamiltonian $H(z)$ such that the mode sorting is exact, we will proceed as in Chapter 4 (Sec. 4.3). We design the invariant first and then obtain the Hamiltonian from it. Applying the boundary conditions $[H(z), I(z)] = 0$ at

$z = 0$ and $z = L$ such that the eigenvectors of $H(z)$ and $I(z)$ coincide at the input and output, the invariant will drive the input eigenstates of $H(z)$ to the output eigenstates of $H(z)$ exactly. Using the invariance condition (5.6), we find

$$\delta(z) = -\dot{\theta}(z)/\sin\varphi(z), \tag{5.10}$$

$$\lambda(z) = -\delta(z)\cot\theta(z)\cos\varphi(z) - \dot{\varphi}(z). \tag{5.11}$$

Using the commutativity of $H(z)$ and $I(z)$ at the input and output and Eq. (5.5), we obtain

$$\begin{aligned}
&\theta(0) = \pi/2,\\
&\varphi(0) = \pi,\\
&\theta(L) = 0,\\
&\dot{\theta}(L) = 0.
\end{aligned} \tag{5.12}$$

These conditions lead to indeterminacies in Eqs. (5.10) and (5.11), so we apply l'Hôpital's rule repeatedly and find the additional boundary conditions [74]

$$\begin{aligned}
&\dot{\theta}(0) = \ddot{\theta}(0) = \dot{\varphi}(0) = 0,\\
&\dddot{\theta}(0) = -\omega_0\dot{\lambda}(0),\\
&\ddot{\varphi}(0) = -\dot{\lambda}(0),\\
&\varphi(L) = \pi/2,\\
&\dot{\varphi}(L) = -\lambda_L/3,
\end{aligned} \tag{5.13}$$

with $\dot{\lambda}(0) \neq 0$. With the boundary conditions in Eq. (5.13), the evolution of the invariant parameters $\theta(z)$ and $\varphi(z)$ can be obtained through interpolation, assuming a polynomial ansatz (see Chapter 4). Then, the Hamiltonian functions δ and λ can be obtained from Eqs. (5.10) and (5.11). We finally use the simplex-based mapping method described in Sec. 4.4 to map the designed Hamiltonian to a realizable waveguide geometry. Device performance will be related to the choice of the interpolation ansatz. It is beyond the scope of this chapter to categorize or evaluate the various ansatz that are possible; rather, we focus on the polynomial ansatz to demonstrate the device concept.

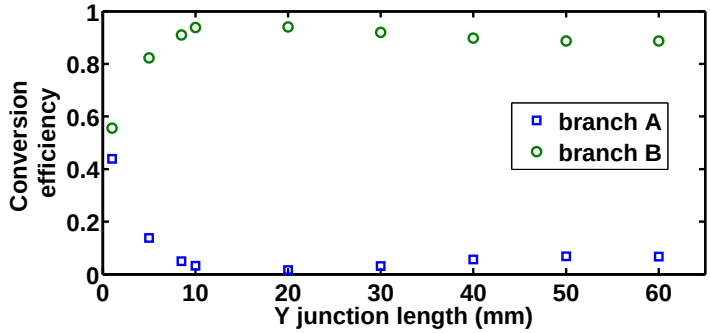

FIGURE 5.2: Conversion efficiencies of a linearly separating Y junction using the second mode as the input for different device lengths

5.3 Numerical results

Now we illustrate the design of a compact mode-sorting asymmetric Y junction in a conventional planar integrated optics platform, and perform beam propagation method (BPM) simulations to verify the designs. The scalar 2D BPM code used in the simulations solves the scalar and paraxial wave equation using the finite difference scheme with the transparent boundary condition. We choose a polymer channel waveguide structure for beam propagation simulations. The design parameters are chosen as follows: 3 μm thick SiO_2 (n =1.46) on a Si (n = 3.48) wafer is used for the bottom cladding layer, the core consists of a 2.4 μm layer of BCB (n = 1.53), and the upper cladding is epoxy (n = 1.50). The device is simulated at 1.55 μm input wavelength and the TE polarization. Subsequent analysis are performed on the 2D structure obtained using the effective index method. For the Y junction input and outputs, we choose an input stem waveguide width of 5.8 μm supporting two modes, and the output single-mode waveguides widths are $W_A(L)$=3.5 μm and $W_B(L)$=3.29 μm. We target a final waveguide separation $D(L)$ of 10 μm so that the coupling between the output branches is negligible. Substituting the corresponding waveguide parameters into Eq. (5.1), MCF=$0.1277/\theta$ (with θ in degrees) indicating the device is a mode sorter for $\theta < 0.3°$. For a conventional linearly separating adiabatic Y junction, this corresponds to a device length of larger than 2 mm to achieve a final separation $D(L)$ of 10 μm. In Fig. 5.2, we show the simulated fractional power in the fundamental modes (conversion efficiency) of waveguides A and B using the second mode as the input for different device lengths. When the device length is greater than 10 mm, the mode-sorting characteristics are well established. The transition from power divider to mode sorter at around 2 mm predicted by MCF calculations is also evident. We also

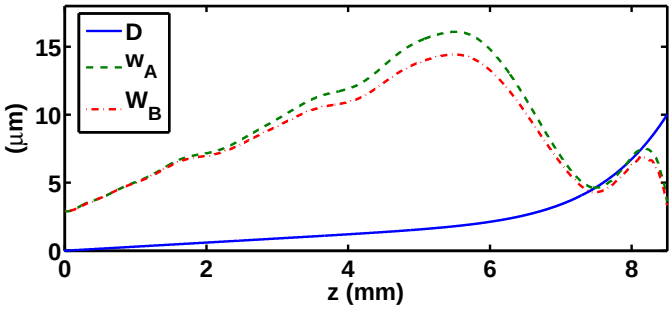

FIGURE 5.3: Parameters for the invariant-based Y junction.

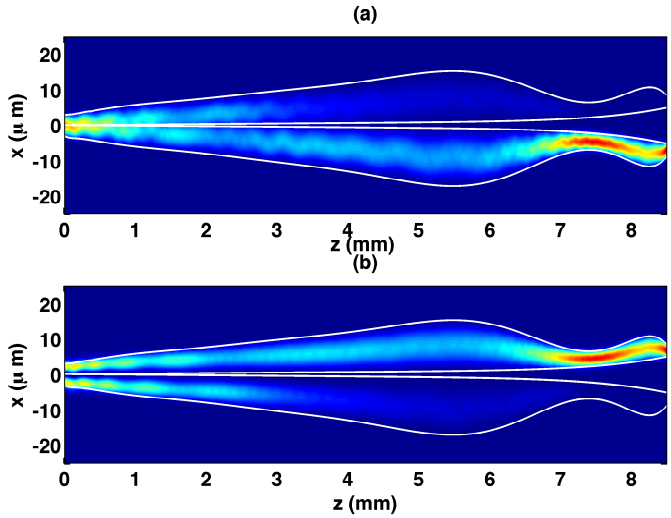

FIGURE 5.4: Mode-sorting operation of the invariant-based Y junction. Input (a) fundamental mode (b) second mode.

observe that the conversion efficiency starts to fall and will oscillate when the length keeps increasing beyond 10 mm, as a result of finite coupling between the supermodes [114].

For the invariant-based design, the boundary conditions in Eq. (5.5) are fixed by the waveguide parameters at the device input and output. To map the Hamiltonian to the waveguide parameters of the Y junction, we choose the widths of waveguides $W_A(z)$ and $W_B(z)$ and the separation $D(z)$ shown in Fig. 5.1 as the free parameters in the simplex search. The resulting parameters are shown in Fig. 5.3 for a $L = 8.5$ mm device. The corresponding Y junction geometry is shown in Fig. 5.4. In Fig. 5.4(a), the BPM results show that the fundamental mode has evolved to waveguide A at the output. And the evolution of the second mode to waveguide B is shown in Fig. 5.4(b). We also show the BPM results for the linearly separating adiabatic Y junction of the same length in Fig. 5.5. In Fig. 5.6, we compare the output field of the invariant-based mode sorter and the linear mode sorter, both at a length of

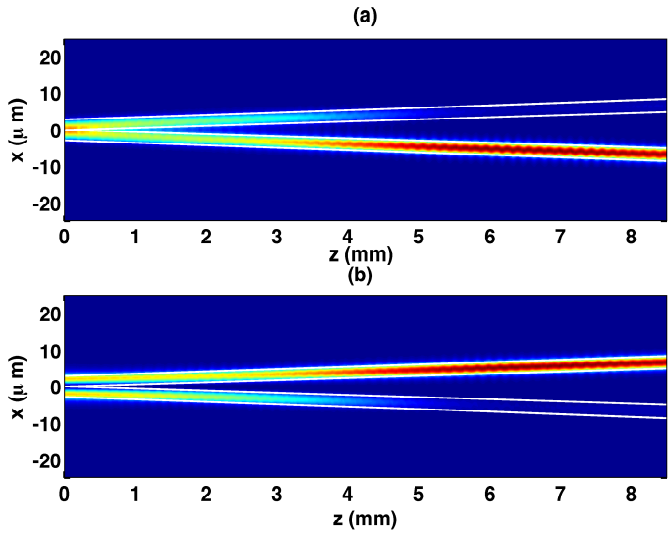

FIGURE 5.5: Mode-sorting operation of the linearly separating Y junction. Input (a) fundamental mode (b) second mode.

8.5 mm. The conversion efficiency of the invariant-based design is calculated to be 0.98 for both modes while the linearly separating design is 0.92 for both modes. The insertion loss of the invariant-based design are 0.267 dB and 0.185 dB for the fundamental and the second modes, respectively, and 0.481 dB and 0.604 dB for the linearly separating design. The higher insertion loss of the linearly separating design can be attributed to coupling into the radiation modes. On the other hand, the evolution of the invariant-based design should follow the eigenstates of the invariant exactly without coupling into the radiation modes. The observed loss can be attributed to small coupling into the radiation modes because the ideal protocol is only approximately mapped to the coordinate space model in the simplex-based mapping [74]. This also results in the conversion efficiency being less than 1. Although the width of the invariant-based design is larger than the linearly separating design, we note from Fig. 5.2 that the conversion efficiency of the linearly separating design would not reach 0.98 even when the length of the junction is increased to 60 mm. As a result, the invariant-based design can achieve high conversion efficiency with a more compact device footprint. The fabrication tolerance is studied by adding width variations δW to W_A and W_B while keeping D unchanged in the simulations. The resulting conversion efficiencies for different δW using the second mode as the input is shown in Fig. 5.7, indicating that the proposed device has a large fabrication tolerance better than 1000 nm.

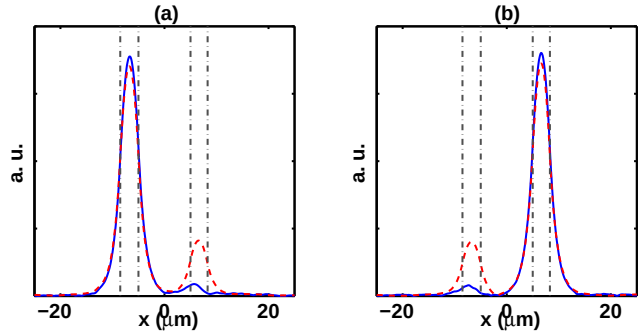

FIGURE 5.6: Output field profile of the Y junctions. Solid: invariant-based. Dashed: linearly separating. Dash-dotted: waveguide walls. Input (a) fundamental mode (b) second mode.

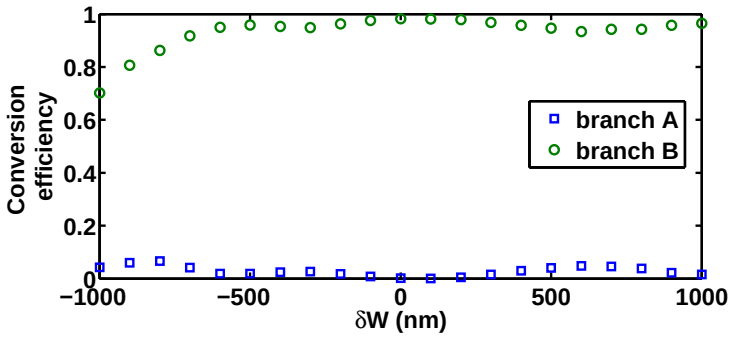

FIGURE 5.7: Conversion efficiencies as a function of width variation using the second mode as the input.

5.4 Conclusions

In conclusion, we demonstrated that the invariant-based inverse engineering approach can be applied successfully to asymmetric Y junction design. By describing the system dynamics using the dynamical invariants, the system evolution can be engineered to achieve mode sorting in a short distance. The compact design exhibits a higher conversion efficiency than the conventional adiabatic design at a shorter device length.

Chapter 6

Fast bias inversion of a double well without residual particle excitation

We design fast bias inversions of an asymmetric double well so that the lowest states in each well stay in the same well they started, free from residual motional excitation. This cannot be done adiabatically, and a sudden bias switch produces in general motional excitation. The residual excitation is suppressed by complementing a predetermined fast bias change with a linear ramp whose time-dependent slope compensates for the displacement of the wells. The process, combined with vibrational multiplexing and demultiplexing, can produce vibrational state inversion without exciting internal states, just by deforming the trap.

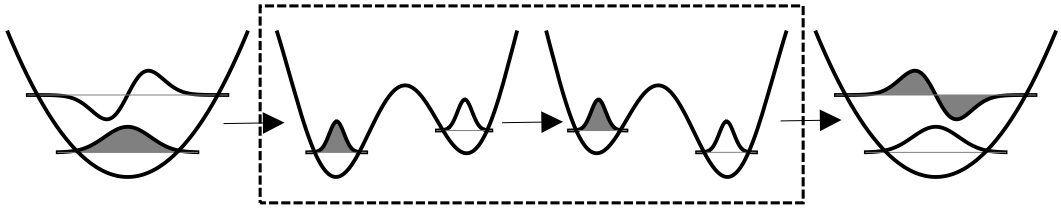

FIGURE 6.1: Schematic representation of demultiplexing (left arrow), bias inversion (framed in dashed line, central arrow), and multiplexing (right arrow). The densities of two one-atom eigenstates are represented in all potentials. In the harmonic potentials (unframed potentials on the left and right charts) the states are the ground state and first excited state. In the two central charts with tilted double wells the states are the lowest for each well. The color (white or gray) indicates how they would evolve sequentially following the fast protocol described in the text. For example, the gray state is initially the ground state of the harmonic oscillator, then it becomes the lowest state of the left well, and remains being the lowest state of that well after the bias inversion. In the last step it becomes the first excited state of the final harmonic oscillator.

6.1 Introduction

In Chapter 4 a protocol to realize fast vibrational state multiplexing or demultiplexing of ultra cold atoms was introduced. By a properly designed time-dependent potential deformation between a harmonic trap and a biased double well, the states of a single atom in a harmonic trap can be dynamically mapped into states localized at each well (vibrational demultiplexing; see the left arrow in Fig. 6.1), or vice versa (multiplexing; see the right arrow in Fig. 6.1), faster than adiabatically and without residual excitation at the final time. It was suggested that these processes may be combined with a bias inversion to produce (i) state inversions, from the ground to the first excited state of the harmonic trap and vice versa, based on trap deformations only (see the evolution of gray and white states in Fig. 6.1), or (ii) to produce vibrationally excited Fock states from an initial ground state [74]. These are basic operations to implement quantum information processing and fundamental studies. Thus the possibility to perform them without exciting internal atomic states as an intermediate step is of much interest. For trapped ions in particular, this amounts to a species-independent approach based entirely on the charge and electric forces. In contrast, π-pulse sequences require specific lasers for each system and a suitable level structure. In general, i.e., both for ions and neutral atoms, a method not using internal-state excitation suppresses decoherence and random kicks due to spontaneous decay. They may be important limiting factors to preserve quantum dynamics with optical transitions [120].

Among the possibilities to avoid decay from an intermediate state in a transition among motional states, one might think of using Stimulated Raman adiabatic passage (STIRAP) [121], which in principle does not populate the upper, intermediate state. This technique, however, is best suited for transitions involving a change in internal state, and its application to purely vibrational transitions (within the same internal state) is not straightforward. Numerical simulations show that several motional states are populated [122], and in fact the experimental applications of STIRAP for trapped ions have been only used for inducing carrier or sideband transitions that involve changing the internal state [123].

The objective of this chapter is to design fast controlled bias inversions of a double well so that the lowest states in each well remain as lowest states without residual excitation. Unlike multiplexing, however, there is no truly adiabatic slow process that achieves this state transformation. In the bias inversion depicted within the dashed-line frame of Fig. 6.1, for example, a slow bias change would preserve the order of the states according to their energy, so that the states represented in the third potential configuration would be interchanged (i.e., the gray state in the right well, and the white one in the left well). Nevertheless, in the limit in which the two wells are effectively independent, which in practice means, for times shorter than the tunneling time among the wells, the intended state transition might indeed be done slowly enough to be considered adiabatic. If we approximate each "isolated" well by a harmonic oscillator, the intended transformation amounts to a "horizontal" displacement along the interwell axis together with a rising or lowering of the energy of the wells. The latter effects, however, do not affect the intrawell dynamics, so we may focus on the displacement. In other words, within the stated approximations the bias inversion amounts to transporting a particle in a harmonic potential. Thus, to achieve a fast transition without residual excitation we may use STA designed to perform fast transport [8]. Specifically, we shall use a compensating-force approach [42, 124], equivalent to the FF scaling technique [7], based on adding to the potential a linear ramp with time-dependent slope to compensate for the effect of the trap motion in the noninertial frame of the trap. We shall compare this approach with a sudden bias switch, a FAQUAD approach [125], or a smooth polynomial connection without compensation. In Sec. 6.2 we introduce the compensating-force approach and Sec. 6.3 describes the alternative methods. In Sec. 6.4 numerical examples are presented with parameters appropriate for trapped ions in multisegmented, linear Paul traps,

and for neutral atoms in optical traps. Finally, in Sec. 6.5 we discuss the results and open questions.

6.2 Compensating-force approach

If the double-well potential with nearly independent wells is subjected to a bias inversion such that the trap frequencies of each well are essentially equal and constant throughout, and the trajectories of the well minima move in parallel, the process may be described by a parallel transport of two rigid harmonic oscillators, one for each well. The Hamiltonian potential near the minima may be approximated as

$$V_0(x - x_0) = \frac{1}{2} m\Omega_0^2 (x - x_0)^2, \tag{6.1}$$

where Ω_0 is the angular frequency and $x_0 = x_0(t)$ is the common notation for either of the two minima.[1] When needed, we may distinguish the minima as $x_{0,\pm}$, with $x_{0,+} > x_{0,-}$. The Hamiltonian $H_0 = p^2/2m + V_0(x - x_0)$ has eigenenergies

$$E_n = \left(n + \frac{1}{2}\right) \hbar\Omega_0, \tag{6.2}$$

and well-known normalized eigenstates $\phi_n(x - x_0)$, proportional to Hermite polynomials [69].

Adding to the Hamiltonian a linear term with an appropriate time-dependent slope, the noninertial effect of the motion of the well will be compensated in the trap frame [42, 124]. To define the trap frame consider the following position and momentum displacement unitary operator

$$\mathcal{U} = e^{ipx_0(t)/\hbar} e^{-im\dot{x}_0(t)x/\hbar}, \tag{6.3}$$

where the overdot represents a time derivative. Starting from the Schrödinger equation

$$i\hbar\partial_t|\psi\rangle = H_0|\psi\rangle, \tag{6.4}$$

the transformed wave function $|\Phi\rangle = \mathcal{U}|\psi\rangle$ obeys

$$i\hbar\partial_t|\Phi\rangle = \mathcal{U}H_0\mathcal{U}^\dagger|\Phi\rangle + i\hbar(\partial_t\mathcal{U})\mathcal{U}^\dagger|\Phi\rangle = H_0'|\Phi\rangle, \tag{6.5}$$

[1] We disregard purely time-dependent functions in each well. Differential phases among the wells depending on these functions can be ignored since the traps are assumed to be independent.

where the IP (trap frame) Hamiltonian is

$$H_0' = \frac{p^2}{2m} + V_0(x) + mx\ddot{x}_0 + \frac{1}{2}m\dot{x}_0^2, \tag{6.6}$$

and $V_0(x) = \frac{1}{2}m\Omega_0^2 x^2$. The term $m\dot{x}_0^2/2$ only depends on time; it does not affect the dynamics and can be ignored. To compensate the motion of the trap, we add $-mx\ddot{x}_0$ to H_0. This produces $-m(x + x_0)\ddot{x}_0$ in the trap frame and the resulting potential in that frame is reduced to $V_0(x)$, again neglecting purely time-dependent functions. $V_0(x)$ does not depend on time, so any stationary state in this trap frame will remain stationary, and excitations are avoided.

6.3 Alternative methods

In this section we discuss three simple alternative approaches to perform the bias inversion. They are all quite natural and simple approaches whose performance can be compared to that of the compensating force approach.

6.3.1 Sudden approach

In the sudden approach the potential is changed abruptly from the initial to the final configuration, but the state of the system remains unchanged immediately after the potential change (in general it will evolve afterwards). If the target state is ψ_{tar} the resulting fidelity is

$$F_s = |\langle\psi(0)|\psi_{tar}\rangle|. \tag{6.7}$$

6.3.2 Fast quasi-adiabatic approach

A quasi-adiabatic method to speed up adiabatic processes when there is one control parameter $\lambda(t)$ is based on distributing the adiabaticity parameter homogeneously in time (see Chapter 3). For instantaneous levels 0 and 1 this means

$$\hbar \left| \frac{\langle\phi_0|\partial_t\phi_1\rangle}{E_0 - E_1} \right| = c, \tag{6.8}$$

where the instantaneous eigenstates ϕ_0, ϕ_1 and eigenenergies E_0, E_1 depend on time through their dependence on λ, and c is constant. By the chain rule this becomes a first order differential equation for $\lambda(t)$, and c is set so that the boundary conditions for $\lambda(t)$ at initial time, $t = 0$, and final time t_f are satisfied. In the transport of a particle with a harmonic oscillator of angular frequency Ω_0 centered at $x_0(t)$ we set $\lambda(t) = x_0(t)$. Using the energies and eigenstates of the first two levels of the harmonic oscillator in Eq. (6.8), the FAQUAD condition becomes simply

$$\frac{m\dot{x}_0(t)}{\sqrt{2\hbar m\Omega_0}} = c. \tag{6.9}$$

The solution is the linear connection

$$x_0(t) = x_0(0) + [x_0(t_f) - x_0(0)]\frac{t}{t_f}. \tag{6.10}$$

The minimal t_f for which a zero of excitation energy appears is $2\pi/\Omega_0$ [73, 125].

6.3.3 Polynomial connection without compensation

The final and initial values of the control parameter may as well be smoothly connected without applying any compensation, for example, using a fifth order polynomial that assures the vanishing of first and second derivatives of the parameter at the boundary times.

6.4 Examples

In the following examples, the potentials and parameters are adapted for a trapped ion in a multisegmented Paul trap, and for a neutral atom in a dipole trap.

6.4.1 Trapped ions

For a trapped ion we consider a simple double-well potential of the form

$$V(x,t) = \beta x^4 + \alpha x^2 + \gamma x, \tag{6.11}$$

with $\alpha(t) < 0$ and $\beta(t) > 0$ [126–128]. α and β are assumed to be constant and $\gamma \equiv \gamma(t)$ time dependent. The bias inversion implies a change of sign of $\gamma(t)$ from $\gamma_0 > 0$ to $-\gamma_0$.

From $\frac{\partial V}{\partial x} = 0$ the condition for the extrema becomes

$$4\beta x^3 + 2\alpha x + \gamma = 0. \tag{6.12}$$

It is useful to define

$$\begin{aligned} A &= 0, \\ B &= \frac{2\alpha}{4\beta}, \\ C &= \frac{\gamma}{4\beta}, \end{aligned} \tag{6.13}$$

and

$$\begin{aligned} Q &= \frac{A^2 - 3B}{9}, \\ R &= \frac{2A^3 - 9AB + 27C}{54}. \end{aligned} \tag{6.14}$$

When $R^2 < Q^3$ there are two minima and one maximum. With $\alpha < 0$ and $\beta > 0$, this is satisfied for

$$|\gamma| < \left(\frac{2}{3}\right)^{3/2} \sqrt{-\frac{\alpha^3}{\beta}}. \tag{6.15}$$

The trajectories of the minima are

$$x_{0,\pm} = -2\sqrt{Q}\cos\left(\frac{\theta + (1 \pm 1)\pi}{3}\right) - \frac{A}{3}, \tag{6.16}$$

where $\theta = \arccos\left(\frac{R}{\sqrt{Q^3}}\right)$, $0 \leqslant \theta \leqslant \pi$ and the roots are taken to be positive. Up to second order in γ they are

$$x_{0,-} \approx -\frac{1}{\sqrt{2}}\sqrt{-\frac{\alpha}{\beta}} + \frac{\gamma}{4\alpha} - \frac{3\gamma^2\sqrt{-\alpha\beta}}{16\sqrt{2}\alpha^3}, \tag{6.17}$$

$$x_{0,+} \approx \frac{1}{\sqrt{2}}\sqrt{-\frac{\alpha}{\beta}} + \frac{\gamma}{4\alpha} + \frac{3\gamma^2\sqrt{-\alpha\beta}}{16\sqrt{2}\alpha^3}. \tag{6.18}$$

The quadratic term in γ is negligible with respect to the linear term when

$$|\gamma| \ll \frac{4\sqrt{2}}{3}\sqrt{-\frac{\alpha^3}{\beta}}, \tag{6.19}$$

which implies that the trajectories for the minima move in parallel. Note that this inequality automatically implies the one in Eq. (6.15). Neglecting the quadratic term, the two minima are given by

$$x_{0,\pm} = \pm\frac{1}{\sqrt{2}}\sqrt{-\frac{\alpha}{\beta}} + \frac{\gamma}{4\alpha}. \tag{6.20}$$

The distance between the minima is

$$\begin{aligned} D &= 2\sqrt{Q}\left\{\cos\left(\frac{\theta}{3}\right) + \sin\left[\frac{1}{6}(\pi + 2\theta)\right]\right\} \\ &\approx \sqrt{2}\sqrt{-\frac{\alpha}{\beta}} + \frac{3\sqrt{-\alpha\beta}}{8\sqrt{2}\alpha^3}\gamma^2. \end{aligned} \tag{6.21}$$

We may also compute the energy bias between the two wells as

$$\delta = \gamma D. \tag{6.22}$$

The distance travelled by each well is, when (6.19) is fulfilled, $d = \gamma_0/(2\alpha)$ [see Eqs. (6.17) and (6.18)], and the effective frequency at each minimum

$$\omega_0 = \sqrt{\frac{1}{m}\left(\frac{d^2V}{dx^2}\right)_{x=x_0}}. \tag{6.23}$$

For Eq. (6.11) the effective frequencies are

$$\begin{aligned} \omega_{0,\pm} &= \sqrt{\frac{2}{m}}\sqrt{\alpha + \frac{2}{3}\beta\left\{A + 6\sqrt{Q}\cos\left[\frac{1}{3}\left(\frac{\theta + (1\pm 1)\pi}{3}\right)\right]\right\}^2} \\ &\approx 2\sqrt{-\frac{\alpha}{m}} \mp \frac{3}{2\sqrt{2}}\sqrt{\frac{\beta}{\alpha^2 m}}\gamma. \end{aligned} \tag{6.24}$$

Hence, comparing the two terms, the condition for the frequencies to be essentially constant

$$\omega_{0,\mp} \approx \Omega_0 \equiv 2\sqrt{-\frac{\alpha}{m}} \tag{6.25}$$

is again the inequality in Eq. (6.19).

In the regime where the inequality (6.19) holds, we can apply the compensating force approach to implement a fast bias inversion. Since the compensating term $-mx\ddot{x}_0$ is equal for both harmonic traps, we add it to V in Eq. (6.11), and the resulting Hamiltonian H is

$$H = \frac{p^2}{2m} + \beta x^4 + \alpha x^2 + (\gamma - m\ddot{x}_0)x. \tag{6.26}$$

Note that the compensation amounts to changing the time dependence of the slope of the linear term from the reference process defined by $\gamma(t)$ to

$$\gamma_{eff}(t) \equiv \gamma(t) - m\ddot{x}_0(t) = \frac{\gamma(t) - m\ddot{\gamma}(t)}{4\alpha}. \tag{6.27}$$

To set $\gamma(t)$ we design a connection between the initial and final configurations. First note the boundary conditions

$$\begin{aligned} \gamma(0) &= \gamma_0 > 0, \\ \gamma(t_f) &= -\gamma_0, \end{aligned} \tag{6.28}$$

which we complement by

$$\begin{aligned} \dot{\gamma}(t_b) &= 0, \\ \ddot{\gamma}(t_b) &= 0, \\ t_b &= 0, t_f, \end{aligned} \tag{6.29}$$

so that $\dot{x}_0(t_b) = \ddot{x}_0(t_b) = 0$. This implies that $\mathcal{U}(t_b) = e^{ipx_0(t_b)/\hbar}$ and $\dot{\mathcal{U}}(t_b) = 0$. Therefore, the Hamiltonians and the wave functions in interaction and Schrödinger pictures transform into each other by a simple coordinate displacement. At intermediate times, we interpolate the function as $\gamma(t) = \sum_{n=0}^{5} c_n t^n$, where the coefficients are found by solving Eqs. (6.28) and (6.29). Finally,

$$\begin{aligned} \gamma(t) &= \gamma(0) + 10[\gamma(t_f) - \gamma(0)]s^3 \\ &- 15[\gamma(t_f) - \gamma(0)]s^4 + 6[\gamma(t_f) - \gamma(0)]s^5, \end{aligned} \tag{6.30}$$

where $s = t/t_f$. This function and examples of γ_{eff} are shown in Fig. 6.2.

In order to compare the robustness of the compensating force method against the alternative ones we consider a $^9Be^+$ ion in the double well with the realistic parameters $\alpha = -4.7$ pN/m and $\beta = 5.2$ mN/m^3, similar to those in [129]. For a

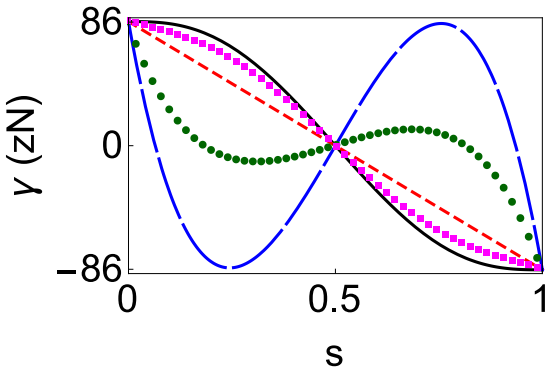

FIGURE 6.2: γ versus $s = t/t_f$ for the polynomial in Eq. (6.30) (solid black line) and FAQUAD (short-dashed red line). $\gamma_0 = 86.4$ zN, $\gamma(t_f) = -\gamma_0$, $\alpha = -4.7$ pN/m, and $\beta = 5.2$ mN/m^3. Also shown are the different effective slopes adding a compensation to the polynomial, $\gamma_{eff}(t) = \gamma(t) - m\ddot{\gamma}(t)/(4\alpha)$, for the mass of ^{9}Be$^+$ and times $t_f = 0.07$ μs (long-dashed blue line); $t_f = 0.1$ μs (green dots); and $t_f = 0.3$ μs (magenta squares).

moderate initial bias compared to the vibrational quanta, such as

$$\gamma_0 \sim \frac{\hbar\Omega_0}{D}, \tag{6.31}$$

the fidelity provided by the sudden approach is one for all practical purposes so we can change the bias abruptly and reach the target state. The displacement of the trap d may be compared with the oscillator characteristic length $a_0 = \sqrt{\hbar/m\Omega_0}$. Their ratio is

$$R = \frac{d}{a_0} = \frac{\gamma_0}{2\alpha}\sqrt{\frac{m\Omega_0}{\hbar}}. \tag{6.32}$$

For the Paul trap $R \approx 0.00065$, which explains the high fidelity of the sudden approach for a moderate bias inversion of the ion. At these bias values there is really no need to apply a more sophisticated protocol than the sudden switch.

Henceforth, we assume a much larger γ_0, but still satisfying the condition (6.19). In particular, for an initial bias of 1000 $\Omega_0\hbar$ (corresponding to $\gamma_0 = 86.4$ zN), the ratio becomes $R \approx 0.65$. The maximum variation of the difference between the trajectories of the minima is 3 pm, about three orders of magnitude less than the displacement of each minimum (9.2 nm), so the minima follow parallel trajectories. Furthermore, the maximum variation of the frequencies in Eq. (6.24) with respect to $\Omega_0 = 2\pi \times 5.6$ MHz is $2\pi \times 3.7$ kHz, so the effective frequency is nearly constant.

Figure 6.3 demonstrates the effect of the compensating-force approach. Starting from the ground state of the lower (left) well, the final evolved state following

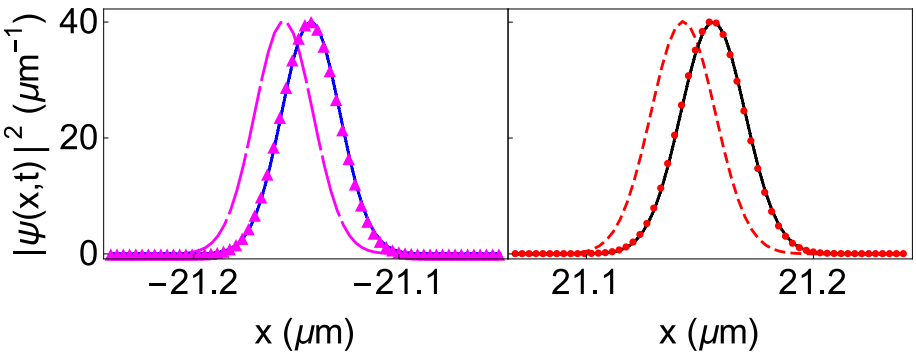

FIGURE 6.3: Left: Ground state of the left well at $t = 0$ (long-dashed magenta line) and at $t = t_f$ (magenta triangles), and final state with the compensating force applied on the double well (solid blue line). Right: Ground state of the right well: at $t = 0$ (short-dashed red line) and at $t = t_f$ (red dots) and final state with the compensating force applied (solid black line). $t_f = 4$ ns and other parameters as in Fig. 6.2 for $^9Be^+$.

the shortcut with compensation stays as the "ground state" of the left well. This is actually defined as the lowest state of the double-well system predominantly located on the left. There is a similar process for the right well. The final states represented are obtained by solving the Schrödinger equation with the full Hamiltonian (6.26).

Figure 6.4 is for the process in the left well. It compares the fidelity at final time and the excitation energy, defined as $E_{ex} = E(t_f) - E_0(t_f)$ where $E(t_f)$ is the final energy after the quantum evolution following the shortcut and $E_0(t_f)$ is the ground state final energy of the upper harmonic well, using the polynomial (6.30) for γ with and without compensation, as well as the results of the FAQUAD approach. The fidelity without compensation tends to the fidelity of the sudden approach (0.89) for very short final times. The method with compensation clearly outperforms the others. In principle, a fundamental limitation of the approach is due to the fact that the inequality (6.19), which guarantees parallel motion and stable frequencies of the wells, should as well be satisfied by γ_{eff}, but, at very short times, the dominant term of $\gamma_{eff} \sim -m\ddot{\gamma}/4\alpha$ may be too large. To estimate this short time limit we combine the mean-value theorem inequality for the maximum [42], $|\ddot{\gamma}|_{max} \geqslant 4\gamma_0/t_f^2$, with Eq. (6.19) for γ_{eff} to find the condition

$$t_f \gg \left(\frac{3m\gamma_0}{4\sqrt{2}}\sqrt{-\frac{\beta}{\alpha^5}}\right)^{1/2}. \tag{6.33}$$

The factor on the right-hand side is 10^{-9} s for this example (see Fig. 6.4), which

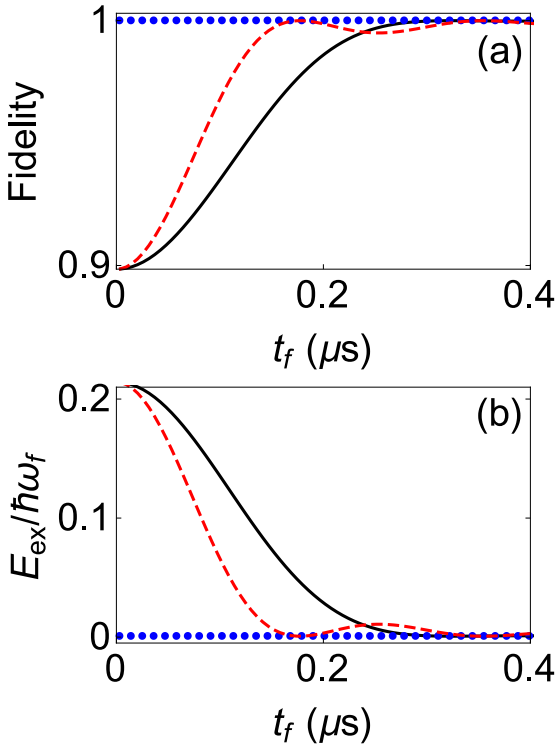

FIGURE 6.4: (a) Fidelity $|\langle\phi_L(t_f)|\psi(t_f)\rangle|$, where $|\phi_L(t_f)\rangle$ is the lowest state located in the left well in the final time configuration, and $|\psi(t_f)\rangle$ is the evolved state following the shortcut at final time. (b) Final excitation energy for the process on the left well using compensating-force (blue dots), fifth degree polynomial in Eq. (6.30) (solid black line), and FAQUAD (short-dashed red line). The parameters are for $^9Be^+$ as in Fig. 6.2.

is several orders of magnitude smaller than $2\pi/\Omega_0$ and does not affect the fidelity in the scale of times shown.

6.4.2 Neutral atoms

The potential introduced in Chapter 4 (Sec. 4.4),

$$V_{na}(x,t) = \frac{1}{2}m\omega^2 x^2 + V_0 \cos^2\left[\frac{\pi(x-\Delta x)}{d_l}\right], \tag{6.34}$$

forms also a double well. It was implemented in [35] with optical dipole potentials, combining a harmonic confinement due to a crossed beam dipole trap with a periodic light shift potential provided by the interference pattern of two mutually coherent laser beams. ω is the angular frequency of the dipole trap about the waist position, V_0 the amplitude, Δx the displacement of the optical lattice relative to the center of the harmonic well, and d_l is the lattice constant. (Double wells

with a controllable bias may be also realized by two optical lattices of different periodicity with controllable intensities and relative phase [82]). Here, the bias inversion implies a change of sign of $\Delta x(t)$ from $\Delta x_0 > 0$ to $-\Delta x_0$.

To check if the conditions to apply the compensating force approach hold here as well, an analysis similar to the one in the previous example is now performed. We approximate the potential around each minimum, $V^{(\pm)}$, up to fourth order. From $\frac{\partial V^{(\pm)}}{\partial x} = 0$ we get a cubic equation for each minimum. The positions of the minima are thus given by

$$x_{0,\pm} = -2\sqrt{Q}\cos\left(\frac{\theta^{(\pm)} - 2\pi}{3}\right) - \frac{A^{(\pm)}}{3}, \tag{6.35}$$

where

$$\begin{aligned} Q &= \frac{2d_l^2\pi^2 V_0 + d_l^4 m\omega^2}{4\pi^4 V_0}, \\ A^{(\pm)} &= -\frac{3}{2}(2\Delta x \pm d_l), \\ \theta^{(\pm)} &= \cos\left[\frac{-3d_l(2\Delta x \pm d_l)m\pi^2\sqrt{V_0}\omega^2}{2(2\pi^2 V_0 + d_l^2 m\omega^2)^{3/2}}\right]^{-1}. \end{aligned} \tag{6.36}$$

Up to a second order in Δx,

$$x_{0,\pm} \approx \pm a + b\Delta x \pm c\Delta x^2, \tag{6.37}$$

where the coefficients are known explicitly but too lengthy to be displayed here. Whenever the quadratic term is negligible with respect to the linear term ($c\Delta x^2 \ll b\Delta x$), we can approximate $x_{0,\pm} = \pm a + b\Delta x$ (parallel motion). The distance between the minima is given by

$$\begin{aligned} D &= \frac{1}{3}\left\{A^{(-)} - A^{(+)} + 6\sqrt{Q}\left[-\cos\left(\frac{\pi + \theta^{(-)}}{3}\right)\right.\right. \\ &+ \left.\left.\cos\left(\frac{\pi + \theta^{(+)}}{3}\right)\right]\right\} \approx 2a + 2c\Delta x^2. \end{aligned} \tag{6.38}$$

Moreover, $\omega_{0,\pm} \approx f \mp g\Delta x$, again with known but lengthy coefficients g and f. As long as $g\Delta x \ll f$, we may set $\omega_{0,\pm} \approx \Omega_0 \equiv f$.

For realistic parameters the conditions for parallel transport of the minima and constant frequency are indeed satisfied. We consider a ^{87}Rb atom in the trap and set the parameters in Chapter 4 after the demultiplexing process, namely,

$d_l = 5.18$ μm, $\omega = 2\pi \times 59.4$ Hz, and $V_0/h = 1.4$ kHz; the time-dependent displacement $\Delta x = \Delta x(t)$ is the control parameter to perform the bias inversion, such that

$$\begin{aligned} \Delta x(0) &= \Delta x_0, \\ \Delta x(t_f) &= -\Delta x_0, \end{aligned} \tag{6.39}$$

with $\Delta x_0 = 200$ nm. We also impose

$$\begin{aligned} \dot{\Delta} x(0) &= 0, \\ \ddot{\Delta} x(0) &= 0, \\ \dot{\Delta} x(t_f) &= 0, \\ \ddot{\Delta} x(t_f) &= 0 \end{aligned} \tag{6.40}$$

to achieve similar conditions in the derivatives of the minima x_0. At intermediate times, we interpolate the function as $\Delta x(t) = \sum_{n=0}^{5} d_n t^n$, where the coefficients are found by solving Eqs. (6.39) and (6.40). Consequently, the connection between the initial and final Hamiltonians is given by the same polynomial in Eq. (6.30) changing $\gamma(t) \to \Delta x(t)$. The double wells are much deeper and tight for trapped ions than for neutral atoms; compare an intrawell angular frequency Ω_0 of $2\pi \times 5.6$ MHz for the ions versus $2\pi \times 0.35$ kHz for the optical trap. Therefore, in this case, for a moderate initial bias compared to the vibrational quanta, the ratio between the displacement of the trap d and the oscillator characteristic length a_0 is $R \approx 0.67$.

With the parameters given at time $t = 0$, the separation of the minima is $D = 5$ μm, the bias between minima $\delta = 2.02 \times 10^{-32}$ J, and the effective angular frequency $\Omega_0 = 2\pi \times 0.35$ kHz, whereas the maximum variation of the frequencies along the process is approximately $2\pi \times 0.2$ Hz. Furthermore, the maximum deviation from D of the minima separation is 1.8 nm, whereas the displacement of each minimum is about 0.4 μm. In summary, the minima do move in parallel with constant, equal frequencies for practical purposes.

To accelerate the bias inversion we add the compensating term to V in Eq. (6.34),

$$H = \frac{p^2}{2m} + \frac{1}{2} m\omega^2 x^2 + V_0 \cos^2\left[\frac{\pi(x - \Delta x)}{d_l}\right] - m x \ddot{x}_0. \tag{6.41}$$

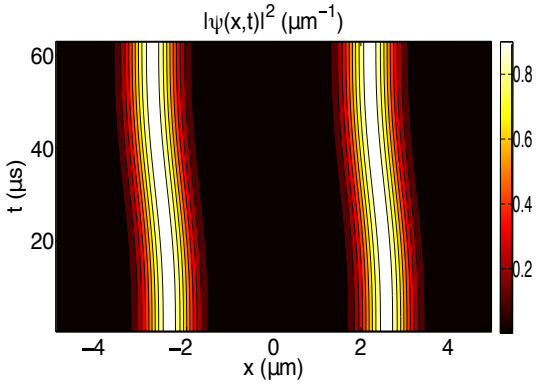

FIGURE 6.5: Evolution of the wave function densities following the shortcut in Eq. (6.41) for states in left and right wells. The parameters are for ^{87}Rb: $d_l = 5.18$ μm, $\omega = 59.4 \times 2\pi$ Hz, $V_0/h = 1.4$ kHz, $\Delta x_0 = 200$ nm, and $t_f = 63$ μs.

Figure 6.5 shows the evolution of the densities. Focusing on the left well, Fig. 6.6(a) demonstrates that the fidelity is exactly one (blue dots) with the compensating force. However, using for the inversion the fifth degree polynomial in Eq. (6.30) [with the change $\gamma(t) \to \Delta x(t)$] without compensation, the fidelity at short final times decreases until the value of the sudden approach, 0.9. Furthermore, the excitation (residual) energy E_{ex} is approximately zero for the shortcut protocol, compared to the excitation without compensation in Fig. 6.6(b).

6.5 Discussion

We have proposed a method to invert the bias of a double-well potential, in the regime of independent wells, to keep the final states motionally unexcited within the same original well. The method treats the bias inversion as a rigid transport of the wells, which is justified for realistic parameters, and applies a "compensating-force" to cancel the excitations. Examples have been worked out for ions or neutral atoms, and comparisons have been provided with a sudden approach, a FAQUAD approach, or a smooth polynomial connection of initial and final bias without compensation. The compensating-force method clearly outperforms the others and gives perfect fidelities under ideal conditions, up to very small times compared, e.g., with the time $2\pi/\Omega_0$ (one oscillation period) where FAQUAD provides a first zero of the excitation energy. The feasibility of the approach may be analyzed in the light of current technology in the two systems examined:

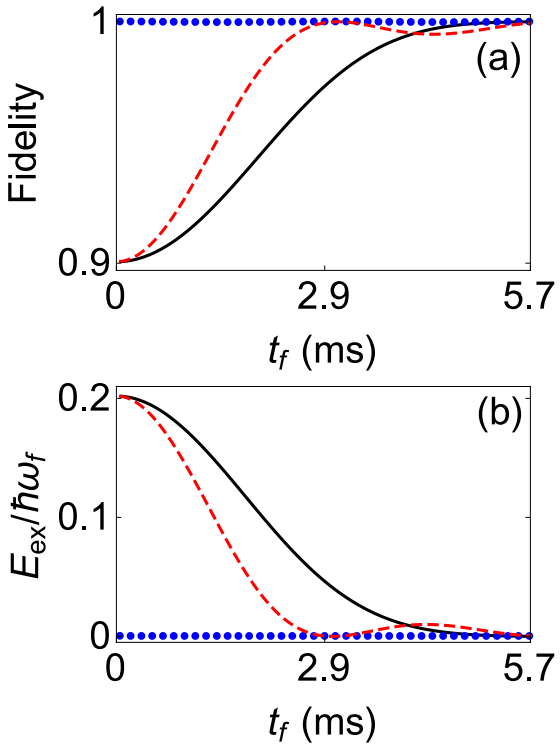

FIGURE 6.6: (a) Fidelity $|\langle\varphi_1(t_f)|\psi(t_f)\rangle|$, where $|\varphi_1(t_f)\rangle$ is the lowest state predominantly of the left well at final time (the first excited state of the double well) and $|\psi(t_f)\rangle$ is the evolved state following the shortcut at final time. (b) Final excitation energy. Compensating-force approach (blue dots), fith degree polynomial in Eq. (6.30) with the change $\gamma(t) \to \Delta x(t)$ without compensation (solid black line), and FAQUAD approach (short-dashed red line). The parameters are chosen for ^{87}Rb: $d_l = 5.18$ μm, $\omega = 59.4 \times 2\pi$ Hz, $V_0/h = 1.4$ kHz, and $\Delta x_0 = 200$ nm.

1. For trapped ions we have considered initial and final values differing by $\Delta\gamma \approx 200$ zN, whereas resolutions of 15 zN of have been reported [130]. As for the timing, much effort is being put into achieving suboscillation-period resolutions for the potential update [131–133] in ion transport experiments. The possibility to switch on and off potentials in a few nanoseconds, much faster than the ion oscillation period, has been demonstrated [133]. The designed bias inversion is thus in reach with current technology.

2. For neutral atoms, the minimal process times t_f are not limited by the method per se but by the technical capabilities to implement the maximal compensating force. This force depends on the maximal acceleration of the well, whose lower bound is known to be $a_{\max} = 2d/t_f^2$ [42]. To implement the compensation with a magnetic field gradient G, the gradient should be of the order of $G \simeq ma_{\max}/\mu_B$ in an amount of time t_f (μ_B is Bohr's

magneton). For rubidium atoms polarized in the magnetic level $F = m_F = 2$ and the transport parameters considered above, this requires a magnetic field gradient on the order of 40 T/m shaped on a time interval $t_f = 63$ μs. This is definitely challenging from an experimental point of view. Alternatively, one can use the dipole force of an out of axis Gaussian laser beam. If the double well is placed on the edge at a distance of $w/2$ where w is the waist and if α_p denotes the polarizability, the local potential slope experienced by the atoms is on the order of $\alpha_p P/w^3$, where P is the power of the beam. The compensation requires that $P/w^3 = m/\alpha_p$. For instance, with an out-of-resonance beam at a wavelength of 1 μm, the polarizability of rubidium-87 atoms is $\alpha_p \simeq 1.3 \times 10^{-36}$ m^{2}s, and the compensation can be performed using a 1W laser with a waist of 20 μm. As for the timing, a submicrosecond time scale for shaping the offset potential is perfectly achievable using a control of the intensity based on acousto-optics modulators.

A relevant feature of the proposed approach is that the reference process used to design the corresponding compensation (we have used a polynomial for simplicity) may be chosen among a broad family of functions satisfying Eqs. (6.28) and (6.29). As in other STA approaches, this flexibility may be used to enhance robustness versus noise and perturbations [68, 134, 135].

The bias inversion put forward here and the multiplexing and demultiplexing protocols developed in [74], see Chapter 4, provide the necessary toolkit to perform vibrational state inversions [104, 105], or Fock state preparations [74]. Applications in optical waveguide design are also feasible [41]. As well, the fast bias inversion is directly applicable to Bose-Einstein condensates [63, 136]. Generalizations for conditions in which rigid transport does not hold are also possible using invariant theory [42], which allows for finding processes without final excitation where both the frequency and position of the well depend on time [137].

Conclusions

In this Thesis a set of Shortcuts-to-Adiabaticity (STA) techniques have been developed and applied to speed up adiabatic processes in systems confines by double-well potentials. The main results can be summarized as follows:

- **Engineering fast and stable splitting of matter waves**
  - Wave-packet splitting is very unstable with respect to slight trap asymmetries. The adiabatic following produces the collapse of the wave into the lower well. We used the fast-forward (FF) approach to accelerate and stabilize the separation.
  - We also introduced a simple moving two-mode model, which combined with sudden and adiabatic approximations provides a stability criterion. This model has also played an important role in the rest of the Thesis.
  - Furthermore, we applied the shortcut to speed up the splitting of a condensate in the mean-field regime.
- **Shortcuts to adiabaticity in three-level systems using Lie transforms**
  - The shortcuts based on the counterdiabatic approach are, in most cases, difficult to implement in the laboratory, so we developed alternative, realizable protocols making use of the dynamical symmetry of the Hamiltonian.
  - The new approaches have been designed by means of a Lie transform. Although the transformations are formally equivalent to interaction-picture (IP) transformations, the resulting IP Hamiltonian and state represent a different physical process from the original one.

  - Mott-insulator transitions and beam splitter implementations have been stabilized and accelerated thanks to the new, Lie-based STA.

- **Fast quasi-adiabatic dynamics**

  - General properties of a "fast-quasi-adiabatic" (FAQUAD) method based on using the time dependence of a control parameter to delocalize in time the transition probability among adiabatic levels have been found.

  - The approach has been applied to different systems where other approaches are not available. In particular, in a two-site boson system and in a many-particle system.

  - Another important result is the discovery that FAQUAD is optimal within the sequence of iterative superadiabatic frames.

- **Vibrational mode multiplexing of ultracold atoms**

  - Processes to achieve fast vibrational-state multiplexing or demultiplexing have been designed. The invariant-based inverse engineering protocol has been applied in a two-mode model and then mapped onto a realistic potential.

  - While protocols calculated with an Optimal Control Theory (OCT) algorithm are quite difficult to implement experimentally, our proposal relies on a smooth potential deformation.

- **Compact and high conversion efficiency mode-sorting asymmetric Y junction using shortcuts to adiabaticity**

  - The power of the approach used to reproduce fast multiplexing and demultiplexing processes is demonstrated in the context of optical waveguides. Specifically, a short mode-sorting asymmetric Y junction has been worked out.

- **Fast bias inversion of a double well without residual particle excitation**

  - The compensating-force method has been applied to realize a fast bias inversion, both for trapped ions and for neutral atoms.

- The combination of the bias inversion and multiplexing/demultiplexing processes can be used to induce vibrational state inversions based on trap deformations only. The possibility of achieving a population inversion without using internal-state excitations is of much interest. In particular, for trapped ions this amounts to a species-independent approach based entirely on the charge and electric forces.

- The implementation of a fast and stable bias inversion could be useful also to produce vibrationally excited Fock states from an initial ground state.

Appendix

Appendix A

Interaction versus asymmetry for adiabatic following

Making some simplifying assumptions, we find the conditions under which the interacting condensate ground state splits adiabatically, instead of collapsing into the deepest well. We consider complete splitting of the trap into separated wells and also $\delta(t_f) \ll \lambda$, so that the noninteracting wave would collapse (see Sec. 1.4). In atomic interferometry, the two split branches of the condensate have to be individually addressed and manipulated during the differential phase accumulation stage, so that tunnelling must be negligible [12, 16, 138]. We also assume that the two ground states of the final wells can be approximated by ground states of harmonic oscillators at $\pm x_f$, with the right one lifted by λ:

$$V_L = \frac{1}{2}m\omega^2(x+x_f)^2, \tag{A.1}$$

$$V_R = \frac{1}{2}m\omega^2(x-x_f)^2 + \lambda. \tag{A.2}$$

The total energy is approximated as $E_{tot} = E_L + E_R$. For $j = L, R$,

$$E_j = N_j \int dx \phi_j \left[-\frac{\hbar^2 \partial_x^2}{2m} + V_j \right] \phi_j + \frac{1}{2} g_1 N_j^2 \int dx |\phi_j|^4, \tag{A.3}$$

where

$$\phi_j(x) = \frac{1}{[\sqrt{\pi} a_0]^{1/2}} e^{[-(x \pm x_f)^2/2a_0^2]}, \tag{A.4}$$

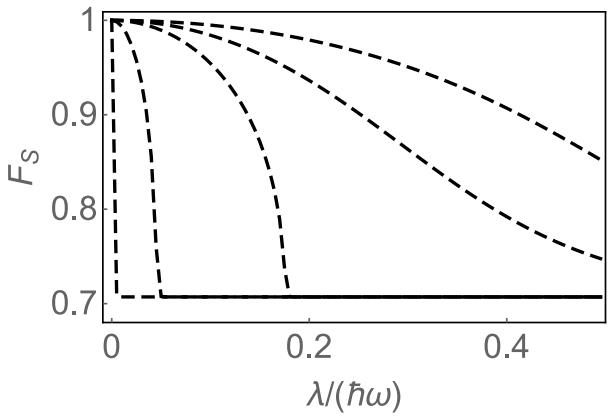

FIGURE A.1: Structural fidelities for the Bose-Einstein condensate. From left to right, $\widehat{g_1}N = 0, 0.138, 0.55, 0.69,$ and 1.38. In all curves $x_f = 4$ μm and $\omega = 780$ rad/s. Equation (1.23) was used to design the potential V_{FF}.

and the total number of particles is $N = N_R + N_L$. The result is

$$E_L = N_L \frac{\hbar\omega}{2} + \frac{\widehat{g_1}}{2\sqrt{2\pi}}\hbar\omega N_L^2, \tag{A.5}$$

$$E_R = N_R \left(\frac{\hbar\omega}{2} + \lambda\right) + \frac{\widehat{g_1}}{2\sqrt{2\pi}}\hbar\omega N_R^2, \tag{A.6}$$

where

$$\widehat{g_1} = g_1/(\hbar\omega a_0). \tag{A.7}$$

From the minimum-energy condition, $\partial E_{tot}/\partial N_R = 0$, it follows that

$$\frac{\Delta N}{N} = \sqrt{2\pi}\frac{\lambda/\hbar\omega}{\widehat{g_1}N}, \tag{A.8}$$

with $\Delta N = N_L - N_R$. (See [21] for a similar treatment in the Thomas-Fermi regime.) Thus, collapse into one well is avoided when $\lambda/(\hbar\omega\widehat{g_1}N) \ll 1$. This relation sets the scale for the uncontrolled and, possibly, unknown asymmetry that may be tolerated to achieve balanced splitting. Adiabatic control of population imbalance requires control of the energy splitting of the order $\lambda \lesssim (\hbar\omega\widehat{g_1}N)$.

Figure A.1 shows the structural fidelity $F_S(\lambda)$ for several values of $\widehat{g_1}N$. The sharp drop at $\widehat{g_1}N = 0$ is substituted by more and more stable curves as $\widehat{g_1}N$ increases. For the splitting described in [34] and [35] using ^{87}Rb, we get $\widehat{g_1}N \approx 9.5$, quite large compared to the values in Fig. A.1. Under these conditions, adiabatic splitting is very stable with respect to minor asymmetries. Moreover, F_S decays slowly with respect to λ, so that the relative population imbalance may be prepared at will by controlling the asymmetry. In [34] and [35] the asymmetry is due to a

potential shift that can be controlled with a standard deviation of 100 nm, whereas a displacement of $\sim 1\mu$m is required for the total collapse into one of the wells.

Appendix B

Lie algebra

The algebra of this three-level system is a four-dimensional Lie Algebra U3S3 according to the classification of four-dimensional Lie algebras in [54]. (For comparison with that work it is useful to rewrite the generators in the skew-Hermitian base $\tilde{G}_k = -iG_k$, $k = 1, 2, 3, 4$.) $U3S3$ is a direct sum of the one-dimensional algebra spanned by the invariant $G_4 - G_3$, that commutes with all members of the algebra, and a three-dimensional SU(2) algebra spanned by $\{G_1, G_2, G_3\}$. Notice that this realization of the three-dimensional (3D) algebra is not spanned by the matrices

$$J_x = \frac{1}{\sqrt{2}} \begin{pmatrix} 0 & 1 & 0 \\ 1 & 0 & 1 \\ 0 & 1 & 0 \end{pmatrix}, J_y = \frac{1}{\sqrt{2}} \begin{pmatrix} 0 & -i & 0 \\ i & 0 & -i \\ 0 & i & 0 \end{pmatrix}, J_z = \begin{pmatrix} 1 & 0 & 0 \\ 0 & 0 & 0 \\ 0 & 0 & -1 \end{pmatrix}, \quad \text{(B.1)}$$

which correspond, in the subspace $|2,0\rangle, |1,1\rangle, |0,2\rangle$, to the operators

$$J_x = \frac{1}{2}\left(a_1^\dagger a_2 + a_2^\dagger a_1\right), \quad \text{(B.2)}$$

$$J_y = \frac{1}{2i}\left(a_1^\dagger a_2 - a_2^\dagger a_1\right), \quad \text{(B.3)}$$

$$J_z = \frac{1}{2}\left(a_1^\dagger a_1 - a_2^\dagger a_2\right). \quad \text{(B.4)}$$

In particular we cannot get the matrices for J_y or J_z by any linear combination of our G_k matrices [see Eqs. (2.3-2.4)]. A second-quantized form for the G_k consistent

with the matrices includes quartic terms in annihilation and creation operators:

$$\begin{aligned} G_1 &= \frac{1}{4}\left(a_1^\dagger a_2 + a_2^\dagger a_1\right), \\ G_2 &= \frac{1}{4i}\left[a_1^\dagger a_2^\dagger\left(a_1 a_1 + a_2 a_2\right) - \left(a_1^\dagger a_1^\dagger + a_2^\dagger a_2^\dagger\right) a_1 a_2\right], \\ G_3 &= \frac{1}{8}\left[\left(a_1^\dagger a_1^\dagger + a_2^\dagger a_2^\dagger\right) a_1 a_1 - 4 a_1^\dagger a_2^\dagger a_1 a_2 + \left(a_1^\dagger a_1^\dagger + a_2^\dagger a_2^\dagger\right) a_2 a_2\right], \\ G_4 &= \frac{1}{4}\left(a_1^\dagger a_1 - a_2^\dagger a_2\right)^2. \end{aligned} \tag{B.5}$$

These second-quantized operators do not form a closed algebra under commutation, but their matrix elements for two particles do.

An invariant (defined in a Lie-algebraic sense) commutes with any member of the algebra. There are generically two independent invariants for $U3S3$ [139]. For the matrix representation in Eqs. (2.3) and (2.4) they are

$$\begin{aligned} I_1 &= G_1^2 = G_2^2 = G_3^2 = \frac{1}{8}\begin{pmatrix} 1 & 0 & 1 \\ 0 & 2 & 0 \\ 1 & 0 & 1 \end{pmatrix}, \\ I_2 &= G_4 - G_3 = \frac{1}{4}\begin{pmatrix} 3 & 0 & -1 \\ 0 & 2 & 0 \\ -1 & 0 & 3 \end{pmatrix}. \end{aligned} \tag{B.6}$$

I_1, which is not in the algebra, has eigenvalues

$$\begin{aligned} \lambda_1^{(2)} &= 1, \\ \lambda_1^{(1,3)} &= \frac{1}{2}, \end{aligned} \tag{B.7}$$

and I_2, a member of the algebra, has eigenvalues

$$\begin{aligned} \lambda_2^{(2)} &= 0, \\ \lambda_2^{(1,3)} &= \frac{1}{4}. \end{aligned} \tag{B.8}$$

The two invariants have the same eigenvectors,

$$\begin{aligned} |u^{(1)}\rangle &= \frac{1}{\sqrt{2}}(|2,0\rangle + |0,2\rangle), \\ |u^{(2)}\rangle &= \frac{1}{\sqrt{2}}(|2,0\rangle - |0,2\rangle), \\ |u^{(3)}\rangle &= |1,1\rangle, \end{aligned} \tag{B.9}$$

with $|u^{(1)}\rangle$ and $|u^{(3)}\rangle$ spanning a degenerate subspace.

Lie-algebraic invariants constructed with time-independent coefficients satisfy as well the equation

$$i\hbar\frac{\partial I_{1,2}}{\partial t} + [H(t), I_{1,2}] = 0 \tag{B.10}$$

so they are also dynamical invariants [6] [i.e., operators that satisfy Eq. (B.10) whose expectation values remain constant]. The degenerate subspace of eigenvectors allows the existence of time-dependent eigenstates of time-independent invariants. In particular, in all the examples in the main text, the dynamics takes place within the degenerate subspace: the initial state is $|u^{(3)}\rangle$ at $t = 0$ and ends up in some combination of $|u^{(1)}\rangle$ and $|u^{(3)}\rangle$ at t_f. The specific state as a function of time is known explicitly, $|\psi_I(t)\rangle = e^{i\alpha(t)G_4}e^{-i\int_0^t E_1 dt'}|\phi_1(t)\rangle$; see Eq. (2.23). Note that $|\phi_1\rangle$ and $|\phi_3\rangle$ in Eqs. (2.11) and (2.13) are two orthogonal combinations of $|u^{(1)}\rangle$ and $|u^{(3)}\rangle$. Also $|u^{(2)}\rangle = |\phi_2\rangle$; see Eq. (2.12). In the nondegenerate subspace spanned by $|u^{(2)}\rangle$ "nothing evolves", other than a phase factor, but the initial states in the examples do not overlap with it.

Bibliography

[1] X. Chen, A. Ruschhaupt, S. Schmidt, A. del Campo, D. Guéry-Odelin, and J. G. Muga, "*Fast Optimal Frictionless Atom Cooling in Harmonic Traps: Shortcut to Adiabaticity*," Phys. Rev. Lett. **104**, 063002 (2010).

[2] M. Demirplak and S. A. Rice, "*Adiabatic Population Transfer with Control Fields*," J. Phys. Chem. A **107**, 9937 (2003).

[3] M. Demirplak and S. A. Rice, "*Assisted adiabatic passage revisited.*," J. Phys. Chem. B **109**, 6838 (2005).

[4] M. Demirplak and S. A. Rice, "*On the consistency, extremal, and global properties of counterdiabatic fields.*," J. Chem. Phys. **129**, 154111 (2008).

[5] M. V. Berry, "*Transitionless quantum driving*," J. Phys. A **42**, 365303 (2009).

[6] H. R. Lewis and W. B. Riesenfeld, "*An Exact Quantum Theory of the Time-Dependent Harmonic Oscillator and of a Charged Particle in a Time-Dependent Electromagnetic Field*," J. Math. Phys. **10**, 1458 (1969).

[7] S. Masuda and K. Nakamura, "*Fast-forward of adiabatic dynamics in quantum mechanics*," Proc. R. Soc. A **466**, 1135 (2010).

[8] E. Torrontegui, S. Ibáñez, S. Martínez-Garaot, M. Modugno, A. del Campo, D. Guéry-Odelin, A. Ruschhaupt, X. Chen, and J. G. Muga, "*Shortcuts to adiabaticity*," Adv. At. Mol. Opt. Phys. **62**, 117 (2013).

[9] U. Hohenester, P. K. Rekdal, A. Borzì, and J. Schmiedmayer, "*Optimal quantum control of Bose-Einstein condensates in magnetic microtraps*," Phys. Rev. A **75**, 023602 (2007).

[10] J. Grond, J. Schmiedmayer, and U. Hohenester, "*Optimizing number squeezing when splitting a mesoscopic condensate*," Phys. Rev. A **79**, 021603 (2009).

[11] J. Grond, G. von Winckel, J. Schmiedmayer, and U. Hohenester, "*Optimal control of number squeezing in trapped Bose-Einstein condensates*," Phys. Rev. A **80**, 053625 (2009).

[12] L. Pezzé, A. Smerzi, G. P. Berman, A. R. Bishop, and L. A. Collins, "*Dephasing and breakdown of adiabaticity in the splitting of Bose-Einstein condensates*," New J. Phys. **7**, 85 (2005).

[13] M. Fattori, C. D'Errico, G. Roati, M. Zaccanti, M. Jona-Lasinio, M. Modugno, M. Inguscio, and G. Modugno, "*Atom Interferometry with a Weakly Interacting Bose-Einstein Condensate*," Phys. Rev. Lett. **100**, 080405 (2008).

[14] M. Gustavsson, E. Haller, M. J. Mark, J. G. Danzl, G. Rojas-Kopeinig, and H.-C. Nägerl, "*Control of Interaction-Induced Dephasing of Bloch Oscillations*," Phys. Rev. Lett. **100**, 080404 (2008).

[15] J. Gea-Banacloche, "*Splitting the wave function of a particle in a box*," Am. J. Phys. **70**, 307 (2002).

[16] Y. Shin, M. Saba, T. A. Pasquini, W. Ketterle, D. E. Pritchard, and A. E. Leanhardt, "*Atom Interferometry with Bose-Einstein Condensates in a Double-Well Potential*," Phys. Rev. Lett. **92**, 050405 (2004).

[17] L. A. Collins, L. Pezzé, A. Smerzi, G. P. Berman, and A. R. Bishop, "*Double-slit interferometry with a Bose-Einstein condensate*," Phys. Rev. A **71**, 033628 (2005).

[18] E. Torrontegui, S. Martínez-Garaot, A. Ruschhaupt, and J. G. Muga, "*Shortcuts to adiabaticity: Fast-forward approach*," Phys. Rev. A **86**, 013601 (2012).

[19] S. Masuda and K. Nakamura, "*Fast-forward problem in quantum mechanics*," Phys. Rev. A **78**, 062108 (2008).

[20] T. Schumm, S. Hofferberth, L. M. Andersson, S. Wildermuth, S. Groth, I. Bar-Joseph, J. Schmiedmayer, and P. Krüger, "*Matter-wave interferometry in a double well on an atom chip*," Nat. Phys. **1**, 57 (2005).

[21] B. V. Hall, S. Whitlock, R. Anderson, P. Hannaford, and A. I. Sidorov, "*Condensate Splitting in an Asymmetric Double Well for Atom Chip Based Sensors*," Phys. Rev. Lett. **98**, 030402 (2007).

[22] X. Chen and J. G. Muga, "*Transient energy excitation in shortcuts to adiabaticity for the time-dependent harmonic oscillator*," Phys. Rev. A **82**, 053403 (2010).

[23] J. Anandan and Y. Aharonov, "*Geometry of quantum evolution*," Phys. Rev. Lett. **65**, 1697 (1990).

[24] J. Javanainen and M. Y. Ivanov, "*Splitting a trap containing a Bose-Einstein condensate: Atom number fluctuations*," Phys. Rev. A **60**, 2351 (1999).

[25] A. Aichmayr, "*Analyzing the Dynamics of an atomic Bose-Einstein-Condensate within a Two-Mode Model*," Bachelor Thesis, Institut für Physik Karl-Franzens-Universität Graz (2010).

[26] C. Menotti, J. R. Anglin, J. I. Cirac, and P. Zoller, "*Dynamic splitting of a Bose-Einstein condensate*," Phys. Rev. A **63**, 023601 (2001).

[27] A. Messiah, *Quantum mechanics*, volume 2. Dover, Mineola, NY, 1999.

[28] C. Ottaviani, V. Ahufinger, R. Corbalán, and J. Mompart, "*Adiabatic splitting, transport, and self-trapping of a Bose-Einstein condensate in a double-well potential*," Phys. Rev. A **81**, 043621 (2010).

[29] E. Torrontegui, X. Chen, M. Modugno, A. Ruschhaupt, D. Guéry-Odelin, and J. G. Muga, "*Fast transitionless expansion of cold atoms in optical Gaussian-beam traps*," Phys. Rev. A **85**, 033605 (2012).

[30] V. Boyer, R. M. Godun, G. Smirne, D. Cassettari, C. M. Chandrashekar, A. B. Deb, Z. J. Laczik, and C. J. Foot, "*Dynamic manipulation of Bose-Einstein condensates with a spatial light modulator*," Phys. Rev. A **73**, 031402 (2006).

[31] X. Chen, I. Lizuain, A. Ruschhaupt, D. Guéry-Odelin, and J. G. Muga, "*Shortcut to Adiabatic Passage in Two- and Three-Level Atoms*," Phys. Rev. Lett. **105**, 123003 (2010).

[32] Y. Ban, X. Chen, E. Y. Sherman, and J. G. Muga, "*Fast and Robust Spin Manipulation in a Quantum Dot by Electric Fields*," Phys. Rev. Lett. **109**, 206602 (2012).

[33] S. Ibáñez, X. Chen, E. Torrontegui, J. G. Muga, and A. Ruschhaupt, "*Multiple Schrödinger Pictures and Dynamics in Shortcuts to Adiabaticity*," Phys. Rev. Lett. **109**, 100403 (2012).

[34] M. Albiez, R. Gati, J. Fölling, S. Hunsmann, M. Cristiani, and M. K. Oberthaler, "*Direct Observation of Tunneling and Nonlinear Self-Trapping in a Single Bosonic Josephson Junction*," Phys. Rev. Lett. **95**, 010402 (2005).

[35] R. Gati, M. Albiez, J. Fölling, B. Hemmerling, and M. K. Oberthaler, "*Realization of a single Josephson junction for Bose-Einstein condensates*," Appl. Phys. B **82**, 207 (2006).

[36] J. Estève, C. Gross, A. Weller, S. Giovanazzi, and M. K. Oberthaler, "*Squeezing and entanglement in a Bose-Einstein condensate.*," Nature **455**, 1216 (2008).

[37] B. Juliá-Díaz, E. Torrontegui, J. Martorell, J. G. Muga, and A. Polls, "*Fast generation of spin-squeezed states in bosonic Josephson junctions*," Phys. Rev. A **86**, 063623 (2012).

[38] J. A. Stickney and A. A. Zozulya, "*Wave-function recombination instability in cold-atom interferometers*," Phys. Rev. A **66**, 053601 (2002).

[39] A. S. Sanz, J. Campos-Martínez, and S. Miret-Artés, "*Transmission properties in waveguides: an optical streamline analysis.*," J. Opt. Soc. Am. A **29**, 695 (2012).

[40] T.-Y. Lin, F.-C. Hsiao, Y.-W. Jhang, C. Hu, and S.-Y. Tseng, "*Mode conversion using optical analogy of shortcut to adiabatic passage in engineered multimode waveguides.*," Opt. Express **20**, 24085 (2012).

[41] S.-Y. Tseng and X. Chen, "*Engineering of fast mode conversion in multimode waveguides.*," Opt. Lett. **37**, 5118 (2012).

[42] E. Torrontegui, S. Ibáñez, X. Chen, A. Ruschhaupt, D. Guéry-Odelin, and J. G. Muga, "*Fast atomic transport without vibrational heating*," Phys. Rev. A **83**, 013415 (2011).

[43] J. G. Muga, X. Chen, S. Ibáñez, I. Lizuain, and A. Ruschhaupt, "*Transitionless quantum drivings for the harmonic oscillator*," J. Phys. B **43**, 085509 (2010).

[44] X. Chen, E. Torrontegui, and J. G. Muga, "*Lewis-Riesenfeld invariants and transitionless quantum driving*," Phys. Rev. A **83**, 062116 (2011).

[45] T. Opatrný and K. Mølmer, "*Partial suppression of nonadiabatic transitions*," New J. Phys. **16**, 015025 (2014).

[46] S. Longhi, "*Quantum-optical analogies using photonic structures*," Laser Photon. Rev. **3**, 243 (2009).

[47] A. Szameit and S. Nolte, "*Discrete optics in femtosecond-laser-written photonic structures*," J. Phys. B **43**, 163001 (2010).

[48] S. Longhi, "*Optical realization of the two-site Bose-Hubbard model in waveguide lattices*," J. Phys. B **44**, 051001 (2011).

[49] M. Ornigotti, G. D. Valle, T. T. Fernandez, A. Coppa, V. Foglietti, P. Laporta, and S. Longhi, "*Visualization of two-photon Rabi oscillations in evanescently coupled optical waveguides*," J. Phys. B **41**, 085402 (2008).

[50] A. A. Rangelov and N. V. Vitanov, "*Achromatic multiple beam splitting by adiabatic passage in optical waveguides*," Phys. Rev. A **85**, 055803 (2012).

[51] K.-H. Chien, C.-S. Yeih, and S.-Y. Tseng, "*Mode Conversion/Splitting in Multimode Waveguides Based on Invariant Engineering*," J. Lightwave Technol. **31**, 3387 (2013).

[52] M. P. A. Fisher, P. B. Weichman, G. Grinstein, and D. S. Fisher, "*Boson localization and the superfluid-insulator transition*," Phys. Rev. B **40**, 546 (1989).

[53] D. Jaksch, C. Bruder, J. I. Cirac, C. W. Gardiner, and P. Zoller, "*Cold Bosonic Atoms in Optical Lattices*," Phys. Rev. Lett. **81**, 3108 (1998).

[54] M. A. H. MacCallum, "*On the classification of the real four-dimensional Lie algebras*," in *On Einstein's Path*, p. 299. Springer, 1999.

[55] D. Bambusi, "*Uniform Nekhoroshev estimates on quantum normal forms*," Nonlinearity **8**, 93 (1995).

[56] J. R. Cary, "*Lie transform perturbation theory for Hamiltonian systems*," Phys. Rep. **79**, 129 (1981).

[57] K. Eckert, M. Lewenstein, R. Corbalán, G. Birkl, W. Ertmer, and J. Mompart, "*Three-level atom optics via the tunneling interaction*," Phys. Rev. A **70**, 023606 (2004).

[58] E. Torrontegui, S. Martínez-Garaot, and J. G. Muga, "*Hamiltonian engineering via invariants and dynamical algebra*," Phys. Rev. A **89**, 043408 (2014).

[59] P. Doria, T. Calarco, and S. Montangero, "*Optimal Control Technique for Many-Body Quantum Dynamics*," Phys. Rev. Lett. **106**, 190501 (2011).

[60] M. Lapert, G. Ferrini, and D. Sugny, "*Optimal control of quantum superpositions in a bosonic Josephson junction*," Phys. Rev. A **85**, 023611 (2012).

[61] D. Stefanatos, J. Ruths, and J.-S. Li, "*Frictionless atom cooling in harmonic traps: A time-optimal approach*," Phys. Rev. A **82**, 063422 (2010).

[62] X. Chen, E. Torrontegui, D. Stefanatos, J.-S. Li, and J. G. Muga, "*Optimal trajectories for efficient atomic transport without final excitation*," Phys. Rev. A **84**, 043415 (2011).

[63] E. Torrontegui, X. Chen, M. Modugno, S. Schmidt, A. Ruschhaupt, and J. G. Muga, "*Fast transport of Bose-Einstein condensates*," New J. Phys. **14**, 013031 (2012).

[64] X. Chen and J. G. Muga, "*Engineering of fast population transfer in three-level systems*," Phys. Rev. A **86**, 033405 (2012).

[65] K. Bergmann, H. Theuer, and B. W. Shore, "*Coherent population transfer among quantum states of atoms and molecules*," Rev. Mod. Phys. **70**, 1003 (1998).

[66] M. N. Kiselev, K. Kikoin, and M. B. Kenmoe, "*SU(3) Landau-Zener interferometry*," Europhys. Lett. **104**, 57004 (2013).

[67] F. Q. Dou, L. B. Fu, and J. Liu, "*High-fidelity fast quantum driving in nonlinear systems*," Phys. Rev. A **89**, 012123 (2014).

[68] A. Ruschhaupt, X. Chen, D. Alonso, and J. G. Muga, "*Optimally robust shortcuts to population inversion in two-level quantum systems*," New J. Phys. **14**, 093040 (2012).

[69] L. I. Schiff, *Quantum mechanics*. McGraw-Hill, New York, 1981.

[70] A. Kastberg, W. D. Phillips, S. L. Rolston, R. J. C. Spreeuw, and P. S. Jessen, "*Adiabatic Cooling of Cesium to 700 nK in an Optical Lattice*," Phys. Rev. Lett. **74**, 1542 (1995).

[71] D. Daems and S. Guérin, "*Adiabatic Quantum Search Scheme With Atoms In a Cavity Driven by Lasers*," Phys. Rev. Lett. **99**, 170503 (2007).

[72] D. Daems, S. Guérin, and N. J. Cerf, "*Quantum search by parallel eigenvalue adiabatic passage*," Phys. Rev. A **78**, 042322 (2008).

[73] R. Bowler, J. Gaebler, Y. Lin, T. R. Tan, D. Hanneke, J. D. Jost, J. P. Home, D. Leibfried, and D. J. Wineland, "*Coherent Diabatic Ion Transport and Separation in a Multizone Trap Array*," Phys. Rev. Lett. **109**, 080502 (2012).

[74] S. Martínez-Garaot, E. Torrontegui, X. Chen, M. Modugno, D. Guéry-Odelin, S.-Y. Tseng, and J. G. Muga, "*Vibrational Mode Multiplexing of Ultracold Atoms*," Phys. Rev. Lett. **111**, 213001 (2013).

[75] S. Guérin, S. Thomas, and H. R. Jauslin, "*Optimization of population transfer by adiabatic passage*," Phys. Rev. A **65**, 023409 (2002).

[76] S. Guérin, V. Hakobyan, and H. R. Jauslin, "*Optimal adiabatic passage by shaped pulses: Efficiency and robustness*," Phys. Rev. A **84**, 013423 (2011).

[77] H. T. Quan and W. H. Zurek, "*Testing quantum adiabaticity with quench echo*," New J. Phys. **12**, 093025 (2010).

[78] J. Roland and N. J. Cerf, "*Quantum search by local adiabatic evolution*," Phys. Rev. A **65**, 042308 (2002).

[79] P. Richerme, C. Senko, J. Smith, A. Lee, S. Korenblit, and C. Monroe, "*Experimental performance of a quantum simulator: Optimizing adiabatic evolution and identifying many-body ground states*," Phys. Rev. A **88**, 012334 (2013).

[80] S. Ibáñez and J. G. Muga, "*Adiabaticity condition for non-Hermitian Hamiltonians*," Phys. Rev. A **89**, 033403 (2014).

[81] M. Anderlini, P. J. Lee, B. L. Brown, J. Sebby-Strabley, W. D. Phillips, and J. V. Porto, "*Controlled exchange interaction between pairs of neutral atoms in an optical lattice.*," Nature **448**, 452 (2007).

[82] S. Fölling, S. Trotzky, P. Cheinet, M. Feld, R. Saers, A. Widera, T. Müller, and I. Bloch, "*Direct observation of second-order atom tunnelling.*," Nature **448**, 1029 (2007).

[83] S. Martínez-Garaot, E. Torrontegui, X. Chen, and J. G. Muga, "*Shortcuts to adiabaticity in three-level systems using Lie transforms*," Phys. Rev. A **89**, 053408 (2014).

[84] M. Girardeau, "*Relationship between Systems of Impenetrable Bosons and Fermions in One Dimension*," J. Math. Phys. **1**, 516 (1960).

[85] D. W. Hallwood, T. Ernst, and J. Brand, "*Robust mesoscopic superposition of strongly correlated ultracold atoms*," Phys. Rev. A **82**, 063623 (2010).

[86] S. Ibáñez, X. Chen, and J. G. Muga, "*Improving shortcuts to adiabaticity by iterative interaction pictures*," Phys. Rev. A **87**, 043402 (2013).

[87] C. Cohen-Tannoudji and D. Guéry-Odelin, *Advances in atomic physics: An overview*. World Scientific, Singapore, 2011.

[88] B. T. Seaman, M. Krämer, D. Z. Anderson, and M. J. Holland, "*Atomtronics: Ultracold-atom analogs of electronic devices*," Phys. Rev. A **75**, 023615 (2007).

[89] A. Ruschhaupt and J. G. Muga, "*Atom diode: A laser device for a unidirectional transmission of ground-state atoms*," Phys. Rev. A **70**, 061604 (R) (2004).

[90] M. G. Raizen, A. M. Dudarev, Q. Niu, and N. J. Fisch, "*Compression of Atomic Phase Space Using an Asymmetric One-Way Barrier*," Phys. Rev. Lett. **94**, 053003 (2005).

[91] J. Reichel and V. Vuletic, *Atom Chips*. John Wiley & Sons, Weinheim, 2011.

[92] G. L. Gattobigio, A. Couvert, G. Reinaudi, B. Georgeot, and D. Guéry-Odelin, "*Optically Guided Beam Splitter for Propagating Matter Waves*," Phys. Rev. Lett. **109**, 030403 (2012).

[93] W. K. Burns and A. F. Milton, "*Mode conversion in planar-dielectric separating waveguides*," IEEE J. Quantum Electron. **11**, 32 (1975).

[94] N. Riesen and J. D. Love, "*Design of mode-sorting asymmetric Y-junctions*," Appl. Opt. **51**, 2778 (2012).

[95] O. A. Collins, S. D. Jenkins, A. Kuzmich, and T. A. B. Kennedy, "*Multiplexed Memory-Insensitive Quantum Repeaters*," Phys. Rev. Lett. **98**, 060502 (2007).

[96] N. Sangouard, C. Simon, H. de Riedmatten, and N. Gisin, "*Quantum repeaters based on atomic ensembles and linear optics*," Rev. Mod. Phys. **83**, 33 (2011).

[97] D. J. Wineland, C. Monroe, W. M. Itano, D. Leibfried, B. E. King, and D. M. Meekhof, "*Experimental issues in coherent quantum-state manipulation of trapped atomic ions*," J. Res. Natl. Inst. Stand. Technol. **103**, 259 (1998).

[98] I. Lizuain, J. G. Muga, and A. Ruschhaupt, "*Laser excitation of transverse modes in an atomic waveguide*," Phys. Rev. A **74**, 053608 (2006).

[99] A. E. Leanhardt, A. P. Chikkatur, D. Kielpinski, Y. Shin, T. L. Gustavson, W. Ketterle, and D. E. Pritchard, "*Propagation of Bose-Einstein Condensates in a Magnetic Waveguide*," Phys. Rev. Lett. **89**, 040401 (2002).

[100] W. Guerin, J.-F. Riou, J. P. Gaebler, V. Josse, P. Bouyer, and A. Aspect, "*Guided Quasicontinuous Atom Laser*," Phys. Rev. Lett. **97**, 200402 (2006).

[101] G. L. Gattobigio, A. Couvert, M. Jeppesen, R. Mathevet, and D. Guéry-Odelin, "*Multimode-to-monomode guided-atom lasers: An entropic analysis*," Phys. Rev. A **80**, 041605 (2009).

[102] E. Torrontegui, S. Martínez-Garaot, M. Modugno, X. Chen, and J. G. Muga, "*Engineering fast and stable splitting of matter waves*," Phys. Rev. A **87**, 033630 (2013).

[103] I. Bouchoule, H. Perrin, A. Kuhn, M. Morinaga, and C. Salomon, "*Neutral atoms prepared in Fock states of a one-dimensional harmonic potential*," Phys. Rev. A **59**, R8 (1999).

[104] R. Bücker, T. Berrada, S. van Frank, J.-F. Schaff, T. Schumm, J. Schmiedmayer, G. Jäger, J. Grond, and U. Hohenester, "*Vibrational state inversion of a Bose-Einstein condensate: optimal control and state tomography*," J. Phys. B **46**, 104012 (2013).

[105] R. Bücker, J. Grond, S. Manz, T. Berrada, T. Betz, C. Koller, U. Hohenester, T. Schumm, A. Perrin, and J. Schmiedmayer, "*Twin-atom beams*," Nat. Phys. **7**, 608 (2011).

[106] H. R. Stuart, "*Dispersive Multiplexing in Multimode Optical Fiber*," Science **289**, 281 (2000).

[107] J. Wang, J.-Y. Yang, I. M. Fazal, N. Ahmed, Y. Yan, H. Huang, Y. Ren, Y. Yue, S. Dolinar, M. Tur, and A. E. Willner, "*Terabit free-space data transmission employing orbital angular momentum multiplexing*," Nat. Photonics **6**, 488 (2012).

[108] S. Berdagué and P. Facq, "*Mode division multiplexing in optical fibers*," Appl. Opt. **21**, 1950 (1982).

[109] V. Liu, D. A. B. Miller, and S. Fan, "*Ultra-compact photonic crystal waveguide spatial mode converter and its connection to the optical diode effect.*," Opt. Express **20**, 28388 (2012).

[110] W. Chen, P. Wang, and J. Yang, "*Mode multi/demultiplexer based on cascaded asymmetric Y-junctions.*," Opt. Express **21**, 25113 (2013).

[111] J. B. Driscoll, R. R. Grote, B. Souhan, J. I. Dadap, M. Lu, and R. M. Osgood, "*Asymmetric Y junctions in silicon waveguides for on-chip mode-division multiplexing.*," Opt. Lett. **38**, 1854 (2013).

[112] J. D. Love and N. Riesen, "*Single-, Few-, and Multimode Y-Junctions*," J. Lightwave Technol. **30**, 304 (2012).

[113] J. D. Love, R. W. C. Vance, and A. Joblin, "*Asymmetric, adiabatic multipronged planar splitters*," Opt. Quantum Electron. **28**, 353 (1996).

[114] X. Sun, H.-C. Liu, and A. Yariv, "*Adiabaticity criterion and the shortest adiabatic mode transformer in a coupled-waveguide system*," Opt. Lett. **34**, 280 (2009).

[115] R. R. A. Syms, "*The digital directional coupler: improved design*," IEEE Photon. Technol. Lett. **4**, 1135 (1992).

[116] G. T. Paloczi, A. Eyal, and A. Yariv, "*Wavelength-insensitive nonadiabatic mode evolution couplers*," IEEE Photon. Technol. Lett. **16**, 515 (2004).

[117] S.-Y. Tseng, "*Counterdiabatic mode-evolution based coupled-waveguide devices.*," Opt. Express **21**, 21224 (2013).

[118] S.-Y. Tseng and Y.-W. Jhang, "*Fast and Robust Beam Coupling in a Three Waveguide Directional Coupler*," IEEE Photon. Technol. Lett. **25**, 2478 (2013).

[119] C.-S. Yeih, H.-X. Cao, and S.-Y. Tseng, "*Shortcut to mode conversion via level crossing in engineered multimode waveguides*," IEEE Photon. Technol. Lett. **26**, 123 (2014).

[120] D. Leibfried, R. Blatt, C. Monroe, and D. Wineland, "*Quantum dynamics of single trapped ions*," Rev. Mod. Phys. **75**, 281 (2003).

[121] K. Bergmann, N. V. Vitanov, and B. W. Shore, "*Perspective: Stimulated Raman adiabatic passage: The status after 25 years.*," J. Chem. Phys. **142**, 170901 (2015).

[122] I. S. Vogelius, *Cooling and manipulating trapped molecular ions*. PhD thesis, Department of Physics and Astronomy, University of Aarhus, 2005.

[123] F. Gebert, Y. Wan, F. Wolf, J. C. Heip, and P. O. Schmidt, "*Detection of motional ground state population of a trapped ion using delayed pulses*," arXiv:1510.00063v1.

[124] M. Palmero, E. Torrontegui, D. Guéry-Odelin, and J. G. Muga, "*Fast transport of two ions in an anharmonic trap*," Phys. Rev. A **88**, 053423 (2013).

[125] S. Martínez-Garaot, A. Ruschhaupt, J. Gillet, T. Busch, and J. G. Muga, "*Fast quasiadiabatic dynamics*," Phys. Rev. A **92**, 043406 (2015).

[126] J. P. Home and A. M. Steane, "*Electrode configurations for fast separation of trapped ions*," Quantum Inf. Comput. **6**, 289 (2006).

[127] A. H. Nizamani and W. K. Hensinger, "*Optimum electrode configurations for fast ion separation in microfabricated surface ion traps*," Appl. Phys. B **106**, 327 (2012).

[128] H. Kaufmann, T. Ruster, C. T. Schmiegelow, F. Schmidt-Kaler, and U. G. Poschinger, "*Dynamics and control of fast ion crystal splitting in segmented Paul traps*," New J. Phys. **16**, 073012 (2014).

[129] A. C. Wilson, Y. Colombe, K. R. Brown, E. Knill, D. Leibfried, and D. J. Wineland, "*Tunable spin-spin interactions and entanglement of ions in separate potential wells.*," Nature **512**, 57 (2014).

[130] T. Ruster, C. Warschburger, H. Kaufmann, C. T. Schmiegelow, A. Walther, M. Hettrich, A. Pfister, V. Kaushal, F. Schmidt-Kaler, and U. G. Poschinger, "*Experimental realization of fast ion separation in segmented Paul traps*," Phys. Rev. A **90**, 033410 (2014).

[131] J. Alonso, F. M. Leupold, B. C. Keitch, and J. P. Home, "*Quantum control of the motional states of trapped ions through fast switching of trapping potentials*," New J. Phys. **15**, 023001 (2013).

[132] R. Bowler, *Coherent Ion Transport in a Multi-electrode Trap Array*. PhD thesis, University of Colorado, 2015.

[133] J. Alonso, F. M. Leupold, Z. U. Soler, M. Fadel, M. Marinelli, B. C. Keitch, V. Negnevitsky, and J. P. Home, "*Fast quantum control and light-matter interactions at the 10,000 quanta level*," `arXiv:1509.06157`.

[134] X.-J. Lu, J. G. Muga, X. Chen, U. G. Poschinger, F. Schmidt-Kaler, and A. Ruschhaupt, "*Fast shuttling of a trapped ion in the presence of noise*," Phys. Rev. A **89**, 063414 (2014).

[135] D. Guéry-Odelin and J. G. Muga, "*Transport in a harmonic trap: Shortcuts to adiabaticity and robust protocols*," Phys. Rev. A **90**, 063425 (2014).

[136] S. Masuda, "*Acceleration of adiabatic transport of interacting particles and rapid manipulations of a dilute Bose gas in the ground state*," Phys. Rev. A **86**, 063624 (2012).

[137] M. Palmero and J. G. Muga, "*Fast excitationless atom transport in a non-rigid trap*," (unpublished) .

[138] J. Grond, U. Hohenester, I. Mazets, and J. Schmiedmayer, "*Atom interferometry with trapped Bose-Einstein condensates: impact of atom-atom interactions*," New J. Phys. **12**, 065036 (2010).

[139] J. Patera, R. T. Sharp, P. Winternitz, and H. Zassenhaus, "*Invariants of real low dimension Lie algebras*," J. Math. Phys. **17**, 986 (1976).